SOUTHWESTERN KANSAS HIGH PLAINS UNSATURATED ZONE PILOT STUDY TO ESTIMATE DARCIAN-BASED GROUNDWATER RECHARGE AT THREE INSTRUMENTED SITES

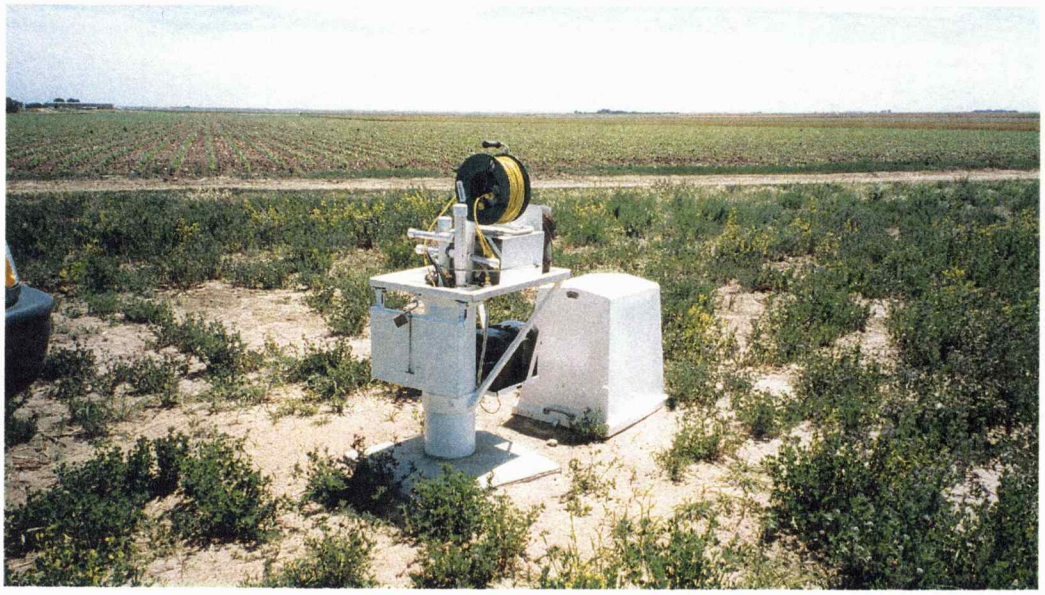

By

Marios Sophocleous, Gerard Kluitenberg, John Healey

Open-File Report 2001-11
Kansas Geological Survey
January 2002

KANSAS GEOLOGICAL SURVEY
OPEN-FILE REPORTS

Disclaimer

The Kansas Geological Survey made a conscientious effort to ensure the accuracy of this report. However, the Kansas Geological Survey does not guarantee this document to be completely free from errors or inaccuracies and disclaims any responsibility or liability for interpretations based on data used in the production of this document or decisions based thereon. This report is intended to make results of research available at the earliest possible date, but is not intended to constitute final or formal publication.

Southwestern Kansas High Plains unsaturated zone pilot study to estimate Darcian-based groundwater recharge at three instrumented sites

By

Marios Sophocleous[1], Gerard Kluitenberg[2], and John Healey[1],

[1]Kansas Geological Survey, The University of Kansas, Lawrence, KS 66047
[2]Department of Agronomy, Kansas State University, Manhattan, KS 66506

Kansas Geological Survey Open-File Report 2001-11
January 2002

Table of Contents

List of Figures

List of Tables

Abstract

Recent improvements in technology make it possible to study the deep vadose zone, well below the rooting depths of plants. Such technology has been employed to monitor, on a continuous basis, the deep pore-water fluxes en route to the High Plains aquifer (HPA). This proof-of-concept pilot study provided, for the first time, information on the quantity and pattern of water fluxes in the deep vadose zone that impact the management of both the quantity and quality of the HPA in Kansas. Our preliminary investigation evaluated the use of heat-dissipation sensors and advanced tensiometers for measuring pore-water pressures in deep boreholes at two irrigated land-use sites (Sites 1 and 2) and one natural grassland site (Site 3). Heat-dissipation sensors yielded excellent estimates of pore-water pressure and proved to be robust and reliable. Limited success was achieved with the advanced tensiometers due to operational problems. Time series data obtained from the heat-dissipation sensors revealed constant pore-water pressures after an equilibration period of 2-3 months. These data indicate steady-state water flow at the points of observation over the duration of the investigation. Darcian methodology was used to obtain estimates of recharge at all three sites. Estimated recharge rates for irrigation land use Sites 1and 2 were appreciably higher (3 mm/yr and 0.6-0.9 mm/yr, respectively) than the estimated recharge rate for native grassland Site 3 (0.1-0.3 mm/yr). In all cases, the estimated annual recharge values were less than one percent of annual precipitation. Although the study sites are representative of irrigated and grassland areas overlying the High Plains aquifer in southwestern Kansas, caution must be exercised in using these flux estimates to draw general conclusions regarding present-day recharge in the region due to the large uncertainty associated with these estimates and the small number of study sites. Improvements in the Darcian methodology employed in this investigation should make it possible to reduce uncertainty in flux estimates in future investigations. Finally, we note that the groundwater levels observed in relatively shallow wells (less than 60-m deep) in the High Plains sediments probably do not represent the Ogallala Formation water levels observed at the generally deep irrigation wells in the area but instead represent perched-type water tables in a saturated subsurface above the locally confined Ogallala Formation.

I. Introduction and Objectives

The High Plains aquifer (HPA) underlies about 79,000 square kilometers (30,500 square miles) area in western and central Kansas, more than 37% of the state. Approximately 98% of ground water withdrawn from the HPA in Kansas is used for irrigated agriculture, which represents 23% of the cropland overlying the HPA (U.S. Department of Agriculture, 1999). In 1990, the total ground-water withdrawal from the Kansas HPA was 5, 012,377 megaliters, ML (4,063,600 ac-ft; McGuire and Sharpe, 1997), representing 83% of all ground-water use and 59.6% of all water use in Kansas. The large annual volume of water withdrawn from the HPA for irrigation purposes has had a substantial effect on water levels in the aquifer. Since 1950 (the beginning of major irrigation development in Kansas), water levels have declined an area-weighted

average of 3.02 m (9.9 ft), or 0.1 m/yr (0.33 ft/yr), from 1950 to 1980, and an area-weighted average of 2.29 m (7.5 ft), or 0.15 m/yr (0.50 ft/yr), from 1980 to 1995 (McGuire and Sharpe, 1997). The average annual area-weighted precipitation in the Kansas HPA region during 1981-1994 was 588 mm (23.16 inches), which is 104% of the 30-year normal (1961-1990) precipitation in the region (McGuire and Sharpe, 1997).

Since 1960, mean annual streamflow in western Kansas has decreased substantially partly due to a decline in baseflow brought about by the above-mentioned ground-water depletion, and partly because of more efficient water-conservation measures reducing surface runoff. Runoff to streams was estimated to have declined by one-half in western Kansas since 1959 (Ratzlaff, 1994).

Widespread water-quality concerns have also emerged with the development of irrigated agriculture in the HPA region. Recent studies (NAS, 1996; Sophocleous, 1998) indicated that agriculture and confined livestock operations are the principal factors related to water-quality problems. Major sources of ground-water contamination are agricultural nutrients (particularly nitrates from nitrogen fertilizers and confined livestock operations), pesticides, and salinity. *However, the quantity and quality of irrigation return-flows and natural recharging water fluxes in the deep vadose zone, en route to the generally deep HPA water table, have not previously been investigated in Kansas.*

The State of Kansas has invested significant financial resources through the Kansas Water Plan to promote water-conservation and pollution-prevention measures. However, the effectiveness of such measures is uncertain, partly because the assessment tools are not readily available. *A major goal of this study is to select and apply some of the most promising and practical tools for performing such evaluations.* Recent improvements in technology make it now possible to study the deep vadose zone, well below the rooting depths of plants, thus allowing us to monitor on a continuous basis the deep pore-water fluxes and sample those pore waters and their possible contaminants en route to the underlying aquifer.

To address the need for consistent and scientifically sound information for managing water resources, the U.S. Geological Survey (USGS) began the National Water-Quality Assessment (NAWQA) Program in 1991. A study unit within this NAWQA program is the High Plains Regional Groundwater study (Dennehy, 2000), which began in 1998 for the purpose of describing the status and trends in water quality in the High Plains aquifer, and providing a better understanding of the natural and human factors that affect groundwater quality (http://webserver.cr.usgs.gov/nawqa/hpgw/HPGW_home.html).

During fiscal year 2000, a USGS study was initiated to determine fluxes of agricultural chemicals to the water table under irrigated fields and grassland in the central High Plains. The Kansas Geological Survey (KGS) and the USGS entered into a cooperative agreement to achieve these objectives. In addition, the KGS cooperated with Kansas State University (KSU) to further enhance the stated objectives. *The specific objectives of this report are to (1) summarize the general hydrogeologic framework of southwestern Kansas where the sites are located, and (2) document the quantification of the deep vadose zone water fluxes reaching the High Plains water table at the studied sites using physically based, Darcian methodologies.*

The general approach used was to drill three boreholes, two in the irrigated agriculture land-use area (Sites 1 [T.26 S.- R.32 W.- 21 ADC] and 2 [T. 26 S.- R. 31 W.- 31 CCD], Fig. 1, with USGS designations as CAL-121 and CAL-122, respectively), and one (USGS designation CNG) in a control (pristine) site (Site 3 [T.34 S.- R.41 W.- 25 ADA], Fig. 1). Depth to water in all sites is less than 60 m (200 ft). At each site, a borehole was drilled from land surface to the water table, and detailed soil and water samples as well as cores were collected by the USGS to characterize sediment texture, hydrologic and thermal parameters, and geochemistry. Field-site lithologic characterization of drill cuttings was mainly the responsibility of KGS. Subsequent to borehole drilling and sampling, the unsaturated zone of each borehole was instrumented with suction lysimeters, gas samplers, advanced tensiometers and heat dissipation sensors. A ground-water monitoring well was also installed at the water table in each

borehole. Pore-water pressure measurements and groundwater-level measurements were the responsibility of KGS, whereas vadose zone gas and water samples as well as groundwater samples were collected regularly at all three sites by the USGS.

Several methods, including environmental tracers and numerical simulations, are being used by the USGS to estimate recharge rates (see McMahon et al., 2002). In this study, we complement the USGS methods by installing advanced tensiometers and ceramic matric potential sensors (based on heat-dissipation technology) in the three boreholes to measure and record the hydraulic gradients near the water table during both the irrigation and non-irrigation seasons. These hydraulic gradient time series, in combination with hydraulic properties of collected cores, determined at the USGS Soil and Rock Properties Laboratory in Sacramento, California, will allow us, for the first time in Kansas, to quantify the deep-vadose-zone water fluxes reaching the HPA water table.

II. Hydrogeologic Environment

1. Physiography and Soils

Sites CAL-121 and CAL-122 are located in irrigated agricultural areas in southern Finney County, and site CNG, the control site, is located in southern Morton County (Fig. 1). Most of Finney County and Morton County are in the High Plains section of the Great Plains physiographic province.

Within Finney County are five, well-defined physiographic areas. These are the High Plains tableland, the Pawnee River drainage area, the Scott-Finney depression, the valley of the Arkansas River, and the sandhills (Latta, 1944). Sites CAL-121 and CAL-122 are located within the Manter-Keith soil association in Finney County, comprising sandy and loamy soils and consisting of transitional areas between the very sandy soils of the sandhills and the loamy soils of the High Plains tableland. The Keith soils in that association (which comprise both CAL-121 and CAL-122 sites) are deep, permeable, and

fertile, and they are well suited to all the dryland and irrigated crops commonly grown (Harner et al., 1965).

Site CNG is located within the Vona-Tivoli association in Morton County that occupies the rolling and hilly sandy lands. The most extensive soil in this association is the Vona loamy fine sand, which occupies the gently rolling areas, including the area of site CNG (Dickey et al., 1963). The native cover consists of mid and tall grasses.

2. Climate

Finney County has a temperate, semiarid, continental climate. The average annual precipitation is about 483 mm (19 inches). Morton County has a semiarid continental climate that is characterized by extreme temperatures and deficiency of moisture in all seasons. The average annual precipitation in Morton County is less than 432 mm (17 inches). In general, the average annual precipitation in southwest Kansas ranges from 381 mm (15 inches) in the west to 508 mm (20 inches) in the eastern part of Groundwater Management District No 3 (GMD3), which covers most of southwestern Kansas; most of this precipitation falls during the warm season from April and September. To a great extent, the amount of rainfall in southwest Kansas depends on the supply of moisture from the Gulf of Mexico. The Rocky Mountains to the west prevent the inflow of moist air from the Pacific Ocean.

The summers in southwestern Kansas are warm, and the winters are cold but not rigorous (Harner et al., 1965). The abundant sunshine and the constant movement of the wind are probably the two most noticeable characteristics of the climate. Marked and significant differences in daily temperature occur in the colder part of the year.

3. Geologic Framework

Tertiary and Quaternary deposits underlie most of the area in southwestern Kansas and are the principal water-yielding beds. The only stratigraphic unit of Tertiary age identified in southwest Kansas, and in western Kansas in general, is the Ogallala Formation of Pliocene age (Gutentag, 1963). Rocks of the Paleocene, Eocene, and

Oligocene Series have been identified in other parts of the High Plains but have not been identified in Kansas. The Pliocene deposits have not been divided in the subsurface, and the broad usage of the term Ogallala Formation encompasses all deposits of Pliocene age observed during drilling (Gutentag, 1963). The Ogallala Formation is a heterogeneous sequence of unconsolidated deposits of clay, silt, sand, and gravel that are principally of alluvial origin. Minor but stratigraphically significant beds of freshwater limestone and lentils of volcanic ash occur in the formation. The type and degree of cementation within the formation varies. Lime-cemented beds of silty sand and gravel (mortar beds) and sandy silt (caliche) occur throughout the formation and form ledges or caprock at the outcrop (Stullken et al., 1985).

The Ogallala Formation was deposited primarily by easterly flowing aggrading streams carrying debris from the Rocky Mountains to the west. A vast plain of braided streams and coalesced alluvial fans was formed. Distribution of sediment types within the Ogallala Formation is largely random (Breyer, 1975). The major identifying feature of braided streams is the coarsening-upward as well as fining-upward sequences of alluvial deposits (Gutentag et al., 1984). This process of coarsening and fining of the alluvial deposits gives a random distribution of sediments in the High Plains aquifer, suggesting that the aquifer is homogeneous on a regional scale. Test holes drilled within a 160-acre tract often show a predominance of clays and silts at one site and of sand and gravel nearby (Stullken et al., 1985).

The Quaternary deposits of southwestern Kansas are of Pleistocene and Holocene age. Considerable thicknesses of both alluvial and eolian deposits occur at the surface of the High Plains in Kansas. Quaternary alluvium (stream-laid clay, silt, sand, and gravel) is the predominant type of Cenozoic deposit in most of southwest Kansas. Pleistocene loess mantles much of the upland areas in western Kansas, and Pleistocene and Holocene dune sands cover a significant part of the southwest areas of the state. Because of the similarity in composition, the contact between the Ogallala Formation and the overlying Pleistocene deposits is difficult to determine from drillers' logs, gamma-ray logs, and some test-hole logs.

Figure 2 shows an east-west cross section depicting the stratigraphy from western Stanton County to the Gray County line across township 28. Sample strip logs, prepared by gluing a representative actual sample of sediment to the log strip at the depth indicated by the driller's log, were used in the interpretation and correlation of the Pliocene-Pleistocene boundary for the Stanton and Grant counties (Gutentag, 1963). The lithology of the wells and test holes has been simplified to show the aquifers (sand and gravel), aquitards (silt), and quasi-aquicludes (clay and caliche). Mixtures of materials were designated as to their major constituent for clarity of illustration. The slopes on the eroded bedrock and Ogallala surfaces in the eastern part of the area are moderate as opposed to steep slopes in the western part. The sediments are thickest where the slopes are moderate (Gutentag, 1963).

In southwest Kansas, south of the Arkansas River, the rocks underlying the High Plains aquifer, or the bedrock, consist of progressively older strata to the south and east--the lower Cretaceous sandstones and shales, the Jurassic and Triassic sandstones and shales, and the Lower and Upper Permian red sandstones, siltstones, gypsum, and dolomite (Fig. 3). The bedrock formations in the vicinity of Sites 1 and 2 are shown by the gamma ray log in Figure 4.

The configuration of the bedrock surface is a composite of subaerial erosional surfaces of several ages (Merriam and Frye, 1954). This surface also has been affected by structural movement and by subsidence associated with the solution of evaporites from Permian rocks (Gutentag et al., 1981). The pre-Ogallala surface south of the Arkansas River has also been modified by post-Ogallala erosion. The irregular bedrock surface in southwest Kansas between the Bear Creek and the Crooked Creek-Fowler faults (Fig. 3) generally slopes at about 2.56 m/km (13.5 feet per mile -- a gradient of 0.0026) to the east-southeast from 1,067 m (3,500 feet) above sea level near the Colorado State line in southwest Stanton County to about 610 m (2,000 feet) above sea level near the town of Meade in Meade County. The Bear Creek and Crooked Creek-Fowler faults in southwest Kansas are attributed to dissolution of halite and gypsum from the Blaine Formation and Flowerpot Shale of the Lower Permian Nippewalla Group (Fig. 4).

Maximum displacement on the bedrock surface across these features is about 76 m (250 feet; Gutentag et al., 1981; Holdoway, 1978).

4. High Plains Aquifer

The High Plains aquifer, which consists of "one or more hydraulically connected geologic units of late Tertiary or Quaternary age" (Gutentag and Weeks, 1980), is considered to be a single hydrologic unit (Stullken et al., 1985). In Kansas, the included geologic units are, in ascending stratigraphic order, the Ogallala Formation of late Tertiary age, and the alluvial and eolian deposits of Quaternary age. The geologic framework of the aquifer consists of a heterogeneous sequence of clay, silt, sand, and gravel that is predominantly of alluvial origin. Dune sands deposited during late Quaternary time also are considered a part of the aquifer because they are hydraulically connected to underlying deposits. Unsaturated Upper Quaternary loess and dune sands overlie the aquifer in most of western Kansas and affect recharge to the aquifer. The High Plains aquifer ranges in saturated thickness from 0 to more than 550 ft (as of the late 1990's), just south and west of Liberal in Seward and Stevens Counties. Generally, the greatest saturated thickness is where the unconsolidated deposits overlie the deepest channels in the bedrock. In some areas the High Plains aquifer is hydraulically connected to the overlying alluvium, such as along the Arkansas and Cimarron river valleys. The Lower Cretaceous Dakota aquifer is also hydraulically connected to the High Plains aquifer in some locations—that is, the Ogallala Formation is not separated from the Dakota Formation by shale, clay, or other low-permeability units (Fig. 4; Coe, 1994). General flow within the aquifer is eastward, as can be seen in the groundwater-level map of Fig. 5. Streams affect local flow patterns as they become discharge or recharge points for the aquifer. Prior to heavy irrigation development, the Arkansas River received baseflow from the High Plains aquifer and the connected alluvial deposits. Under these conditions, groundwater naturally flowed towards the river. Now the water table has declined below the streambed so that the flowing river may be a recharge source for the underlying sediments (Coe, 1994).

The natural hydrologic cycle in the High Plains aquifer in southwestern Kansas is depicted by a generalized block diagram (Fig. 6). Water enters the aquifers by underflow from the west; by seepage from streams, especially in times of high flow; and by recharge of precipitation within the area. Water is discharged to the east and south by underflow, by seepage to perennial streams, and by evapotranspiration (ET) where the water table is shallow (although in southwestern Kansas, discharge by ET is negligible because the water table in most of the area is too far below the land surface). This natural cycle has been modified by human activities to include discharge from the aquifer by pumpage from wells and recharge to the aquifer from deep percolation of applied irrigation water.

III. Methodology

The major objective of this pilot study was to employ state-of-the-science technology to quantify deep-vadose-zone water fluxes reaching the High Plains aquifer. This technology consists of Advanced Tensiometers (AT) and Heat Dissipation (HD) sensors in combination with a data acquisition and control system to measure the pore-water pressure head in the deep vadose zone.

1. Sensors

a. Advanced Tensiometers

Tensiometers are used to obtain measurements of soil-water potential between 0 and about -1,000 cm H_2O (Cassel and Klute, 1986), although their practical lower limit attainable in the field is about -900 cm, due to air coming out of solution (degassing) at higher tension. Multiple tensiometers are used in a profile to calculate hydraulic gradients to determine the direction of water movement and to estimate water flux using unsaturated hydraulic conductivity.

Tensiometers consist of three components: a porous cup, a pressure sensor, and a reservoir filled with water connecting the porous cup to the pressure sensor. Conventional tensiometers are equipped with the pressure sensor mounted above the land

surface, limiting installations to a few meters below the land surface. The length of the water column adds to the vacuum in conventional tensiometers, thereby reducing the effective range by the length of the water column. Tensiometers have been constructed with a pressure transducer buried at or near the sensing tip to circumvent this depth limitation and to allow automated data collection (Klute and Peters, 1962; Strebel et al., 1973; Williams, 1978; Trotter, 1984; Nyhan and Drennon, 1990). However, this technique does not provide easy access for field calibration, replacement, or maintenance of the transducer (Hubbell and Sisson, 1996; 1998). Conventional tensiometers exhibit significant diurnal measurement fluctuations from temperature changes in the transducer-tensiometer system (Watson and Jackson, 1967) and the gases trapped in the tensiometer (Cassell and Klute, 1986). As a result, the instruments have to be serviced regularly to remove air that can accumulate and influence tensiometer measurements.

A new design for permanently installed tensiometers was presented by Hubbell and Sisson (1998). This design allows soil moisture potential measurements at any depth, reduces measurement errors from diurnal temperature effects, uses a replaceable transducer, allows in-place sensor calibration and verification, and reduces field maintenance requirements. This tensiometer, the Advanced Tensiometer (AT), is shown in Figure 7. It consists of a permanently installed casing (B) and a removable transducer assembly (A). The permanently installed casing is equipped with a porous ceramic cup on the bottom, an adapter containing a reservoir of water, and casing that extends to the land surface. The removable transducer assembly consists of a rubber gasket and a pressure transducer attached to an inner guide tube for installing the transducer assembly from the land surface. The transducer assembly is lowered into the casing until the gasket seats into the permanently installed adapter. The Advanced Tensiometer is activated by filling the porous cup/adapter with water, and sliding the pressure transducer assembly (A) inside the casing (B) until the stopper/gasket seats in the adapter (C). Figure 8 shows the porous ceramic cup and adapter in lower hand, and the transducer with a rubber gasket attached to an inner polyethylene guide tube in upper hand. About 100 mL of water is poured between the inner guide tube and the outer tensiometer assembly, and the inner guide-tube assembly is raised a few centimeters to fill the cup

and adapter (Fig. 7C). The weight of the inner guide tube and transducer presses the stopper into the adapter while the water moving from the reservoir into the surrounding unsaturated sediments applies a force that also holds the stopper in place. Additional details about the construction and installation of Advanced Tensiometers are given by Hubbell and Sisson (1998).

The advanced tensiometer is serviced (deaired) by raising the inner guide tube allowing the water reservoir to refill from water located above the stopper. Servicing must be performed before readings are affected by air entrapment in the water reservoir. The inner guide tube and stopper need only to be pulled up a few centimeters in order to service the Advanced Tensiometer. Water is added to the tensiometer periodically to maintain a small volume of water above the stopper. Excess water that is not required to fill the sealed bottom chamber adjacent to the porous cup is retained above the stopper and used to fill the chamber at a later time. The tensiometer readings equilibrate a few hours after servicing.

b. Heat Dissipation Sensors

The Heat Dissipation (HD) sensor for measuring soil matric-potential consists of a thermocouple wire pair and heater wire enclosed in a hypodermic needle that is embedded in a cylindrical porous ceramic body (Fig. 9). The sensor operates by passing an electric current through the heater wire and measuring the thermocouple temperature rise with time. The rate of heat dissipating through the ceramic from the needle is dependent on the thermal conductivity of the ceramic, which will change with water content. When placed in contact with the soil, the sensor should equilibrate to the same water potential as the soil. In our case, temperatures are measured one second after heating starts, and again 20 seconds after heating starts (Appendix A). The difference in temperature between the early and late reading is used to compute matric potential. The thermocouple temperature was also measured just before the initiation of heating, so that the in-situ sediment temperature can be recorded. Assuming a unique water retention curve for the ceramic, the temperature rise of the sensor for a particular electrical current and heating time can be calibrated against known soil matric-potentials (Reece, 1996).

These sensors exhibit several desirable characteristics for water-potential measurement. They have a water potential range of approximately -100 to -10^6 cm H_2O (-0.1 to -1,000 bars) and a sensitivity that is approximately proportional to water potential. Therefore, they have good resolution in the wet range and are still capable of responding to changes in water potential of dry soils.

c. Water-level Pressure Transducers

The PXD-261 pressure transducer (In-Situ Inc.) is a fully submersible transducer for monitoring changes in water level. The small diameter of the PXD-261 permits access to one-inch diameter wells, and long cable lengths do not compromise accuracy. Such pressure transducers are ideal for short- or long-term monitoring in field environments.

A pressure transducer senses changes in pressure exerted by a column of water or other fluid above an internal strain gauge. A pressure transducer measures change in pressure within its stated range. The sensing of pressure change by the strain gauge is translated electronically to a 4-20 mA signal sent to the data logger. An advantage of current output transducers over voltage output transducers is that the current signal remains constant over very long cable leads.

Terminal input modules connect directly to the data logger's input terminals to provide completion resistors for resistive bridge measurements, voltage dividers, and precision current shunts. The CURS100 (Campbell Scientific, Inc.) 100-ohm current shunt terminal input module converts a current signal (e.g., 4-20 mA) to a voltage that is measured by the 21X datalogger (Campbell Scientific, Inc.). The 100-ohm resistor used for the current shunt allows currents up to 50 mA to be read on a ±5000 mV range (for the Campbell Scientific, Inc. 21X datalogger employed in this study).

2. Sensor Calibration

a. Advanced Tensiometers

The AT pressure transducers (Honeywell 26PCC-type, differential, compensated pressure transducers with a pressure range of 103 kPa (15 psi), with fluorosilicone seal and straight port) were calibrated at the Idaho National Engineering and Environmental Laboratories (INEEL) in Idaho Falls, Idaho using specified pressure/vacuum values ranging from -700 to +200 cm H_2O. Linear calibration curves with $R^2 = 0.9999$ were typical. Appendix B contains all the resulting calibration curves.

b. Heat Dissipation sensors

The Heat Dissipation (HD) sensors (Campbell Scientific, Inc. 229 Soil Water Potential Probe) were calibrated at the USGS Soil and Rock Properties laboratory in Sacramento, California. Much of the variation due to heating methods and sensor to sensor variation can be removed by a normalization procedure based on the saturated and oven dry temperature responses,

$$T^* = \frac{\Delta T_d - \Delta T}{\Delta T_d - \Delta T_w}, \qquad \text{(i)}$$

where ΔT is the temperature rise of the line heat source of the HD sensor due to heating, and subscripts w and d indicate the values for a fully saturated matrix and an oven-dry matrix, respectively (Flint et al., 2002). This normalization reduced the matric potential (Ψ)-temperature rise (ΔT) response of HD sensors to a single relationship, which is well fitted by a van Genuchten-type equation (Flint et al., 2002):

$$\Psi = \Psi_0 [(T^*)^{-n} - 1]^m, \qquad \text{(ii)}$$

where Ψ_0, n, and m are empirical constants. Sensor calibrations are temperature dependent, and this temperature dependence is well described by a dielectric mixing model similar to that described by Campbell et al. (1994). A fifth order polynomial was fit to the model predictions that allows the correction of measurements at any temperature to values at the calibration temperature (Flint et al., 2002).

Sensors were calibrated following the general procedures described in Flint et al. (2002). A six-point calibration was performed and the data were fit to eq. (ii) above

using optimization techniques. The ΔT_w point in eq. (i) was obtained in a water bath at 20C after vacuum saturation. The pressure plate apparatus was used to obtain data points at –0.11, –0.5, and –3 bars. These points were chosen based on the assumption that the matric potentials we would encounter in the deep vadose zone of western Kansas would likely fall within that range. All HD sensors were air-dried, sealed in double plastic bags with desiccant, and placed in a temperature controlled chamber at 20C to obtain a data point equivalent to –1300 bars. The ΔT_d point in eq. (i) {equivalent to –10,000 bars} was determined by applying the quadratic function described in Flint et al. (2001). Appendix C contains the HD sensor calibration data.

c. Water-level pressure transducers

The water-level pressure transducers (PXD sensors) were calibrated at the Kansas Geological Survey by lowering them into an observation well a set distance below the water table and gradually raising or lowering them a set depth increment, recording the mV response from the datalogger (21X), and fitting a straight line through the data. The responses were perfectly linear, and Appendix D contains the resulting calibration curves.

3. Datalogging

A Campbell Scientific, Inc. 21X datalogger in combination with a SM4M storage module and a 12V deep-cycle marine battery was employed at each monitoring site. A CE8 50mA current excitation module was also used at each site to control heating of the HD sensors. Figure 10 shows the 21X datalogger and CE8 current excitation module inside a weatherproof enclosure. To conserve energy and reduce battery drain, the datalogger was programmed to collect data once daily (at midnight) from all sensors. The datalogging software with which we programmed the 21X dataloggers for each site is shown in Appendix A. Data were retrieved to a portable PC through an SC32A optically isolated RS232 interface for direct connection to the 21X. An SC532 9-pin peripheral to RS232 interface was employed to retrieve data from the SM4M storage modules. The Campbell Scientific Inc. PC208W software program was employed for all data retrievals.

4. Laboratory hydraulic property analyses of cores at sensor locations

The cores collected from the field sites in their 6-in aluminum liners were immediately capped with plastic cups at their two ends and further wrapped in plastic wrap and an additional heat-sealable wrap by USGS personnel to minimize moisture loss. The cores from the AT-HD sensor locations were sent to the USGS Soil and Rock Properties Laboratory for determination of physical properties. These cores were analyzed for the following items: bulk density, porosity, particle size distribution, gravimetric moisture content at field sampling, particle density, thermal properties, and moisture retention from pressure plate extractors and relative humidity equilibration techniques at the following gas pressures (in bars): 0, 0.03, 0.08, 0.20, 0.49, 0.98, 4.90, and 663.0. Unsaturated hydraulic conductivity values for some of those cores, using the centrifuge method, were planned but were not available during the writing of this report.

5. Retention curve and unsaturated hydraulic conductivity function fitting

Accurate in-situ measurement of the unsaturated hydraulic conductivity has remained especially cumbersome and time-consuming (van Genuchten et al., 1998). One alternative to direct measurement of the unsaturated hydraulic conductivity is to use theoretical methods, which predict the conductivity from more easily measured soil-water retention data. Methods of this type are generally based on statistical pore-size distribution models, a large number of which have appeared in the soil science and petroleum engineering literature during the past several decades (see Mualem, 1986 for a review). Implementation of these predictive conductivity models still requires independently measured soil-water retention data.

Water flow in variably saturated soils is traditionally described with the Richards equation:

$$C(h)\frac{\partial h}{\partial t} = \frac{\partial}{\partial z}\left(K(h)\frac{\partial h}{\partial z} - K(h) \right), \qquad (1)$$

where h is the pore-water pressure head (with dimension L), t is time (T), z is soil depth (L), $K(h)$ is the hydraulic conductivity function (LT^{-1}), and $C(h)$ is the soil-water capacity function (L^{-1}), approximated by the slope $(d\theta / dh)$ of the soil-water retention curve, $\theta(h)$,

in which θ is the volumetric water content (L^3L^{-3}). The solution of the Richards equation requires knowledge of the unsaturated soil hydraulic functions $\theta(h)$ and $K(h)$ or $K(\theta)$.

The RETC (RETention Curve) computer program (van Genuchten et al., 1991) for describing the hydraulic properties of unsaturated soils (publically available at http://www.ussl.ars.usda.gov/MODELS/retc.html) uses the parametric models of Brooks-Corey (1964) and van Genuchten (1980) to represent the soil water retention curve, and the theoretical pore-size distribution models of Mualem (1976) and Burdine (1953) to predict the unsaturated hydraulic conductivity function from observed soil water retention data.

The van Genuchten parametric model is a continuously differentiable (smooth) equation with attractive properties:

$$S_e = \frac{\theta - \theta_r}{\theta_s - \theta_r} = \left[1 + (\alpha h)^n\right]^{-m}, \tag{2}$$

where n and m are empirical constants affecting the shape of the retention curve. S_e is the effective degree of saturation, also called the reduced water content $(0 \le S_e \le 1)$; θ_r and θ_s are the residual and saturated water contents, respectively; and α is an empirical parameter (L^{-1}) whose inverse is often referred to as the *air entry value* or *bubbling pressure*. For notational convenience, h and α are taken positive for unsaturated soils (i.e., h denotes suction). Van Genuchten et al. (1991) found that $m = 1 - 1/n$ seems to perform best for many soils.

The model of Mualem (1976) for predicting the relative hydraulic conductivity, K, can be written, in the simpler case where $m = 1 - 1/n$, as:

$$K(S_e) = K_s S_e^l \left[1 - \left(1 - S_e^{1/m}\right)^m\right]^2, \tag{3}$$

or in terms of the pressure head:

$$K(h) = \frac{K_s \left\{1 - (\alpha h)^{mn}\left[1 + (\alpha h)^n\right]^{-m}\right\}^2}{\left[1 + (\alpha h)^n\right]^{ml}}, \tag{4}$$

where K_s is the hydraulic conductivity at saturation, and l is a pore-connectivity parameter estimated by Mualem [1976] to be about 0.5 as an average for many soils.

RETC uses a nonlinear least-squares optimization approach to estimate the unknown model parameters from observed retention and/or hydraulic conductivity or diffusivity data. The aim of the curve-fitting process is to find an equation that maximizes the sum of squares associated with the model, while minimizing the residual sum of squares, SSQ (Van Genuchten et al., 1998). The residual sum of squares reflects the degree of bias (lack of fit) and the contribution of random errors. Referring to SSQ as the objective function $O(\tilde{b})$, in which $\tilde{b}$ represents the unknown parameter vector, RETC minimizes $O(\tilde{b})$ iteratively by means of a weighted, least-squares approach based on Marquardt's maximum neighborhood method (Marquardt, 1963). In our case, the parameter vector $\tilde{b}$ included only the parameters α and n. The saturated and residual water contents were determined in the USGS Soil and Rock Properties Laboratory (the water content corresponding to a relative humidity oven measurement equivalent to –663 bars was considered residual water content), as did the saturated hydraulic conductivities. However, in order to check the results of the optimization procedure on some of the experimentally determined parameters, the saturated and residual water contents were also treated as fitted parameters, both of which matched exceptionally well.

6. Unsaturated zone Darcian methodology for recharge estimation

Measurements below the plant root zone, using principles of soil physics, can be used to estimate recharge. Recharge is water reaching the ground water. It is measured as a flux, which is a volume of water per unit area per unit time, usually reported as mm/year. Deep drainage is the term more commonly used by soil physicists. This is defined as the downward flux of water below the depth to which plants extract water (the plant root zone). Provided there are no other sinks for water below the root zone, the deep drainage should be equal to recharge. This will be true when hydrological conditions are such that a steady state has been reached so that the deep drainage and recharge are constant with time. Under conditions of changing deep drainage and recharge, however, the deep drainage flux measured just beneath the root zone is unlikely

to be equal to the recharge to the groundwater at some (often considerably) deeper depth at that time. The deep drainage flux measured just beneath the root zone should, therefore, be considered as potential recharge. It will eventually reach the groundwater and become recharge, after a delay determined by the magnitude of the flux, the water storage capacity of the strata above the groundwater, and the depth to the groundwater (Bond, 1998).

Flow in unsaturated soils is governed by Darcy-Buckingham equation. This equation for one-dimensional, vertical unsaturated soil water flow can be written as:

$$q = -K(\theta)\frac{dH}{dz} \cong -K(\theta)\frac{\Delta H}{\Delta z} = -K(\theta)\frac{\Delta[h(\theta)+z]}{\Delta z} = -K(\theta)\left[\frac{\Delta h(\theta)}{\Delta z}+1\right], \quad (5)$$

where $H\ (=h+z)$ represents the hydraulic head, θ represents water content, z is the elevation head (the direction of the vertical z-axis is taken positive upwards), and $K(\theta)$, $h(\theta)$ indicate that hydraulic conductivity, K, and pore water pressure head or suction, h, are both dependent on water content. Equation (5) can be used to calculate soil-water flux at any instant in time or while the flow is steady state—that is, while the water content is not changing with time. When soil-water flow is not steady, Eq. (5) is combined with the law of conservation of mass (in this case, water) to derive the equation commonly used to model soil water flow, known as the *Richards Equation,* Eq. (1).

Use of Darcian methods to determine the deep drainage flux requires measurements to be made at a depth below the bottom of the root zone, so that the flux represents water that will eventually reach the groundwater as recharge (Sophocleous and Perry, 1985; 1987). Unless measured immediately above the water table, however, the value does not represent recharge at the time of measurement, but rather recharge that will occur at some later time depending on the travel time to the groundwater (Bond, 1998). When applied, these methods yield the drainage flux at specific instants in time. If sufficient measurements are made relative to the rate of change of the drainage flux, then these can be integrated over time to determine the cumulative drainage for the desired period (Rose and Stern, 1965).

The application of the Darcy's Law method to measure the deep drainage flux requires the simultaneous determination of hydraulic conductivity, $K(\theta)$ or $K(h)$, and hydraulic gradient, $\Delta H / \Delta z = \Delta[h(\theta) + z] / \Delta z$, at some depth below the root zone. The hydraulic gradient is measured by placing tensiometers and/or heat dissipation (HD) sensors above and below the chosen depth. The accuracy of the gradient measurements is determined by the accuracy of the method used to measure soil-water suction in the employed sensors, the vertical distance between the two sensors, and the magnitude of the hydraulic gradient.

The greatest uncertainty in the application of Darcian methods is associated with the value of the hydraulic conductivity. Hydraulic conductivity changes as water content (θ) and soil-water suction (h) change. Therefore, to obtain the value of hydraulic conductivity for calculating drainage flux from this method, the $K(\theta)$ or $K(h)$ relationship appropriate for the depth and location where the hydraulic gradient measurements were made is required. A measurement of θ or h at the mid-depth between the two tensiometers or HD sensors used to determine the hydraulic gradient is often used to obtain the value of K, or the average of the hydraulic conductivity values at the two sensor locations is often employed to be used in the flux calculation. The $K(\theta)$ and $K(h)$ relationships are usually very steep—that is, a small change in θ or h produces a large change in K (refer to Figs. 23–25 later on). This introduces a major source of uncertainty—namely, that associated with interpolating K from the $K(\theta)$ or $K(h)$ relationship; a small uncertainty in θ or h translates to a large uncertainty in K.

In the case of stratified, layered systems (rather than single, unstratified ones), the hydraulic conductivity, K, of each of the soil/sediment layers of the stratified system is different because of the various types of soil/sediment. Besides, the K perpendicular to the stratified layers or bedding planes is different from that parallel to the stratification. It is therefore necessary to determine a weighted K for the compound, stratified sediment system.

Consider the layered, water-saturated formation shown in Fig. 11. Each layer is homogeneous and isotropic with hydraulic conductivity values K_1, K_2,..., K_n. Consider flow perpendicular to the layering. The specific discharge q must be the same entering the system as it is leaving; in fact, it must be constant throughout the system. Let Δh_1 be the head loss across the first layer, Δh_2 across the second layer, and so on. The total head loss is then $\Delta h = \Delta h_1 + \Delta h_2 + \cdots + \Delta h_n$, and from Darcy's law,

$$q = \frac{K_1 \Delta h_1}{d_1} = \frac{K_2 \Delta h_2}{d_2} = \ldots = \frac{K_n \Delta h_n}{d_n} = \frac{K_z \Delta h}{d}, \tag{6}$$

where K_z is an equivalent vertical hydraulic conductivity for the system of layers, d_i is the thickness of each layer i, where $i = 1, 2, \ldots n$, and d is the total thickness of the layered formation. Solving the outside relationship of Eq. (6) for K_z and using the inside relationships for Δh_1, Δh_2,..., leads to (Freeze and Cherry, 1979):

$$K_z = \frac{d}{\sum_{i=1}^{n} d_i / K_i}, \tag{7}$$

which represents the harmonic average hydraulic conductivity of a system of layers in series. For unsaturated, layered systems, the corresponding equations are similar but more complex (Bear et al., 1968).

In order to estimate Darcian water fluxes, it is preferable to install the ATs and HD sensors close together near the water table, from which recharging gradients could be more accurately determined. However, in order to gain a better understanding of the entire vadose system, it was decided to install the few available sensors at shallow, intermediate, and deep depths.

IV. Drilling, Installation, and Completion

1. Drilling

As Hammermeister et al. (1985) emphasized, investigators studying both saturated and unsaturated flow and transport phenomena in the field often need borehole

geologic samples that have physical and chemical properties representative of the formation rock. In addition, these same investigators often require that the formation rock be relatively undisturbed by drilling and coring activities, so that in-situ borehole testing can be initiated under ambient conditions. In practice, it is impossible to obtain completely undisturbed geologic samples (core and cuttings) or to drill a borehole without disturbing the surrounding formation rock. Therefore, the goal of most investigators has been to minimize the disturbance of both geologic samples and formation rock.

Standard rotary-drilling and rotary-coring methods utilizing polymer mud or air foam as drilling fluids have been used successfully to drill difficult-to-drill rock types. Polymer mud or air foam help stabilize the walls of holes, prevent lost circulation, cool and lubricate the bit, and efficiently remove cuttings from the hole. Unfortunately they also contain varying proportions of water; therefore, they may significantly alter the water content of geologic samples, as well as formation rock, and impact its water quality (Hammermeister et al., 1985).

After careful consideration of a variety of methods, the USGS Odex 115 drilling system was selected for drilling the boreholes. This method was developed in Sweden for drilling through and casing off unconsolidated overburden, such as glacial till overlying bedrock. This method drills and advances casing equally well through unconsolidated deposits and consolidated bedrock (Hammermeister et al., 1985).

The Odex 115 method used a downhole percussion hammer to drill and ream at the bottom of a casing. A pilot bit, in conjunction with an eccentric reamer, drills a hole slightly larger than the outside diameter of the casing (Fig. 12). The percussion hammer also impacts on the casing through a shoe attached to the bottom joint of the casing. Thus the casing is advanced downward as the hole is drilled deeper. Drill cuttings are returned to the surface through the inside of the casing, thereby minimizing the disturbance of borehole walls with drilling fluids. Drill cuttings were collected for every foot depth

drilled for field identification and later textural and chemical analyses in the lab. Figure 13 shows the Odex drill rig in the field.

For core collection, the USGS Odex 115 system was used to drill and drive the casing down to the desired depth for coring. The drill rod assembly was then pulled out and a coring assembly was inserted. Core was then collected using a 10-cm (4-in) diameter, 0.6-m (2-ft) long core barrel with a 0.15-m (1/2-ft) shoe. (Four, 15-cm {6-in}-long aluminum liners can be inserted in the core barrel.)

2. Installation/Completion

The Odex 115 drilling system advanced a steel casing with an outside diameter of 20.3- cm (8-in) into the entire depth of the drill hole. Upon drilling completion, a 5-cm (2-in), schedule-40, PVC observation well with a 3-m (10-ft) screen (0.254 mm {0.010 in} slot) at the bottom was installed and sand-packed up to well above the top of the well screen; then granular bentonite was poured in up to near the depth of the selected deepest AT installation. The Odex steel casing was gradually lifted approximately 3 m (10 ft) above the zone to be instrumented. Instruments were installed and packing material was added up to the bottom of the casing, and the process was repeated as needed. Depth measurements were periodically done to check for possible hole caving, and correct depth locations.

The 31.75 mm (1-1/4 in), schedule-80 PVC casing that was permanently connected to the AT system —consisting of the porous cup epoxied into a specially machined PVC water-reservoir adapter, which in turn was epoxied to the bottom of the PVC casing —formed the base on which all other sensors (HDs , suction lysimeters, and gas tubes) were attached at a predetermined spacing. (The PVC casing was equipped with O-ring screw joints.) As a general rule, the HDs were attached within 0.3 m (1 ft) of the AT porous ceramic. (To protect the fragile ceramic of the HD sensor, it was first covered with a silica-flour slurry and wrapped in wet cheese cloth.) Figure 14 shows the AT permanently installed casing and the attached HD sensor approximately 0.3 m (1 ft) above the AT porous ceramic cup. An approximately 0.6-m (2-ft)-thick silica sand layer

was first put on top of the granular bentonite, followed by an approximately 0.6-m (2-ft)-thick dry silica flour layer, in which the AT porous cup and the HD sensor were embedded. To confirm that the AT and HD sensors were covered with silica flour, a thin layer of white, very fine sand ("sugar-powder" sand) was added on top of the silica flour, and subsequently sounding it to confirm that the depths measured were those expected. For the rationale and consequences of using dry fill-in materials in the borehole, the reader is referred to the next section (V.4). A 0.6-m (2-ft) silica sand layer usually was separating the suction lysimeter from the underlying silica flour. The suction lysimeter was also embedded in approximately 0.46-m (1.5-ft) of silica flour, followed by another silica sand layer. If a gas-sampling port followed, that was embedded in coarse sand followed by granular bentonite until the next level of AT-HD sensor system installation.

In each drilled hole, three AT assemblies at shallow, intermediate, and deep depths were installed, resulting in three 3.2-cm (1-1/4-in) PVC pipes, one 5-cm (2-in) observation well pipe, and several copper tubings (for the gas samplers) and polyethylene tubings (for the suction lysimeters) protruding at the surface. The well completion for each borehole is shown in Figs. 15–17, which also display the number and location of the various sensors installed in each site. The filled borehole and instrumentation were enclosed in a 20.3-cm (8-in) diameter steel outer casing set in concrete, over which a housing platform, designed and built at the KGS, was installed. An insulated fiberglass cover was installed over the platform to protect it from weather elements. Figure 18 shows the housing platform. The three protruding pipes with the side tubes (filled with drierite) are the three AT units; the reel with the yellow cable is connected to the water-level pressure transducer; underneath the reel is the datalogger unit (not visible in the picture). The battery housing unit is visible underneath the platform, and the fiberglass cover is on the ground of Site 2. Figure 19 shows the fiberglass cover over the platform. The battery housing is also visible.

V. Results and Discussion

1. 2000-2001 local climate

The average daily air temperatures in Garden City and Elkhart during the 2000 and 2001 calendar years are shown in Figs. 20 and 21, respectively. All weather data were obtained from the Weather Data Library, Kansas State University. Note the high air temperatures during July and August, and the abnormally low air temperatures starting from November 6 onwards, as well as the cold spells of September 23–25, and October 5–9. Figure 20 also displays the daily potential evapotranspiration in Garden City, using a modified Penman equation (Mary Knapp, State Climatologist, e-mail communication, Feb. 2001). Potential evapotranspiration totaled 1,936 mm (76.23 inches) in Garden City for calendar year 2000, and 2,008 mm (79.06 inches) for 2001.

The daily precipitation values for Elkhart and Garden City during calendar years 2000 and 2001 are shown in Figs. 21 and 22, respectively. The total 2000 precipitation for Elkhart and Garden City were 543 mm (21.37 in) and 470 mm (18.52 in), respectively. The average daily station barometric pressure for Garden City is also shown in Fig. 22. The average barometric pressure did not fluctuate very much around the 68.6 cm (27 inches)-of-mercury mark.

2. Site lithology

The drilled cuttings were blown out of the drilled hole by the Odex system and collected into 18.9-L (5-gal) plastic buckets. One drilled foot depth increment from the 20.3-cm (8-in) diameter hole usually filled up the bucket, from which a sub-sample was taken with a scoop into plastic bags for further analysis. The samples were quickly described in the field by hand-feel, visual inspection, and using dilute HCL acid to check for presence of carbonates.

The lithologic log for each site is graphically presented in Figs. 15–17. Because of the large size of each incremental foot sample, the sub-samples taken for later textural analysis may be different from the bucket sample described on site. Site CAL-121 was

the "sandiest" of all sites, with the most clayey sample detected only in the 41.4–42.7 m (136–140 ft) depth interval. Site CAL-122 was the most clayey of all sites. In fact, the clay encountered beyond the 45.7-m (150-ft) depth was so "heavy" (plastic) that the drill had difficulty penetrating through because of its sticking inside the casing, especially the plastic blue clay beyond the depth of 49.4 m (162 ft). Finally, after reaching the 67 m (220 ft) depth, still in blue clay, the decision was made to cease further drilling and complete an observation well on top of this deep clay layer. The grassland site, CNG, was the "siltiest" of all sites, with the greatest variety of reddish and yellowish colorations, and with gravel that occasionally was much different from the other two sites in that it was non-granitic, black, and most probably of volcanic origin. All sites included appreciable amounts of gravel, predominantly quartzitic, as well as significant numbers of caliche nodules.

3. Unsaturated hydraulic property fitting on laboratory analyses of collected cores at sensor locations

At each site, three AT sensors (and three or two HD sensors) were installed at three levels of the unsaturated zone: shallow, intermediate, and deep. Cores were collected at each one of these locations and were sent to the USGS lab in Sacramento, California for saturated hydraulic conductivity and retention curve analyses, among others. These data were entered into the RETC program to predict the unsaturated hydraulic conductivity function from observed soil-water retention data. The fitted water characteristic and unsaturated hydraulic conductivity functions for two depth levels at which the hydraulic gradients were calculated for each site are shown graphically in Figures 23-25. The R^2 statistic for regression of observed vs. fitted values for the retention data was generally better than 98% for all sites. The fitted parameters for the cores corresponding to sensor locations at each site are shown in Table 1.

Table 1. Fitted van Genuchten parameters for sampled cores at sensor locations for all sites.

Site	Depth interval, m (ft)	K-sat[1] (cm/day)	θ^{1}_{s} (dim.)	θ^{1}_{r} (dim.)	Parameter[2]			
					α (cm^{-1})	std error	n	std error
1	20.1 – 20.3 (66 – 66.5)	100	0.3480	0.0280	0.0637	0.0093	1.5410	0.0426
	35.4 – 35.5 (116 – 116.5)	64	0.3240	0.0100	0.3352	0.0684	1.337	0.0195
2	9.9 – 10.1 (32.5 – 33)	9.8	0.4450	0.0300	0.0193	0.0045	1.4139	0.0513
	22.1 – 23.8 (72.5 – 78)	160.3	0.2110	0.0210	0.2020	0.0990	1.4226	0.0723
	35.4 – 35.5 (116 – 116.5)	0.035[3]	0.3460	0.0300	0.2238	0.0676	1.3570	0.0342
3	23.6 – 23.8 (77.5 – 78)	0.1	0.4600	0.0370	0.0207	0.0048	1.2969	0.0305
	41.5 – 41.6 (136 – 136.5)	124.4	0.3880	0.0290	0.0245	0.0057	1.7487	0.1379

[1] Core saturated hydraulic conductivity (K-sat), saturated water content (θ_s), and residual (θ_r) water content (taken as the water content corresponding to the gas pressure of 663 bars in the water retention curve) determined in the laboratory by the USGS.

[2] $m = (1 - 1/n)$; $l = 0.5$

[3] This value, as explained in note 4 of Table 4, is suspect. A more representative value for that depth is considered to be the value indicated for depth 22.1-23.8 m above.

4. Measured time series of matric potentials, sediment temperatures, and water-table levels

a. Pore-water pressure head

The soil-water pressure head or matric-potential sensors, consisting of advanced tensiometers (AT) and heat dissipation (HD) sensors, were spaced approximately 0.3 m (1 ft) apart, with the AT at the lower end of the spaced interval. At all sites, sensors installed at the deepest depths, ranging from 35.7 m (117 ft; Sites 1 and 2) to 42 m (138 ft; Site 3) are labeled with the suffix 1; those installed at intermediate depths, ranging from 20.4 m (67 ft; Site 1) to 23.5–23.8 m (77–78 ft; Sites 2 and 3, respectively), are labeled with the suffix 2; and those installed at the shallow depths, ranging from 6.7 m (22 ft; Site 1) to 9.8–11 m (32–36 ft; Sites 2 and 3, respectively), are labeled with the suffix 3.

The time series of soil-water pressure head (matric-potential or suction) for HD matric-potential sensors for all sites since measurements were initiated are shown in Figures 26–28. The HD sensors took at least 2 to 3 months (from their installation on March 25, 2000, for Site 1; April 3, 2000, for Site 2; and April 10, 2000, for Site 3) to equilibrate with the surrounding soil. A major contributing factor to this delayed equilibration was the dry silica flour filling in the 20.3-cm (8-inch) borehole at the depth intervals in which the sensors were embedded (the native soil moisture content was also relatively very low). Dry materials were used to backfill the borehole to avoid introducing extraneous fluids in the borehole that might alter soil-water chemistry. However, after this relatively long equilibration time, the matric-potential is relatively stable. Only the shallowest HD sensor from Site 1 (HDS3 at 6.4 m {21 ft}) failed to stabilize at a constant matric potential and instead showed fluctuations, which probably indicate a leakage problem from the nearby AT ceramic cup assembly.

The matric-potential time series based on the ATs are also shown in Figures 26–28. We encountered several problems with these sensors. At Site 1, the AT3 unit malfunctioned after just a few months of operation during late spring of 2000, and resumed operating from the spring of the following year (2001). The abrupt lowering of the AT3 readings (in absolute value) during June 2001 is due to the servicing of the AT. Units AT1 and AT2 seemed to have operated satisfactorily after a relatively long time of questionable, low (near zero) readings. At Site 2, units AT2 and 3 displayed questionable near-zero readings for a significant period of time. The abrupt lowering of the AT2 readings during November and December 2000, and March and June 2001 are due to servicing of the tensiometer. The AT3 seemed to be operating satisfactorily only from March 2001 onwards. Unit AT1, after a long period of questionable readings, seemed to be operating satisfactorily near the end of the 2000 year and continuing in 2001, although with appreciable noise. Site 3 was so dry, that the matric potentials were generally beyond the range of the ATs. We tested all ATs for mechanical integrity by removing the pressure transducer assembly, inserting the lower end with the pressure transducer and rubber stopper into a specially machined PVC tube sealed at the other end, and applying a known vacuum, usually 0.6 bars at the other end of the assembly

(polyethylene tubing) through a vacuum pump, to check if the assembly could hold and maintain vacuum. All ATs passed this test except AT2 of Site 3 that we pronounced defective. For the particular depths at Sites 1 and 2, where the matric potentials are within the tensiometer range, the ATs are within 0.11 to 0.15 bars of the HD sensor readings. This may be considered satisfactory, given the different operation principles and sensing ranges of the ATs and HD sensors. Despite the extra care we took in constructing, testing, checking, and servicing the ATs, their performance was too often problematic and not satisfactory.

b. Sediment temperatures

The sediment temperatures from the HD sensors are shown for each site in Figures 29 – 31. The 21X datalogger's reference temperature in the instrument panel at the surface is also shown. The deeper temperatures were stable with time as expected. It is interesting to see the penetration of the annual temperature wave (shown in Figs. 29 and 30) down to the shallow (6.4 m; 21-ft) temperature sensor at Site 1, and in a much more subdued fashion to the shallowest (9.4-m; 31-ft) temperature sensor at Site 2. This was initially surprising, as we were not expecting the annual temperature wave to penetrate that deep in the sediments. We were, however, fortunate to have the USGS analyze some of the collected cores for thermal properties.

The transient heat-flow equation for the simple case where the thermal conductivity, λ [$W/(m\ C)$] is constant, can be written in the familiar form:

$$\partial T/\partial t = \kappa\, \partial^2 T/\partial^2 z, \qquad (8)$$

where T is soil temperature [C], t is time [s], z is depth [m], $\kappa = \lambda / C_v$ is the soil thermal diffusivity [m^2/s], and C_v is the volumetric heat capacity [$J/(m^3 C)$]. According to Eq. (8), the location in the soil where temperature will change the fastest with time is the location where the change with depth of the temperature gradient is largest (Campbell and Norman, 1998). To understand, at least qualitatively, the spatial and temporal patterns in sediment temperature, it is instructive to look at a few simple analytical solutions to Eq. (8).

If the soil is assumed to be infinitely deep, with uniform thermal properties, and a surface temperature that varies sinusoidally according to the equation,

$$T(0,t) = Tavg + A(0)\sin\left[\omega(t - t_o)\right], \tag{9}$$

then the temperature at any depth and time is given by (Campbell and Norman, 1998):

$$T(z,t) = Tavg + A(0)\exp(-z/D)\sin\left[\omega(t - t_o) - z/D\right], \tag{10}$$

where t_o is a phase shift. $Tavg$ is the average temperature over a temperature cycle, $A(0)$ is the amplitude of the temperature fluctuations (half the difference between the minimum and maximum), and $\omega = 2\pi/\tau$ is the angular frequency, with τ being the period of the temperature fluctuations. For annual fluctuations, $\omega = 2\times10^{-7}\,s^{-1}$. The coefficient D in Eq. (10) is the soil damping depth, which determines how much the amplitude of the temperature variation is attenuated with depth, and is calculated as

$$D = \sqrt{2\kappa/\omega} \tag{11}$$

When $z = D$, the exponential in Eq. (10) has a value of 0.37, indicating that the amplitude of temperature fluctuations at that depth is 37% of the amplitude at the surface. At $z = 2D$, the amplitude is 0.14 $A(0)$, and at $z = 3D$ the amplitude is 0.05 $A(0)$. The damping depth therefore gives useful information about the depth to which temperature fluctuations penetrate into the soil. Even though the surface temperature is not exactly sinusoidal, the damping depth still gives a good idea of how deep diurnal and annual temperature fluctuations will penetrate (Campbell and Norman, 1998).

The thermal diffusivities of the sediments at sensor locations as determined from collected cores at sampled field moisture content by the USGS are presented in Table 2. The relatively high thermal diffusivities κ of the sediments from the three sites reflect the high quartz content in the sandy sediments encountered, and probably the relatively high bulk density of the sediments (Table 2). Here we calculate the annual damping depth for Site 1, which has the shallowest HD sensor (6.4 m; 21 ft) and exhibited the most pronounced temperature wave at that depth (Figure 29). Taking the measured κ value at a depth of 21 ft, $0.819\times10^{-6}m^2/s$, as representative, the damping depth using the annual wave angular frequency is:

$D = \sqrt{2\kappa/\omega} = \sqrt{2\times0.819\times10^{-6}m^2s^{-1}/2\times10^{-7}s^{-1}} = 2.86\ m = 9.39$ ft. Thus, at a depth

$z = 2D = 5.72m \approx 19$ ft, which is close to the HD sensor depth of 6.4 m (21 ft), the soil temperature amplitude would be 14% the annual wave amplitude at the surface. Thus, the temperature pattern at 6.4 m (21 ft) does seem plausible. At $z = 3D = 8.58m \approx 28$ ft, which is close to the shallow temperature sensor at Site 2 (9.75 m; 32 ft), the temperature amplitude would be 5% of the amplitude at the surface, which is close to what we observe at Site 2. In addition, the damping depth also affects the phase of the temperature wave as can be observed at Sites 1 and 2.

Another surprising item from Figs. 29–31 is the simultaneous, short-term drop in soil temperature at all monitored depths at all sites around September 24, 2000, October 7, 2000 and November 1, 2000, as well as a longer-term temperature drop beginning November 6, 2000. These relatively small soil-temperature depressions coincide with air temperature drops as can be seen from the instrument panel temperatures (Figs. 29–31) and air temperatures at nearby climatic stations (Figs. 20 and 21). It is possible that the reference (thermistor) temperature, measured inside the 21X datalogger, may have been affected by the sudden drops in air temperature observed at the sites, thus affecting the recorded temperatures.

c. Water level hydrographs

The observed water levels at the monitored sites are shown in Fig. 32. The surprising item here is that the water levels are nearly stable, with occasional, short-term depressions, most probably correlating with water-quality sampling that required evacuation of several casing volumes. However, Sites 1 and 2 are located in heavily irrigated areas and are surrounded by hundreds of irrigation wells; many sections in townships 26 and 27 south and ranges 32 and 31 west, in which Sites 1 and 2 are located, have four irrigation wells per section (Fig. 33). Monitored wells in the vicinity of Sites 1 and 2 show steadily declining water levels (Fig. 34), which raises the question of why our monitored sites did not show such declines? In order to answer this question, it is necessary to look at the nearby surrounding irrigation wells. Generally, these wells are more than 90 m (300 ft) deep (well 26S-32W-22ABB is 115.2-m {378-ft} deep, well 27S-32W-6CBB is 90.8-m {298-ft} deep, and well 27S-32W-19CCD is 121.9-m {400-

ft} deep) and are screened at the bottom. Depth to water level in this area is generally between 30 m (100 ft) and 60 m (200 ft). The general groundwater flow direction in the vicinity of the sites is southeastwards (Fig. 5).

Table 2. Thermal diffusivities and other properties of soil core samples at field moisture content (USGS lab analyses)

Site	Sample depth m (ft)	Bulk density (g/cm^3)	Volumetric Water Content (cm^3/cm^3)	Initial Saturation (%)	Sand (%)	Gravel (%)	Thermal Diffusivity (mm^2/s)
1(CAL-121)	6.4 (21)	1.60	0.085	0.21	74	5	0.819
	20.1 (66)	1.88	0.070	0.23	70	25	0.835
	35.4 (116)	1.83	0.081	0.24	87	9	0.576
2(CAL-122)	9.9 (32.5)	1.81	0.118	0.36	83	3	0.760
	23.6 (77.5)	1.76	0.090	0.33	87	11	0.794
	35.4 (116)	1.89			64	30	0.545
3(CNG)	11.4 (37.5)	1.69	0.167	0.44	60	2	0.999
	23.6 (77.5)	1.99	0.173*	0.73	59	7	0.957
	41.5 (136)	1.72	0.071	0.19	89	0	0.740

*This value seems high given that most of the sediment was relatively dry. The gravimetric water content for sample depth 23.3–23.5 m (76.5–77 ft), which has the same texture as that sample (sandy loam), was determined as 0.08.

The Ogallala Formation is difficult to distinguish from the undiffertiated Pleistocene deposits in this area. However, in log 15 (surface elevation, 888.3 m {2,914.5 ft}) in NW Sec. 12, T. 26 S., R. 33 W., near Sites 1 and 2, Latta (1944) distinguished the Ogallala Formation (from the undifferentiated Pleistocene deposits), starting from a depth of 97.8 m (321 ft) below land surface (see also the cross section in Fig. 2, as well as Fig. 4). Paleontologic age determination seems to be the most important tool in the differentiation of the Pleistocene from Pliocene deposits (Gutentag, 1963). The boreholes at Sites 1 (surface elevation, 873.6 m {2,866 ft}) and 2 (surface elevation, 862.9 m {2,831 ft}) are 52 m (171 ft) and 67 m (220 ft) deep, with well depths 52 m (170 ft) and 47.4 m (155.5 ft), respectively; thus, these wells most probably never reached the Ogallala Formation.

The massive clay from 45.7 m (150 ft) to beyond 67 m (220 ft) at Site 2, and the general occurrence of clay layers in the neighborhood of 61 m (200 ft) depth and beyond in the vicinity of Site 1 (based on examined drillers logs), clearly indicate locally confined conditions for the Ogallala aquifer proper in the area. The depths of the irrigation wells and their screen locations, as well as the water-level depths mentioned above, are evidence of the confined nature of the Ogallala Formation aquifer proper in the area. This explains why the monitored water levels at the sites showed no water level declines despite being surrounded by active irrigation wells: the irrigation wells were pumping from the deep portions of the Ogallala Formation, which is confined in the area by relatively thick clays, which in turn create perched-type water tables above the Ogallala aquifer proper. These perched-type water tables are probably the ones monitored at the sites, not the Ogallala aquifer water levels. (The sediment column between the Ogallala Formation proper and the perched-type water table is saturated.)

The grassland site in Morton County, Site 3, with no irrigation development in the vicinity, showed a relatively stable water-level hydrograph as expected (Fig. 32).

5. Estimated water fluxes reaching the water table and estimation uncertainties

a. Darcian recharge estimation

The gradient of the hydraulic head, $H(=h+z)$, is the driving force for the flow of fluids in porous media and, hence, for the recharging fluxes to the High Plains aquifer. Following equilibration of the heat-dissipation sensors with the surrounding native sediments, the deep-vadose-zone hydraulic-head gradients were remarkably constant throughout the 2000-2001 observation (Figs. 26–28) for all 3 sites. The direction of flow can be discerned from Eq. (5), where we see that, if $\Delta H / \Delta z > 0$, the flow will be downward (because the calculated flux, q, will be negative, opposite to the direction of the vertical z-axis, which is taken positive upwards as mentioned previously.) Conversely, if $\Delta H / \Delta z < 0$, the flow will be upward. This conclusion merely reiterates the main point of Darcy's law, that water flows down a gradient in hydraulic head (Hornberger et al., 1998). The measured hydraulic-head gradients for all sites (following equilibration of the HD sensors with the in-situ environment) are shown in Table 3.

Table 3. Measured hydraulic-head gradients and estimated water fluxes in deep, unsaturated High Plains sediments based on heat-dissipation sensors.

Site ID	Landuse	Depth interval m (ft)	Avg. hydraulic head gradient[1] (dimensionless)	Direction of flow	Estimated Darcian water fluxes[2] (mm/yr)
(1)	(2)	(3)	(4)	(5)	(6)
1(CAL-121)	irrigated cropland	20.1–35.4 (66–116)	1.013	downwards	3
2(CAL-122)	irrigated cropland	9.4–35.4 (31–116)	0.861	downwards	0.6–0.9[3]
3(CNG)	native grassland	23.5–41.8 (77–137)	0.467	downwards	0.1–0.3

[1] Hydraulic gradient based on late time (2001) data.

[2] Assuming arithmetic average of the two hydraulic conductivities at the end members of the depth interval shown in col. 3. See also Table 4 for K-sat values.

[3] See footnote 4 in Table 4 for this flux estimate.

Based on the fitted, unsaturated hydraulic-conductivity functions at the locations where the sensors were emplaced (Figs. 23–25; see the previous section *c*, and also Table 4), we can estimate the hydraulic conductivity at those locations from the measured matric potential from the HD sensors shown in Figs. 26–28. Table 4 shows the field-measured pore-water pressures using the HD sensors, as well as the corresponding saturated and unsaturated hydraulic conductivity values, which were determined as outlined previously in the methodology section.

Knowing the average hydraulic conductivity of the sediment column between the two HD sensors and the measured hydraulic-head gradient (Table 3), we can then calculate the downward water fluxes recharging the High Plains aquifer. Although this process sounds simple enough, it is fraught with large uncertainties because, among other things, the sediment column between the two sensors is heterogeneous with unknown hydraulic properties. Assuming the collected cores are representative of the in-situ conditions, we only know (or rather estimated) the hydraulic-conductivity function at the two end locations of the measured sediment column, while the hydraulic-conductivity functions and other hydraulic properties of the various heterogeneous sediments in the column between the sensor locations remain unknown. Therefore, given such

circumstances, we need to make additional approximations for the estimation of the recharging fluxes and bracket these estimates within appropriate limits.

Table 4. Sediment-water hydraulic properties at sensor locations for all sites

Site	Depth, m (ft)	K-sat[1] (cm/day)	Avg. Pore-water[2] pressure (cm H_2O)	K-unsat. (cm/day)	K-avg[3] (cm/day)
1	20.1–20.3 (66 – 66.5)	100	–230	1.55×10^{-3}	
					7.8×10^{-4}
	35.4–35.5 (116 – 116.5)	64	–250	7.93×10^{-6}	
2	9.9–10.1 (32.5 – 33)	9.8	–640	4.04×10^{-4}	
					{2.3×10^{-4} to 2.7×10^{-4}}
	35.4–35.5 (116 – 116.5)	(160.3)[4]	–280 to –220	(6.30×10^{-5} to 1.32×10^{-4})	
3	23.6–23.8 (77.5 – 78)	0.15	–1675 to –1500	4.71×10^{-7} to 6.37×10^{-7}	
					8.2×10^{-5} to 1.9×10^{-4}
	41.5–41.6 (136 – 136.5)	124.4	–870 to –700	1.64×10^{-4} to 3.85×10^{-4}	

[1] Average value of 4 to 7 saturated hydraulic conductivity determinations from sampled cores. These lab analyses were performed by the USGS.

[2] Field-measured values based on Heat Dissipation sensors.

[3] Averaged unsaturated hydraulic conductivity (K-avg) based on the two endpoint depth intervals, which are indicated in column 2.

[4]The saturated hydraulic conductivity (K-sat) value for this depth was measured in the USGS lab as 0.035 cm/day. Such value seems unreasonably low, given that the core and the sediments collected from that depth, as both described in the field, indicate medium to coarse sand and gravel. These collected sediments were subsequently texturally analyzed by the USGS and were characterized as sand. Given this uncertainty, the core from depth 23.5–23.8 m (77–78 ft), which is of the same texture as that of the core from the 35.4–35.7 m (116–117 ft) interval, is considered more representative of site conditions, thus the estimate in parentheses. Even if the value of 0.035 cm/day for K-sat is true, then the corresponding K-unsat for the average measured range of pore pressures for that depth (–280 to –220 cm) would be 1.56×10^{-8} cm/day to 3.12×10^{-8} cm/day, respectively, resulting in a K-avg value (for the two considered endpoint depth intervals indicated in col. 2) of 2.02×10^{-4} cm/day.

Assuming that the arithmetic average of the two, end-member, unsaturated hydraulic conductivities of the analyzed depth intervals (Tables 3 and 4), based on Figs. 23–25, is representative of the entire sediment column within that depth interval, the estimated recharging fluxes, based on Eq. (5), are shown in the last column of Table 3. These recharge estimates should probably be considered as upper limits because, if instead of the arithmetic average, the harmonic average of hydraulic conductivities (eq. 7) was employed in the Darcian flux calculation [Eq.(5)], the resulting flux would be significantly less. It is interesting to note that the hydraulic head gradients between the deepest HD sensor and the groundwater level at each site were approximately 0.75 for Sites 1 and 2, whereas for Site 3 was nearly zero. Also, it is worth pointing out that the hydraulic head between the measured locations is assumed to vary linearly with depth, so that a linear average hydraulic gradient was employed in eq (5).

In order to obtain an upper limit on groundwater recharge in the study region, consider the following hydrologic observations that were extracted from Sophocleous (1998). Average annual precipitation is approximately 483 mm (19 in). Average annual potential evapotranspiration or shallow lake evaporation is approximately 1,524 to 1,778 mm (60 to 70 in). Average annual runoff is approximately 2.5 mm (0.1 in). Depth to water table in the vicinity of the instrumented sites is generally greater than 45.7 m (150 ft), resulting in a relatively thick vadose zone. Reported amount of irrigation from groundwater in the southwest Kansas Groundwater Management District No. 3 (GMD3) for 1997, for example, was 2, 283,453 ML (1,851,225 acre-ft), irrigating a total area of 636,504 ha (1,572,818 acres). Given that the GMD3 area is 2,182,181 ha (5,392,229 acres or 8,425 square miles), the total amount of water withdrawals from the aquifer (assuming that approximately the whole GMD3 is underlain by the High Plains aquifer) is on the order of 100 mm/yr (4 in/yr). The rate of irrigation development increased significantly during the 1970's and early 1980's. Such rates of withdrawals in south-western Kansas during the last 50 years caused severe declines in water levels because they are much greater than the rate of recharge into the alluvial and High Plains aquifers. In fact, the Kansas Governor's Task Force on Water Resources estimated in its interim report (Dec. 1977) that in the GMD3 region, withdrawals approximated 18 times the

recharge, which was estimated at that time (1975) to be 7 mm/yr (0.29 in/yr) over the region. Thus, the order of magnitude of actual recharge in the High Plains aquifer of southwestern Kansas is definitely less that 100 mm/yr (4 in/yr), and most likely less than or equal to the aforementioned Task Force estimate.

b. Error analysis of estimated fluxes

Reliable field measurements can be achieved by using properly designed and calibrated field instrumentation in combination with careful field installation involving minimum soil disturbance and appropriate spacing. However, even if appropriate precautions are taken, the field researcher is faced with many difficulties in assuring the long-term accuracy of the instrumentation. Thus, the difficulties of accurately specifying the water flux at some location in the subsurface profile are considerable.

In order to determine the magnitude of the uncertainty involved in every experimental measurement, an error analysis similar to the ones performed by Gardner (1986), Hanks and Jacobs (1971), Fritton (1974), and Fluhler et al. (1976), among others, was carried out. If a calculated quantity F (in the present case, the Darcian water flux, q) is a function of several independent variables x_i, representing measured input data, that is $F = f(x_1, x_2, \ldots, x_n)$ and these input data are in error by $\pm\Delta x_1$, $\pm\Delta x_2$, ..., $\pm\Delta x_n$, respectively, then these errors will cause an error ΔF in the computed result F. Expanding the function f in a Taylor series, and neglecting all higher order terms, as the Δx_i's will be small quantities, one obtains (Doebelin, 1990):

$$f(x_1 \pm \Delta x_1,\ x_2 \pm \Delta x_2, \ldots,\ x_n \pm \Delta x_n) = f(x_1,\ x_2, \ldots,\ x_n) + \Delta x_1 \partial f / \partial x_1 + \Delta x_2 \partial f / \partial x_2 + \ldots + \Delta x_n \partial f / \partial x_n \quad (12)$$

The absolute error E_a is given by

$$E_a = |\Delta F| = \left|\Delta x_1 \frac{\partial f}{\partial x_1}\right| + \left|\Delta x_2 \frac{\partial f}{\partial x_2}\right| + \ldots \left|\Delta x_n \frac{\partial f}{\partial x_n}\right|, \quad (13)$$

where the absolute value signs are used to avoid possible reduction of the total error by negative signs of partial derivatives associated with positive Δx_i's, or vice versa. Thus,

the actual error ΔF will never exceed E_a as long as the Δx_i's do not exceed their estimated values. The form of Eq. (13) is useful because it indicates which variables (Δx_i's) exert the strongest influence on the accuracy of the overall result. The maximum error approach is different from the standard error approach (Beers, 1957; Bevington and Robinson, 1992), in which a statistical average of the errors Δx_i's likely to be present—usually the root-mean-square errors—is estimated.

Taking approximate measures of the uncertainty in the various parameters involved in calculating the water flux, Eq. (5), we can illustrate the practical usefulness of the maximum error approach. The results of this analysis are detailed in Table 5. For error analysis, it is necessary to arrive at an estimate of error (Δx_i) for each of the variables. These error estimates could be standard deviations, 95% confidence intervals, ranges, or other measures of error. In the present case, the absolute-error estimates employed here (column 4 of Table 5) were empirical estimates based on the instrumentation and experiments used for this study. The variable x_i exerting the greatest influence on the accuracy of the overall result is underlined in column 6 of the table for the example calculations shown there. In the present case, the uncertainty in the flux estimate (8×10^{-4} cm/day, col. 7 of Table 5) is at least equal or larger than the magnitude of the estimated water flux (7.9×10^{-4} cm/day, lower col. 1 of Table 5).

It should be noted that for this analysis no errors were assigned to the problem of measuring true field conditions caused by instrumentation emplacement and the resulting disturbance of the soil, field heterogeneities, annual heat-wave influences (Hanks and Tanner, 1972), data smoothing, departure of reality from theory, scaling issues, and other factors. Because the computed errors depend on the magnitude of the variables involved in the error analysis, representative data from some depth interval (20.1–35.4 m; 66–116 ft in the example shown in Table 5), where the time change in various physical properties is not pronounced, were chosen. *The purpose of this exercise is not to present a precise and detailed error analysis but to get a general feeling of the approximate maximum errors involved in this type of field calculation.*

Table 5. Maximum error analysis for pore-water flux parameters at Site 1[1]

Equation & magnitude of F (i.e., water flux, q)	x_i	magnitude of x_i	Approx. maximum abs. error Δx_i	$(\partial F / \partial x_i)\Delta x_i$	Contrib. to abs. error of term x_i	Total absolute error[2] (cm/day)	Total relative error (in %)
(1)	(2)	(3)	(4)	(5)	(6)	(7)	(8)
$q = -K(h)\frac{H_i - H_{i+1}}{\Delta z}$	$K(h)$	7.8×10^{-4} cm/day	7.8×10^{-4} cm/day	$\left[-\frac{H_i - H_{i+1}}{\Delta z}\right]\Delta K(h)$	7.9×10^{-4}		
	H_i	733 cm (h = -250 cm)	15 cm	$\left[-\frac{K(h)}{\Delta z}\right]\Delta H_i$	7.7×10^{-6}		
	H_{i+1}	2,277 cm (h = -230 cm)	15 cm	$\left[\frac{K(h)}{\Delta z}\right]\Delta H_{i+1}$	7.7×10^{-6}		
	Δz ($=z_i - z_{i+1}$)	-1,524 cm	15 cm	$K(h)\left[\frac{H_i - H_{i+1}}{(\Delta z)^2}\right]\Delta(\Delta z)$	3×10^{-7}		
$q = -7.9 \times 10^{-4}$ cm/day						8×10^{-4}	102

[1]Data from a depth interval 20.1–35.4 m (66–116 ft) from Site 1 during the year 2000 measurement period. See text for explanation of symbols.

[2] Sum of error components in col. (6).

Fluhler et al. (1976) investigated the relative errors of hydraulic conductivities determined from a transient drainage field experiment. They found that in the wet range of the hydraulic-conductivity function, errors are 20-30% of the K-value. In the drier range, where K-values are small (as in this case study), the relative errors may be >100%. One should not be discouraged by the error analysis shown above because any other field method to estimate water and other fluxes would most likely result in similar, if not greater, uncertainties (Fluhler et al., 1976). The maximum error analysis can be used as criterion for selecting the best field method from others available.

VI. Conclusions and Recommendations

Our major conclusions and recommendations are listed below:

1. The driving forces for fluids in the deep vadose zone of the High Plains aquifer were measured and displayed for the first time in Kansas during May 2000 to September 2001. During the observation time period, a stable, steady driving force for fluid movement was measured.

2. The HD sensors proved to be more reliable and robust sensors than the ATs in our particular implementation. The ATs, which were proven worthwhile in other studies, need more attention than the HD sensors.

3. Concern with water quality/water-contamination problems resulted in emplacing the sensors in dry silica flour and fine silica sand, instead of in a slurry of such materials. This resulted in relatively long equilibration times of sensors with the native environment.

4. A better design for water flux estimation near the water table, given the limited number of sensors employed in this study, would have been to place the pore-water pressure-head sensors closer together at depth (near the water table), instead of scattering them throughout the vadose-zone profile as shallow, intermediate and deep sensors. Such a design would have reduced, but not eliminated, the uncertainty of averaging hydraulic conductivities between sensors as well as the uncertainties in employing a linear gradient, and the assumption of steady-state conditions involved in Darcian-type flux estimations.

5. Despite the large uncertainties involved in estimating ground-water recharge to the High Plains aquifer, and the large heterogeneity characterizing this aquifer, the values of recharge estimated for the High Plains aquifer based on the three sites are probably representative of present-day recharge, although the reader is cautioned that we are dealing with only three sites. Even taking into consideration more than 100%

VI. Conclusions and Recommendations

1. Heat dissipation (HD) sensors appear to be a useful tool for measuring sediment matric potential in deep boreholes. Most HD sensors installed in this study functioned as expected and provided matric potential data with excellent precision (low noise). Heat dissipation sensors appear to be reliable and robust. We recommend them for use in future investigations requiring measurements of sediment matric potential. The only apparent disadvantage of HD sensors is the rather elaborate calibration procedure required in order to achieve accurate results.

2. The use of Advanced Tensiometers (AT) for measuring sediment matric potential met with limited success. This was due, in part, to the fact that some of the sediment matric potentials (as documented with HD sensors) approached or exceeded the theoretical lower limit for tensiometry. However, problems with AT operation and employed transducers also contributed to the lack of success. Additional development and testing of this instrument appears to be necessary before it can be used on a routine basis to provide reliable estimates of sediment matric potential in borehole investigations.

3. Time series of matric potential data obtained with the HD sensors showed that it took approximately 2 to 3 months for the dry backfill in the boreholes to reach hydraulic equilibrium with the adjacent sediment. It may be possible to reduce this equilibration time in future investigations by using a silica flour/silica sand slurry instead of dry material.

4. Time series of matric potential data obtained with most of the HD sensors showed that, following the 2- to 3-month equilibration period, sediment matric potentials remained constant throughout the remainder of the period of investigation. These data indicate steady-state water flow at the points of observation over the duration of the investigation. It must be realized, however, that these observations represent only snap-shots in space and time of water flow throughout the entire vadose zone.

Increased sampling density with depth and/or much longer monitoring periods would be necessary to confirm whether or not flow throughout the vadose zone below the root zone is proceeding at steady-state.

5. Darcian methodology was used to obtain estimates of recharge at all the three investigation sites. Estimated recharge rates for the irrigated land-use sites (Sites 1 and 2) were appreciably higher (3 mm/yr and 0.6-0.9 mm/yr, respectively) than the estimated recharge rate for the natural grassland site (Site 3; 0.1-0.3 mm/yr). In all cases the estimated annual recharge values were less than one percent of annual precipitation. Although the large uncertainty associated with these estimates and the small number of study sites precludes using these flux estimates alone to draw firm conclusions regarding present-day recharge in the region, the irrigated and natural grassland sites selected are representative of irrigated and grassland areas overlying the High Plains aquifer in southwestern Kansas.

6. The Darcian methodology employed in this investigation was applied over large depth intervals encompassing considerable vertical heterogeneity in sediment hydraulic properties. Large uncertainty in flux estimates resulted from the fact that the hydraulic properties for these large depth intervals were only partially characterized. Furthermore, the assumption of steady-state water flow, required in employing Darcian methodology, may be questionable over large depth intervals. We recommend that small depth intervals be used for applying Darcian flux methodology in future investigations.

7. Shallow wells completed near the water table do not usually tap the Ogallala Formation water levels as do most irrigation wells in the area but rather a water table of "perched-type" character on top of some lower permeability unit, although the entire underlying sediment column is saturated. As shown in Fig. 2, the Ogallala Formation top in the study area usually lies below the 60-m (200-ft) depth mark, and is locally confined by clayey layers of variable thickness. Therefore, extra care needs to be used in interpreting water-level and related data.

8. The Darcian-based water-flux estimation aspect of this High Plains aquifer program was a pilot study of recharge assessment. Despite the low performance of some state-of-the-art sensors, this study showed that deep-vadose-zone hydrology, a mostly unexplored frontier due to technological obstacles, can be monitored and analyzed. More instrumented sites, similar to the ones employed here (and taking advantage of the experience gained during this study), in combination with additional methodologies are needed to assess the deep vadose zone water (and chemical) fluxes reaching the High Plains aquifer.

Acknowledgments

The authors thank Kevin Dennehy and Peter McMahon of the USGS for their offer of collaboration on this study. The unsaturated zone study design and implementation was funded primarily by the USGS's National Water-Quality Assessment (NAWQA) Program High Plains Regional Groundwater Study without whom this study would not have been possible. The authors acknowledge the contributions of Kevin Dennehy and Peter McMahon, USGS, Denver, CO for securing the unsaturated zone study sites --the owners of which are also thanked for their permissions to use their land in this study-- and for developing and implementing the overall study design, and Kevin Ellett, USGS, Sacramento, CA for calibration of heat dissipation sensors and determination of sediment physical properties. These three USGS personnel shared their expertise and provided constructive reviews that improved this report. Joel Hubbell and Buck Sisson of the INEEL in Idaho Falls, ID, provided various AT components, and answered numerous questions regarding the AT sensors. They also provided review comments of an earlier version of this manuscript. Lee Allison, KGS Director, provided unscheduled seed money support for this project. Bill Hargrove, Director of the KCARE program at Kansas State University matched the KGS monetary contribution for this project. Bill Harrison, KGS Deputy Director, arranged for a visit to INEEL labs to meet with the inventors of Advanced Tensiometers (AT), and arranged for them to provide components of ATs for this study. He also provided continued encouragement for this project. Don Whittemore, KGS Geohydrology Section Chief, made limited section funds available for this project. Dave Young gamma logged one borehole in Finney County. Margaret Townsend and Al Macfarlane offered financial support from their unspent project funds and provided moral support. Jim Butler made one datalogger available for this project. Brett Bennett assisted with advice and assembly of electronic components. Sam Perkins assisted in assembling the ATs and also provided miscellaneous other assistance.

References

Bear, J., Zaslavsky, D., and Irmay, S., 1968. Physical principles of water percolation and seepage. Unesco, Paris, 465 p.

Beers, Yardley, 1957. Introduction to the Theory of Error. 2nd ed., Addison-Wesley, Cambridge, Mass., 65 p.

Bevington, P.R., and Robinson, D.K., 1992. Data Reduction and Error Analysis for the Physical Sciences. 2nd ed., McGraw Hill, New York, 328 p.

Bond, W., 1998. Soil Physical Methods for Estimating Recharge. In: Zhang, L. (ed.), The Basics of Recharge and Discharge, Part 3. CSIRO Publishing, Australia, 17 p.

Breyer, John, 1975. The classification of Ogallala sediments in western Nebraska, in Studies on Cenozoic paleontology and stratigraphy, Claude W. Hibbard Memorial, v. 3, Papers on Paleontology No. 12: Museum of Paleontology, University of Michigan, 1-8 p.

Brooks, R.H., and Corey, A.T., 1964. Hydraulic properties of porous media. Hydrology Paper No. 3, Colorado State Univ., Fort Collins, Colorado, 27 p.

Burdine, N.T., 1953. Relative permeability calculations from pore-size distribution data. Petrol. Trans. Am. Inst. Min. Eng., 198:71-77.

Campbell, G.S., Jungbauer, J.D. Jr., Bidlake, W.R., and Hungerford, R.D., 1994. Predicting the effect of temperature on soil thermal conductivity. Soil Sci., 158:307-313.

Campbell, G.L. and Norman, J.M., 1998. An Introduction to Environmental Biophysics. 2nd ed. Springer-Verlag, New York, 286 p.

Cassel, D.K., and Klute, A., 1986. Water potential: Tensiometry. In Methods of soil analysis, Part 1. Physical and Mineralogical Methods. In: A. Klute (ed.), Agronomy Monograph No. 9, 2nd Ed. American Society of Agronomy, Madison, WI, p. 563-596.

Coe, D.K., 1994. Southwest Kansas Groundwater Management District Groundwater Quality. Southwest Kansas Groundwater Management District, Garden City, KS, 19 p.

Dennehy, K.F., 2000. High Plains regional groundwater study. U.S. Geol. Survey Fact Sheet FS-091-00, 6 p.

Dickey, H.P., Swafford, W.R., and Markley, Q.L., 1963. Soil Survey of Morton County, Kansas. U.S. Dept. of Agric., Soil Conserv. Service, Series 1960, No. 8, 51 p.

Doebelin, E.O., 1990. Measurement Systems: Application and Design. 4th edition McGraw Hill, New York, 960 p.

Flint, A.L., Campbell, G.S., Bilskie, J., and Calissendorff, C., 2002. Calibration and temperature correction of heat dissipation matric potential sensors. Soil Sci. Amer. J., *in press*.

Fluhler, H., Ardakani, M.S., and Stolzy, L.H., 1976. Error propagation in determining hydraulic conductivities from successive water content and pressure head profiles. Soil Sci. Soc. Amer. J., 40:830-836.

Freeze, R.A., and Cherry, J.A., 1979. Groundwater. Prentice-Hall, Englewood Cliffs, NJ, 604 p.

Fritton, D.D., 1974. Evaluation of experimental procedures by error analysis. J. Agron. Educ., 3:43-48.

Gardner, W.H., 1986. Water Content. In: A. Klute (ed.), Methods of Soil Analysis, Part 1, 2nd ed., Agronomy Monographs 9, Madison, WI, p. 493-544.

Gutentag, E.D., 1963. Studies of the Pleistocene and Pliocene deposits in southwestern Kansas: Kansas Acad. Sci. Trans., 66(4): 606-621.

Gutentag, E.D., and Weeks, J.B., 1980. Water table in the High Plains aquifer in 1978 in parts of Colorado, Kansas, Nebraska, New Mexico, Oklahoma, South Dakota, Texas, and Wyoming: U.S. Geological Survey Hydrologic Investigations Atlas HA-642, scale 1:2,500,000, 1 sheet.

Gutentag, E.D., Lobmeyer, D.H., and Slagle, S.E., 1981. Geohydrology of southwestern Kansas: Kansas Geological Survey Irrigation Series 7, 73 p.

Gutentag, E.D., Heimes, F.J., Krothe, N.C., Luckey, R.R., and Weeks, J.B., 1984, Geohydrology of the High Plains aquifer in parts of Colorado, Kansas, Nebraska, New Mexico, Oklahoma, South Dakota, Texas, and Wyoming: U.S. Geological Survey Professional Paper 1400-B, 63 p.

Hammermeister, D.P., Blout, D.O., and McDaniel, J.C., 1985. Drilling and coring methods that minimize the disturbance of cuttings, core, and rock formation in the unsaturated zone, Yucca Mountain, Nevada. Conference on Characterization and

Monitoring of the Vadose (Unsaturated) Zone Proceedings, National Water Well Association, Denver, CO, p. 507-541.

Hanks, R.J., and Jacobs, H.S., 1971. Comparison of the colorimetric and flux meter measurements of soil heat flow. Soil Sci. Soc. Amer. Proc., 35:671-674.

Hanks, R.J., and Tanner, C.B., 1972. Colorimetric and flux meter measurements of soil heat flow. Soil Sci. Soc. Amer. Proc., 36:537-538.

Harner, R.F., Agell, R.C., Lobmeyer, M.A., and Jantz, D.R., 1965. Soil survey of Finney County, Kansas: U.S. Dept. Agriculture Soil Conserv. Service, ser. 1961, no. 30, 91 p.

Holdoway, Katrine, 1978. Deposition of evaporites and redbeds of the Nippewalla Group (Permian), western Kansas: Kansas Geological Survey Bulletin 215, 45 p.

Hornberger, G.M., Raffensperger, J.P., Wiberg, P.L., and Eshleman, K.N., 1998. Elements of Physical Hydrology. The Johns Hopkins Univ. Press, Baltimore, MD., 302 p.

Hubbell, J. M. and Sisson, J. B., 1996. Portable tensiometer use in deep boreholes. Soil Science, 161(6):376-381.

Hubbell, J.M., and Sisson, J.B., 1998. Advanced tensiometer for shallow or deep soil water potential measurements. Soil. Sci., 163:271-277.

Klute, A., and Peters, D.B., 1962. A recording tensiometer with a short response time. Soil Soc. Sci. Am. Proc., 26:87-88.

Latta, B.F., 1944. Geology and ground water resources of Finney and Gray Counties, Kansas: Kansas Geol. Survey Bull. 55, 272 p.

McGuire, V. L., and Sharpe, J. B., 1997. Water-level changes in the High Plains aquifer—predevelopment to 1995. U.S. Geological Survey, Water-Resources Investigations Report 97-4081.

McMahon, P.B., Dennehy, K.F., Ellett, K., Sophocleous, M.A., Paschke, R.L., Michel, R.L., and Hurlbut, D., 2002. Evaluation of recharge rates beneath grassland and irrigated fields in the central High Plains, southwestern Kansas, 2000-01. U.S. Geological Survey, Water-Resources Investigations Report, in preparation.

Marquardt, D.W., 1963. An algorithm for least-squares estimation of nonlinear parameters. J. Soc. Ind. Appl. Math. 11:431-441.

Merriam, D.F., and Frye, J.C., 1954. Additional studies of the Cenozoic of western Kansas. Kansas Geol. Survey Bull. 109, pt. 4, 16 p.

Mualem, Y., 1976. A new model for predicting the hydraulic conductivity of unsaturated porous media. Water Resour. Res., 12:513-522.

Mualem, Y., 1986. Hydraulic conductivity of unsaturated soils: Prediction and formulas. In A. Klute (ed.), Methods of Soil Analysis. Part 1. Physical and Mineralogical Methods. Agron. Monogr. 9, 2nd ed. American Society of Agronomy, Madison, Wisconsin, p. 799-823.

NAS (National Academy of Sciences), 1996. A New Era For Irrigation. National Academy Press, Washington, DC, 216 p.

Nyhan, J.W., and Drennon, B.J., 1990. Tensiometer data acquisition system for hydrologic studies requiring high temporal resolution. Soil Sci. Soc. Am. J., 54:293-296.

Ratzlaff, J. R., 1994. Timing and magnitude of changes in runoff for Kansas watersheds, 1940-1990. Transactions of the Kansas Academy of Science, 97(1-2): 26-35.

Reece, C.F., 1996. Evaluation of a line heat dissipation sensor for measuring soil matric potential. Soil Sci. Soc. Am. J., 60:1022-1028.

Rose, C.W., and Stern, W.R., 1965. The drainage component of the water balance equation. Aust. J. Soil Res., 3:95-100.

Sophocleous, M.A., and Perry, C.A., 1985. Experimental studies in natural groundwater recharge dynamics: The analysis of observed recharge events: Journal of Hydrology, 81(3/4):297-332.

Sophocleous, M.A., and Perry, C.A., 1987. Natural groundwater recharge instrumentation and computation at sites in south-central Kansas. U.S. Geological Survey, Water Resources Investigations Report 87-4097, 48 p.

Sophocleous, M.A. (ed.), 1998. Perspectives on Sustainable Development of Water Resources in Kansas. Kansas Geol. Survey, Bull. 239, 239 p.

Strebel, O., Renger, M., and Giesel, W., 1973. Soil-suction measurements for evaluation of vertical water flow at greater depths with a pressure transducer tensiometer. J. Hydrol., 18:367-370.

Stullken, L.E., Watts, K.R., and Lindgren, R.J., 1985. Geohydrology of the High Plains aquifer, Western Kansas. U.S. Geol. Surv., Water-Resourc. Inv. Rpt 85-4198, 86 p.

Trotter, C.M. 1984. Errors in reading tensiometer vacuum with pressure transducers. Soil Sci., 138:314-316.

U.S. Department of Agriculture, 1999. 1997 Census of Agriculture. Geographic Area Series, Vol. 1, CD-ROM set.

van Genuchten, M.Th., 1980. A closed-form equation for predicting the hydraulic conductivity of unsaturated soils. Soil Sc. Soc. Am. J., 44:892-898.

van Genuchten, M. Th., Leij, F.J., and Yates, S.R., 1991. The RETC Code for Quantifying the Hydraulic Functions of Unsaturated Soils, Version 1.0. EPA Report 600/2-91/065, U.S. Salinity Laboratory, USDA, ARS, Riverside, California, 85 p.

van Genuchten, M.Th., Simunek, J., Leij, F.J., and Sejna, M., 1998. RETC, Version 6.0: Code for Quantifying the Hydraulic Functions of Unsaturated Soils. Available at http://www.ussl.ars.usda.gov/MODELS/retc.html.

Watson, K.K., and Jackson, R.D., 1967. Temperature effects in a tensiometer-pressure transducer system. Soil Science Society of America Journal, 31: 156-160.

Williams, T., 1978. An automatic scanning and recording tensiometer system. J. Hydrol., 39:175-183.

APPENDIX A

Datalogging programs

```
;{21X} :S/N6953
;Program: HPA1 - 02/28/00 version for 3 tensiom. transds. (ATs), 3 HDPs,
& 1 WL transd.
;Modified 3/13/00; 5/11/00 (SITE 1 field test)
*Table 1 Program
  01: 3600          Execution Interval (seconds)

1:  If time is (P92)
 1: 0         Minutes into a
 2: 1440      Minute Interval
 3: 11        Set Flag 1 High

2:  Batt Voltage (P10)
 1: 18        Loc [ _________ ]

3:  Internal Temperature (P17)
 1: 5         Loc [ _________ ]

4:  If Flag/Input (P91)
 1: 11        Do if Flag 1 is High
 2: 30        Then Do

5:  Volt (Diff) (P2)   :1 WL transd.
 1: 1         Reps
 2: 5         5000 mV Slow Range
 3: 1         DIFF Channel
 4: 1         Loc [ _________ ] ;1
 5: 0.0715    Mult; XD4935
 6: -28.442   Offset

6:  Full Bridge (P6)   : AT1 tensiom.
 1: 1         Reps
 2: 2         15 mV Slow Range
 3: 2         DIFF Channel
 4: 1         Excite 1 plus reps
 5: 5000      mV Excitation
 6: 2         Loc [ _________ ] ;2
 7: -148.57   Mult ; ID38
 8: -107.14   Offset

7:  Full Bridge (P6)   : AT2 tensiom.
 1: 1         Reps
 2: 2         15 mV Slow Range
 3: 3         DIFF Channel
 4: 2         Excite 1 plus reps
 5: 5000      mV Excitation
 6: 3         Loc [ _________ ] ;3
 7: -147.87   Mult ; ID39
 8: -107.42   Offset

8:  Full Bridge (P6)   : AT3 tensiom.
 1: 1         Reps
 2: 2         15 mV Slow Range
 3: 4         DIFF Channel
 4: 3         Excite 1 plus reps
 5: 5000      mV Excitation
 6: 4         Loc [ _________ ] ;4
 7: -148.60   Mult ; ID40
 8: -105.34   Offset

9:  Thermocouple Temp (DIFF) (P14)
```

```
 1: 3         Reps
 2: 1         5 mV Slow Range
 3: 6         DIFF Channel
 4: 1         Type T (Copper-Constantan)
 5: 5         Ref Temp (Deg. C) Loc [ _________ ]
 6: 6         Loc [ _________ ] ;Tinit 6,7,8
 7: 1.0       Mult
 8: 0.0       Offset

10:  Set Port (P20)
 1: 1         Set High
 2: 1         Port Number

11:  Excitation with Delay (P22)
 1: 4         Ex Channel
 2: 0         Delay w/Ex (units = 0.01 sec)
 3: 100       Delay After Ex (units = 0.01 sec)
 4: 0         mV Excitation

12:  Thermocouple Temp (DIFF) (P14)
 1: 3         Reps
 2: 1         5 mV Slow Range
 3: 6         DIFF Channel
 4: 1         Type T (Copper-Constantan)
 5: 5         Ref Temp (Deg. C) Loc [ _________ ]
 6: 9         Loc [ _________ ] ;T(t=1s)9,10,11
 7: 1.0       Mult
 8: 0.0       Offset

13:  Excitation with Delay (P22)
 1: 4         Ex Channel
 2: 0         Delay w/Ex (units = 0.01 sec)
 3: 2000      Delay After Ex (units = 0.01 sec)
 4: 0         mV Excitation

14:  Thermocouple Temp (DIFF) (P14)
 1: 3         Reps
 2: 1         5 mV Slow Range
 3: 6         DIFF Channel
 4: 1         Type T (Copper-Constantan)
 5: 5         Ref Temp (Deg. C) Loc [ _________ ]
 6: 12        Loc [ _________ ] ;T(t=20s)12,13,14
 7: 1.0       Mult
 8: 0.0       Offset

15:  Set Port (P20)
 1: 0         Set Low
 2: 1         Port Number

16:  Beginning of Loop (P87)
 1: 0         Delay
 2: 3         Loop Count

17:  Z=X-Y (P35)
 1: 12     -- X Loc [ _________ ]
 2: 9      -- Y Loc [ _________ ]
 3: 15     -- Z Loc [ _________ ] ;15,16,17

18:  End (P95)

19:  Do (P86)
```

```
 1: 10       Set Output Flag High

20:  Real Time (P77)
 1: 0110     Day,Hour/Minute (midnight = 0000)

21:  Resolution (P78)
 1: 1        High Resolution

22:  Sample (P70)
 1: 1        Reps
 2: 1        Loc [ _________ ] ;1 WL xd

23:  Sample (P70)
 1: 3        Reps
 2: 2        Loc [ _________ ] ;2,3,4 ATs

24:  Resolution (P78)
 1: 0        Low Resolution

25:  Sample (P70)
 1: 4        Reps
 2: 5        Loc [ _________ ] ;5,6,7,8 Tref, Tinit123

26:  Sample (P70)
 1: 3        Reps
 2: 15       Loc [ _________ ] ;DT20-1 15,16,17

27:  Sample (P70)
 1: 1        Reps
 2: 18       Loc [ _________ ] ;Battery V

28:  End (P95)

29:  Serial Out (P96)
 1: 30       SM192/SM716/CSM1

30:  Do (P86)
 1: 21       Set Flag 1 Low
```

```
;{21X} :S/N1227
;Program: HPA1 - 02/28/00 version for 3 tensiom. transds. (ATs), 2 HDPs,
& 1 WL transd.
;Modified 3/13/00; 5/11/00 (SITE 2 field test)
*Table 1 Program
  01: 3600          Execution Interval (seconds)

1:  If time is (P92)
 1: 0         Minutes into a
 2: 1440      Minute Interval
 3: 11        Set Flag 1 High

2:  Batt Voltage (P10)
 1: 18        Loc [ _________ ]

3:  Internal Temperature (P17)
 1: 5         Loc [ _________ ]

4:  If Flag/Input (P91)
 1: 11        Do if Flag 1 is High
 2: 30        Then Do

5:  Volt (Diff) (P2)   :1 WL transd.
 1: 1         Reps
 2: 5         5000 mV Slow Range
 3: 1         DIFF Channel
 4: 1         Loc [ _________ ] ;1
 5: 0.1443    Mult ; XD705
 6: -58.277   Offset

6:  Full Bridge (P6)   : AT1 tensiom.
 1: 1         Reps
 2: 2         15 mV Slow Range
 3: 2         DIFF Channel
 4: 1         Excite 1 plus reps
 5: 5000      mV Excitation
 6: 2         Loc [ _________ ] ;2
 7: -149.63   Mult ; ID41
 8: -111.67   Offset

7:  Full Bridge (P6)   : AT2 tensiom.
 1: 1         Reps
 2: 2         15 mV Slow Range
 3: 3         DIFF Channel
 4: 2         Excite 1 plus reps
 5: 5000      mV Excitation
 6: 3         Loc [ _________ ] ;3
 7: -147.68   Mult ; ID42
 8: -105.83   Offset

8:  Full Bridge (P6)   : AT3 tensiom.
 1: 1         Reps
 2: 2         15 mV Slow Range
 3: 4         DIFF Channel
 4: 3         Excite 1 plus reps
 5: 5000      mV Excitation
 6: 4         Loc [ _________ ] ;4
 7: -148.81   Mult ; ID43
 8: -109.97   Offset

9:  Thermocouple Temp (DIFF) (P14)
```

```
 1: 2         Reps
 2: 1         5 mV Slow Range
 3: 6         DIFF Channel
 4: 1         Type T (Copper-Constantan)
 5: 5         Ref Temp (Deg. C) Loc [ _________ ]
 6: 6         Loc [ _________ ] ;Tinit 6,7,8
 7: 1.0       Mult
 8: 0.0       Offset

10:  Set Port (P20)
 1: 1         Set High
 2: 1         Port Number

11:  Excitation with Delay (P22)
 1: 4         Ex Channel
 2: 0         Delay w/Ex (units = 0.01 sec)
 3: 100       Delay After Ex (units = 0.01 sec)
 4: 0         mV Excitation

12:  Thermocouple Temp (DIFF) (P14)
 1: 2         Reps
 2: 1         5 mV Slow Range
 3: 6         DIFF Channel
 4: 1         Type T (Copper-Constantan)
 5: 5         Ref Temp (Deg. C) Loc [ _________ ]
 6: 9         Loc [ _________ ] ;T(t=1s)9,10,11
 7: 1.0       Mult
 8: 0.0       Offset

13:  Excitation with Delay (P22)
 1: 4         Ex Channel
 2: 0         Delay w/Ex (units = 0.01 sec)
 3: 2000      Delay After Ex (units = 0.01 sec)
 4: 0         mV Excitation

14:  Thermocouple Temp (DIFF) (P14)
 1: 2         Reps
 2: 1         5 mV Slow Range
 3: 6         DIFF Channel
 4: 1         Type T (Copper-Constantan)
 5: 5         Ref Temp (Deg. C) Loc [ _________ ]
 6: 12        Loc [ _________ ] ;T(t=20s)12,13,14
 7: 1.0       Mult
 8: 0.0       Offset

15:  Set Port (P20)
 1: 0         Set Low
 2: 1         Port Number

16:  Beginning of Loop (P87)
 1: 0         Delay
 2: 2         Loop Count

17:  Z=X-Y (P35)
 1: 12     -- X Loc [ _________ ]
 2: 9      -- Y Loc [ _________ ]
 3: 15     -- Z Loc [ _________ ] ;15,16,17

18:  End (P95)

19:  Do (P86)
```

```
 1: 10       Set Output Flag High

20:  Real Time (P77)
 1: 0110     Day,Hour/Minute (midnight = 0000)

21:  Resolution (P78)
 1: 1        High Resolution

22:  Sample (P70)
 1: 1        Reps
 2: 1        Loc [ _________ ] ;1 WL xd

23:  Sample (P70)
 1: 3        Reps
 2: 2        Loc [ _________ ] ;2,3,4 ATs

24:  Resolution (P78)
 1: 0        Low Resolution

25:  Sample (P70)
 1: 4        Reps
 2: 5        Loc [ _________ ] ;5,6,7,8 Tref, Tinit123

26:  Sample (P70)
 1: 3        Reps
 2: 15       Loc [ _________ ] ;DT20-1 15,16,17

27:  Sample (P70)
 1: 1        Reps
 2: 18       Loc [ _________ ] ;Battery V

28:  End (P95)

29:  Serial Out (P96)
 1: 30       SM192/SM716/CSM1

30:  Do (P86)
 1: 21       Set Flag 1 Low
```

```
;{21X} :S/N8279
;Program: HPA1 - 02/28/00 version for 3 tensiom. transds. (ATs), 2 HDPs,
& 1 WL transd.
;Modified 3/13/00; 5/11/00 (SITE 3 field test)

*Table 1 Program
  01: 3600          Execution Interval (seconds)

1:  If time is (P92)
 1: 0         Minutes into a
 2: 1440      Minute Interval
 3: 11        Set Flag 1 High

2:  Batt Voltage (P10)
 1: 18        Loc [ _________ ]

3:  Internal Temperature (P17)
 1: 5         Loc [ _________ ]

4:  If Flag/Input (P91)
 1: 11        Do if Flag 1 is High
 2: 30        Then Do

5:  Volt (Diff) (P2)   :1 WL transd.
 1: 1         Reps
 2: 5         5000 mV Slow Range
 3: 1         DIFF Channel
 4: 1         Loc [ _________ ] ;1
 5: 0.1423    Mult ; XD4658
 6: -56.538   Offset

6:  Full Bridge (P6)   : AT1 tensiom.
 1: 1         Reps
 2: 2         15 mV Slow Range
 3: 2         DIFF Channel
 4: 1         Excite 1 plus reps
 5: 5000      mV Excitation
 6: 2         Loc [ _________ ] ;2
 7: -147.87   Mult ; ID37
 8: -101.46   Offset

7:  Full Bridge (P6)   : AT2 tensiom.
 1: 1         Reps
 2: 2         15 mV Slow Range
 3: 3         DIFF Channel
 4: 2         Excite 1 plus reps
 5: 5000      mV Excitation
 6: 3         Loc [ _________ ] ;3
 7: -148.40   Mult ; ID44
 8: -107.52   Offset

8:  Full Bridge (P6)   : AT3 tensiom.
 1: 1         Reps
 2: 2         15 mV Slow Range
 3: 4         DIFF Channel
 4: 3         Excite 1 plus reps
 5: 5000      mV Excitation
 6: 4         Loc [ _________ ] ;4
 7: -148.38   Mult ; ID45
 8: -104.20   Offset
```

```
 9:  Thermocouple Temp (DIFF) (P14)
  1: 2          Reps
  2: 1          5 mV Slow Range
  3: 6          DIFF Channel
  4: 1          Type T (Copper-Constantan)
  5: 5          Ref Temp (Deg. C) Loc [ _________ ]
  6: 6          Loc [ _________ ] ;Tinit 6,7,8
  7: 1.0        Mult
  8: 0.0        Offset

 10:  Set Port (P20)
  1: 1          Set High
  2: 1          Port Number

 11:  Excitation with Delay (P22)
  1: 4          Ex Channel
  2: 0          Delay w/Ex (units = 0.01 sec)
  3: 100        Delay After Ex (units = 0.01 sec)
  4: 0          mV Excitation

 12:  Thermocouple Temp (DIFF) (P14)
  1: 2          Reps
  2: 1          5 mV Slow Range
  3: 6          DIFF Channel
  4: 1          Type T (Copper-Constantan)
  5: 5          Ref Temp (Deg. C) Loc [ _________ ]
  6: 9          Loc [ _________ ] ;T(t=1s)9,10,11
  7: 1.0        Mult
  8: 0.0        Offset

 13:  Excitation with Delay (P22)
  1: 4          Ex Channel
  2: 0          Delay w/Ex (units = 0.01 sec)
  3: 2000       Delay After Ex (units = 0.01 sec)
  4: 0          mV Excitation

 14:  Thermocouple Temp (DIFF) (P14)
  1: 2          Reps
  2: 1          5 mV Slow Range
  3: 6          DIFF Channel
  4: 1          Type T (Copper-Constantan)
  5: 5          Ref Temp (Deg. C) Loc [ _________ ]
  6: 12         Loc [ _________ ] ;T(t=20s)12,13,14
  7: 1.0        Mult
  8: 0.0        Offset

 15:  Set Port (P20)
  1: 0          Set Low
  2: 1          Port Number

 16:  Beginning of Loop (P87)
  1: 0          Delay
  2: 2          Loop Count

 17:  Z=X-Y (P35)
  1: 12     -- X Loc [ _________ ]
  2: 9      -- Y Loc [ _________ ]
  3: 15     -- Z Loc [ _________ ] ;15,16,17

 18:  End (P95)
```

```
19:  Do (P86)
 1: 10       Set Output Flag High

20:  Real Time (P77)
 1: 0110     Day,Hour/Minute (midnight = 0000)

21:  Resolution (P78)
 1: 1        High Resolution

22:  Sample (P70)
 1: 1        Reps
 2: 1        Loc [ _________ ] ;1 WL xd

23:  Sample (P70)
 1: 3        Reps
 2: 2        Loc [ _________ ] ;2,3,4 ATs

24:  Resolution (P78)
 1: 0        Low Resolution

25:  Sample (P70)
 1: 4        Reps
 2: 5        Loc [ _________ ] ;5,6,7,8 Tref, Tinit123

26:  Sample (P70)
 1: 3        Reps
 2: 15       Loc [ _________ ] ;DT20-1 15,16,17

27:  Sample (P70)
 1: 1        Reps
 2: 18       Loc [ _________ ] ;Battery V

28:  End (P95)

29:  Serial Out (P96)
 1: 30       SM192/SM716/CSM1

30:  Do (P86)
 1: 21       Set Flag 1 Low
```

APPENDIX B

AT calibration curves

Site 1, AT1

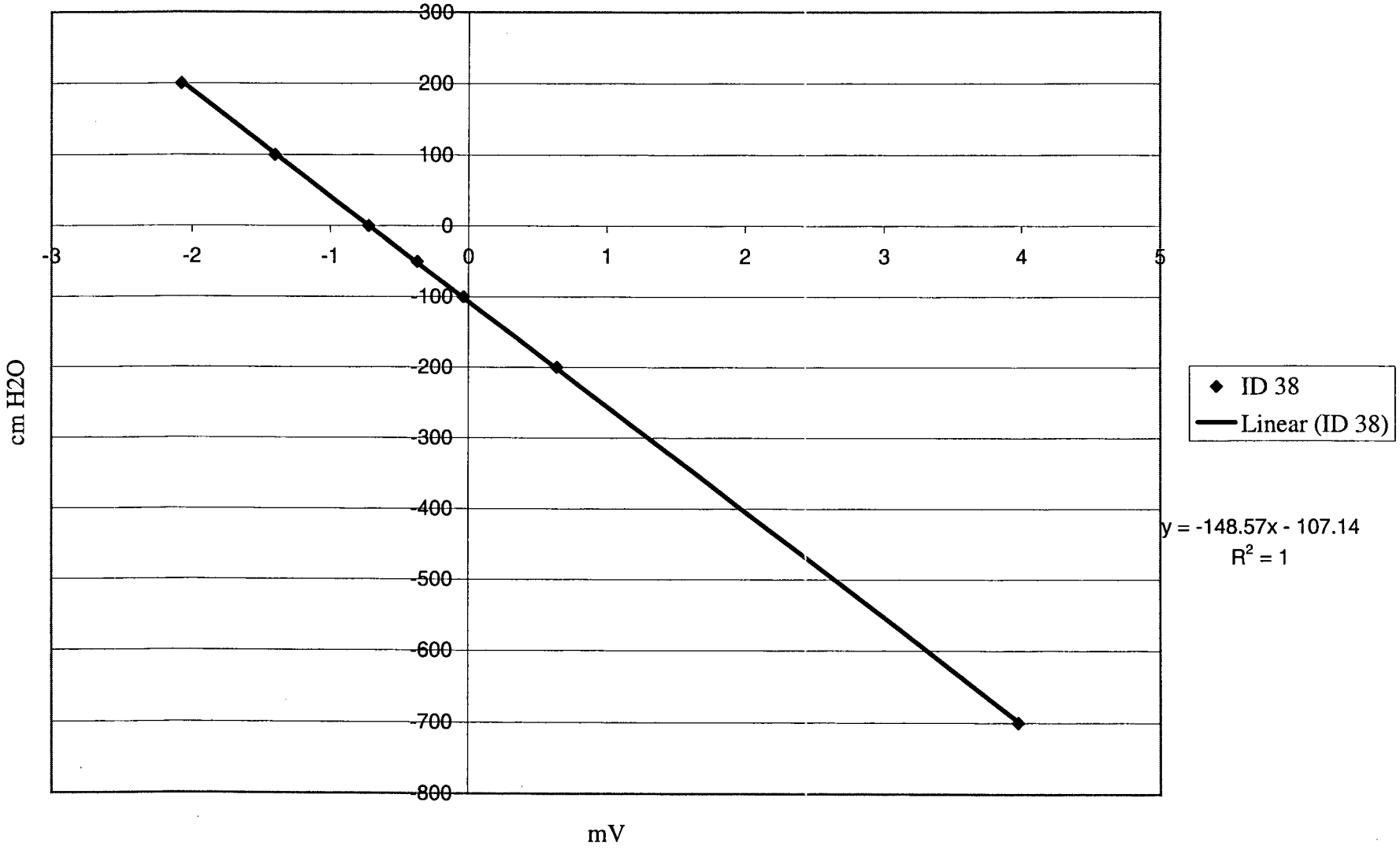
300
200
100
0
-100
-200
-300
-400
-500
-600
-700
-800
-3
-2
-1
0
1
2
3
4
5
cm H2O
mV
ID 38
Linear (ID 38)
y = -148.57x - 107.14
R2 = 1

Site 1, AT2

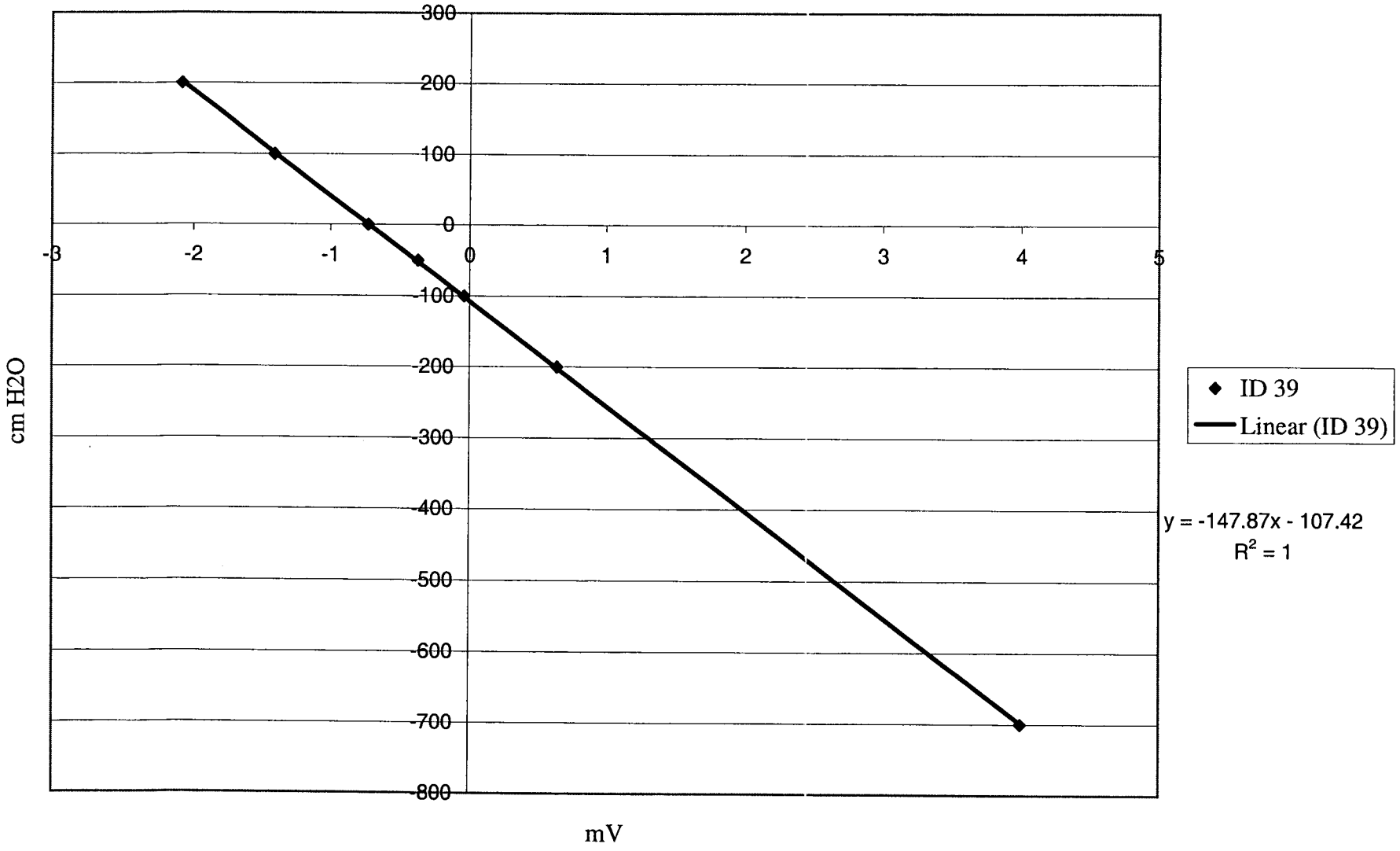
300
200
100
0
-100
-200
-300
-400
-500
-600
-700
-800
-3
-2
-1
0
1
2
3
4
5
cm H2O
mV
ID 39
Linear (ID 39)
y = -147.87x - 107.42
R2 = 1

Site 1, AT3

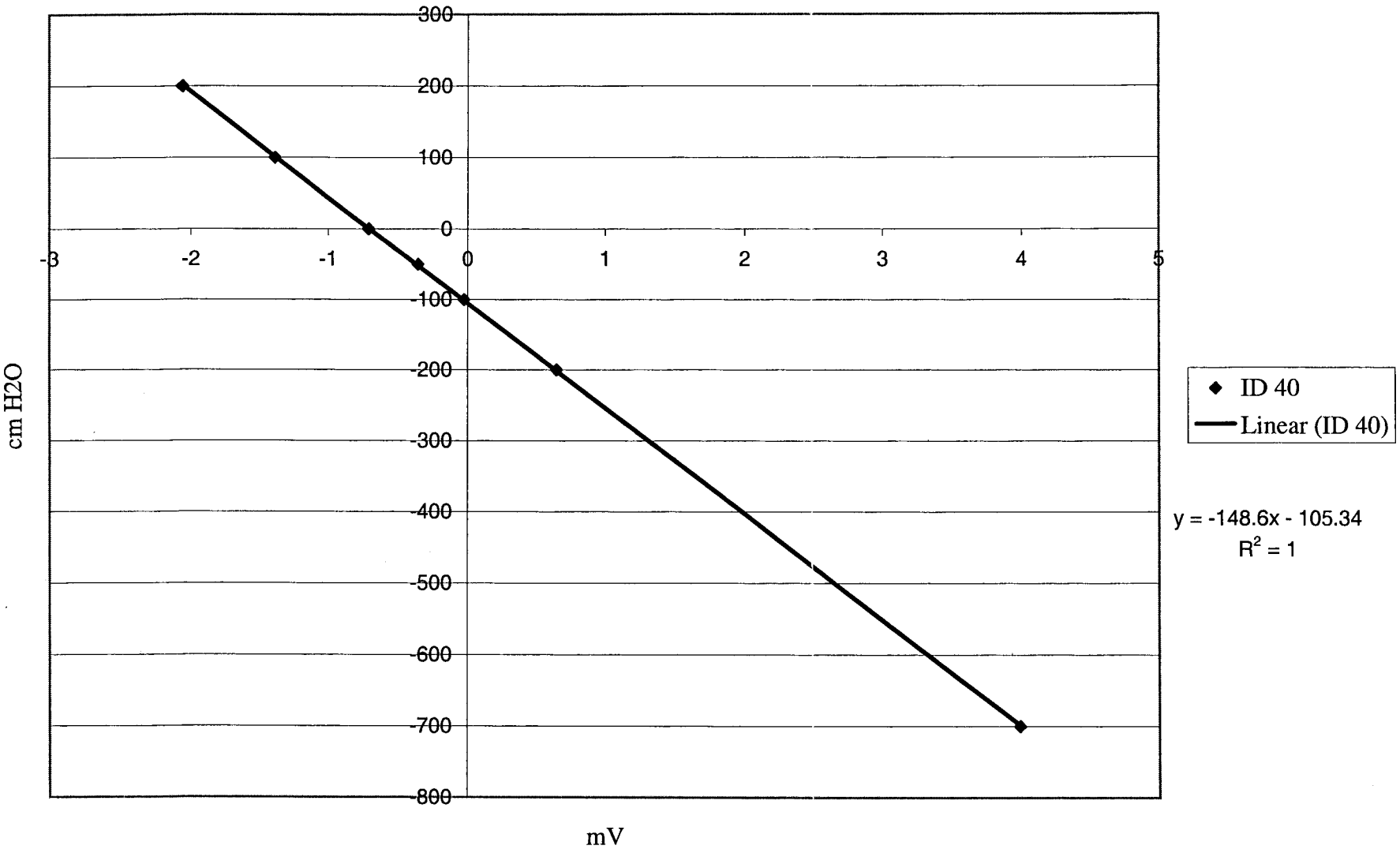
300
200
100
0
-100
-200
-300
-400
-500
-600
-700
-800
-3
-2
-1
0
1
2
3
4
5
cm H2O
mV
ID 40
Linear (ID 40)
y = -148.6x - 105.34
R2 = 1

Site 2, AT1

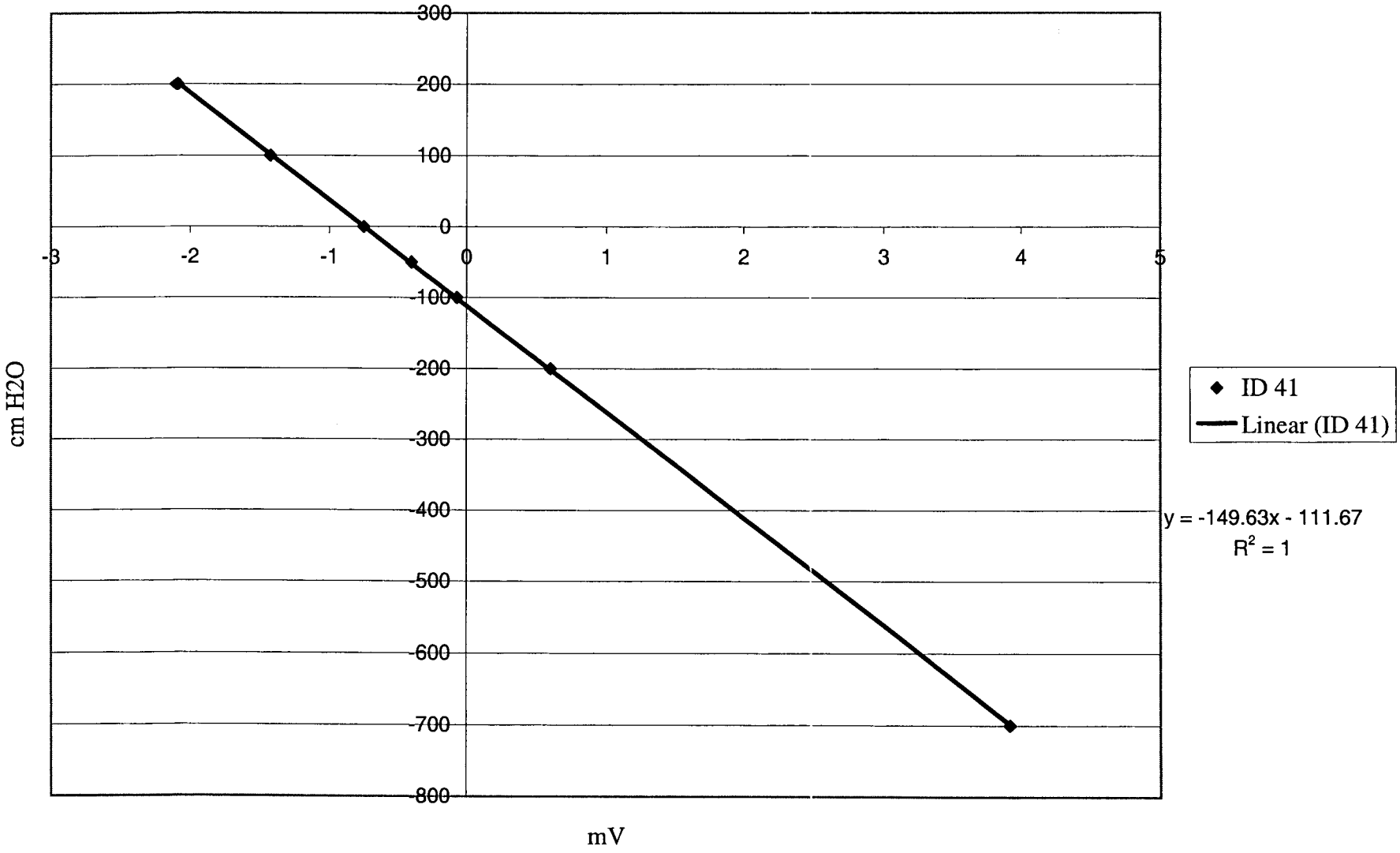
300
200
100
0
-100
-200
-300
-400
-500
-600
-700
-800
-3
-2
-1
0
1
2
3
4
5
cm H2O
mV
ID 41
Linear (ID 41)
y = -149.63x - 111.67
R2 = 1

Site 2, AT2

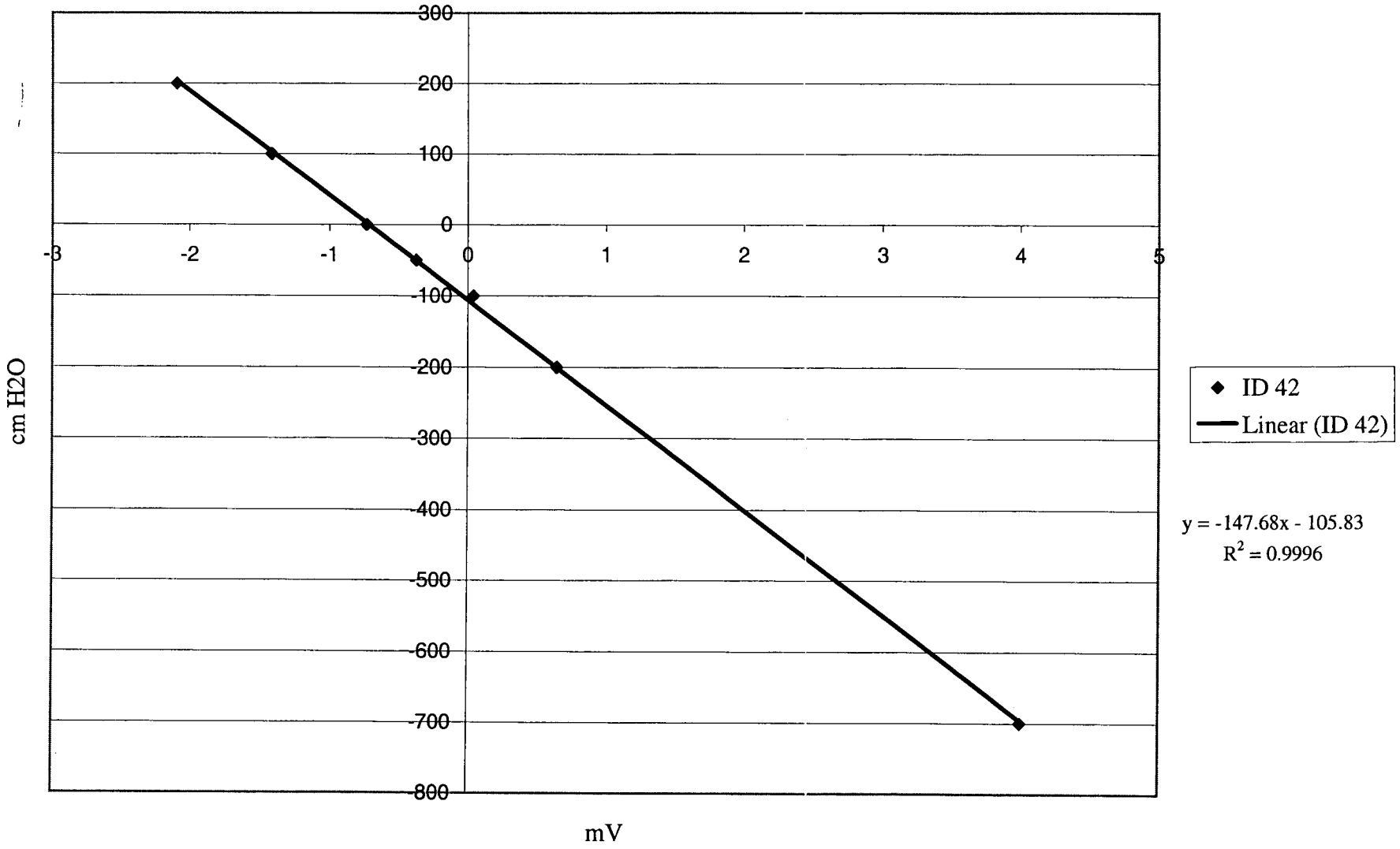
300
200
100
0
-100
-200
-300
-400
-500
-600
-700
-800
-3
-2
-1
0
1
2
3
4
5
cm H2O
mV
ID 42
Linear (ID 42)
y = -147.68x - 105.83
R2 = 0.9996

Site 2, AT3

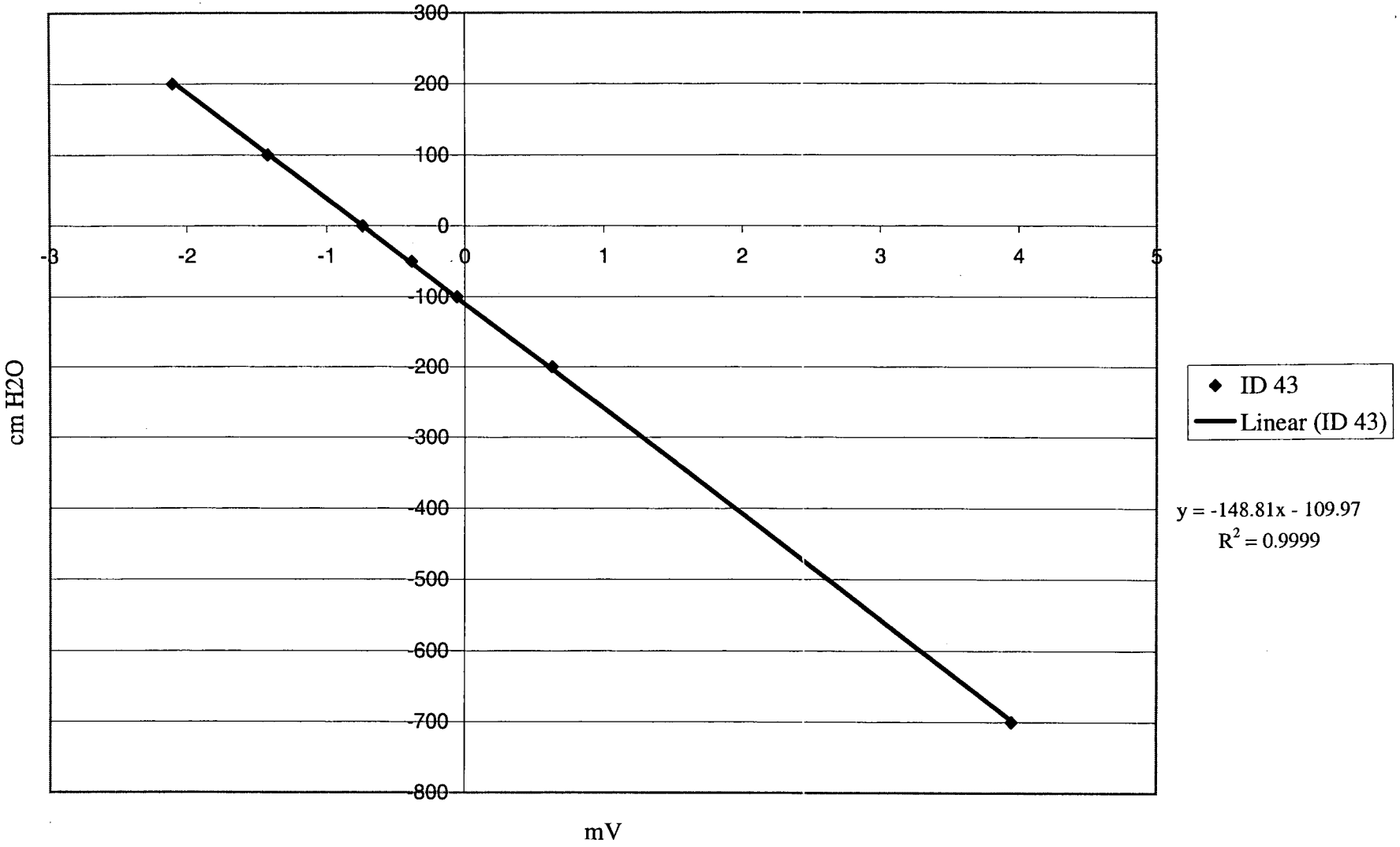
300
200
100
0
-100
-200
-300
-400
-500
-600
-700
-800
-3
-2
-1
0
1
2
3
4
5
cm H2O
mV
ID 43
Linear (ID 43)
y = -148.81x - 109.97
R2 = 0.9999

Site 3, AT1

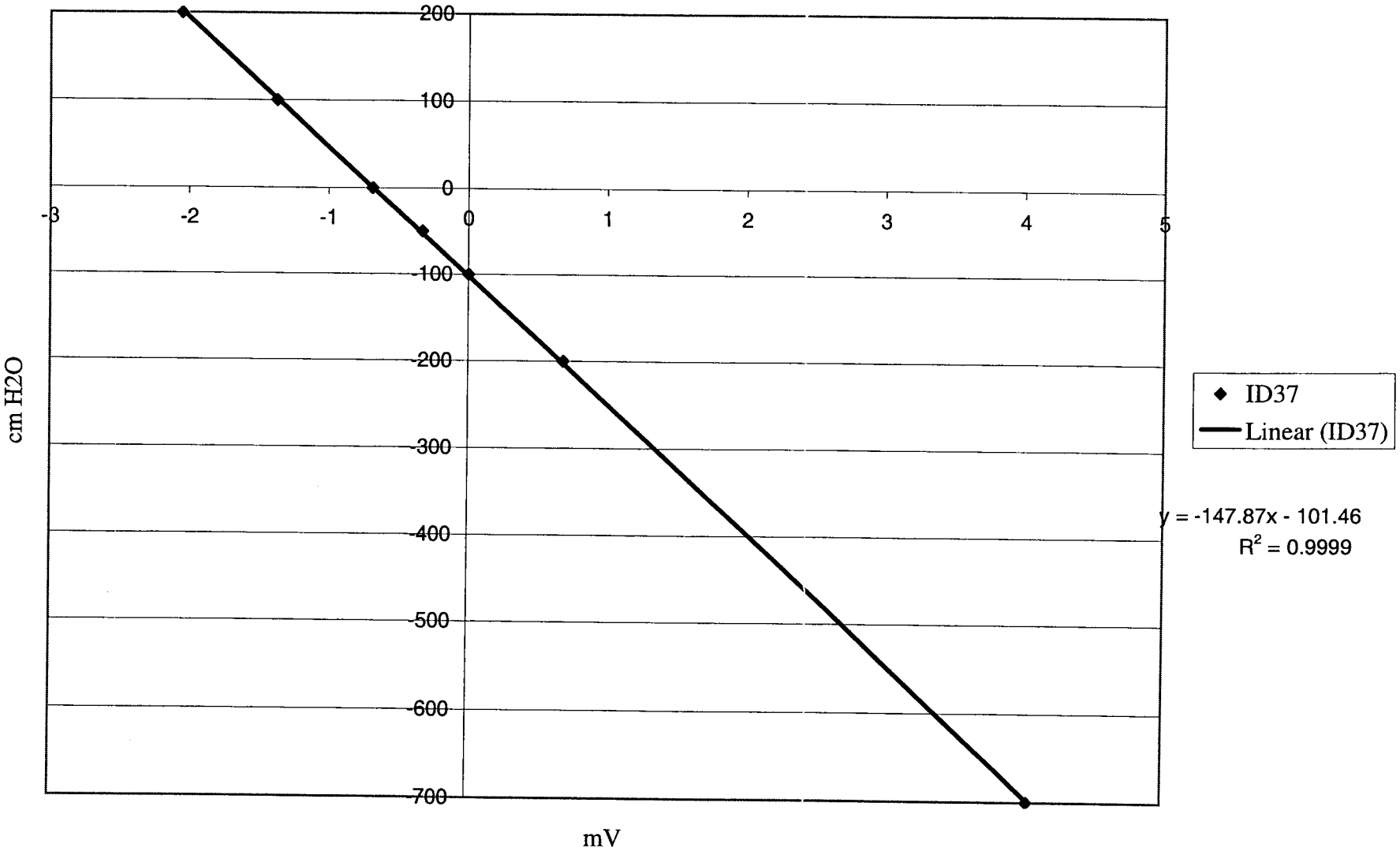
200
100
0
-100
-200
-300
-400
-500
-600
-700
-3
-2
-1
0
1
2
3
4
5
cm H2O
mV
ID37
Linear (ID37)
y = -147.87x - 101.46
R2 = 0.9999

Site 3, AT2

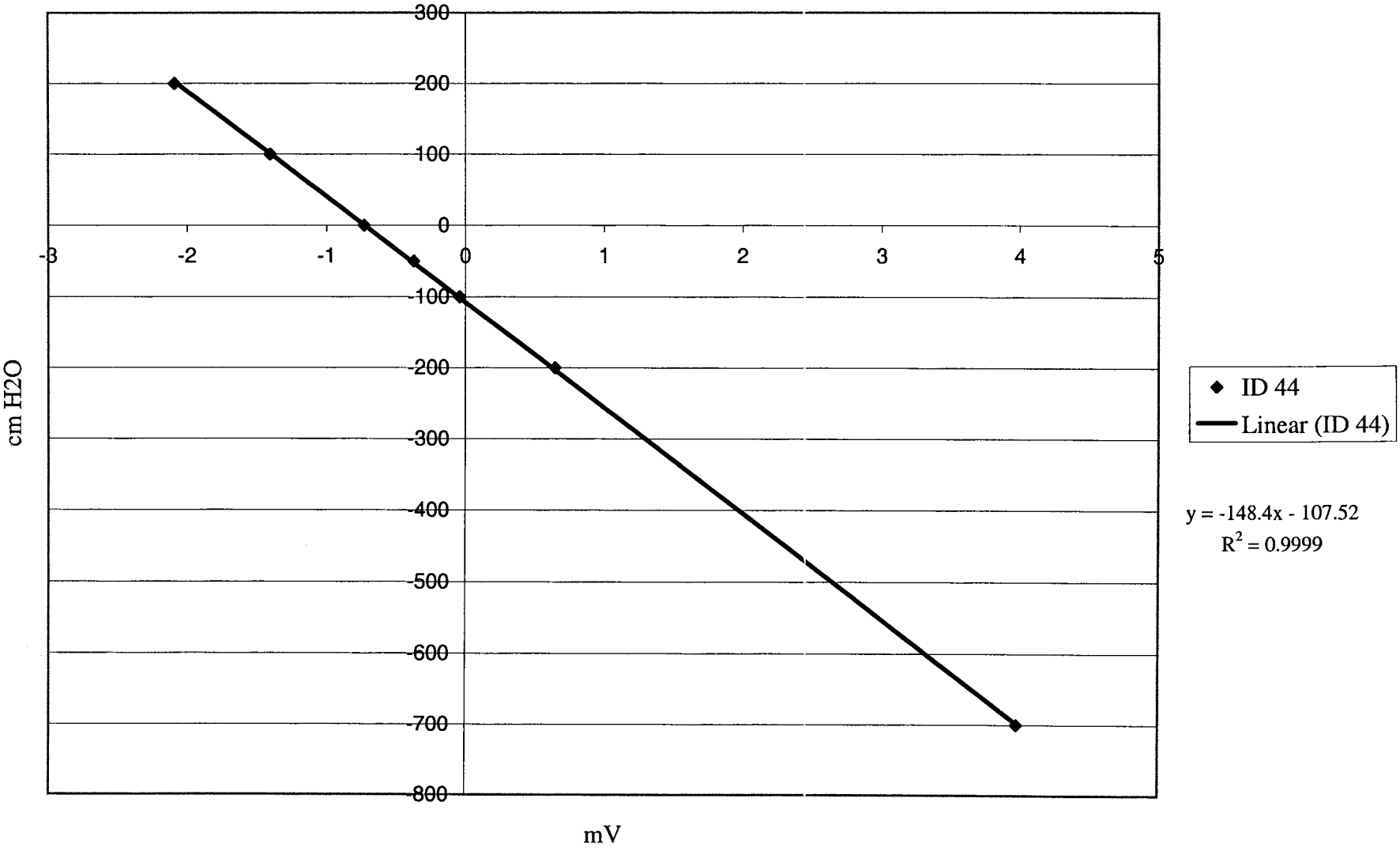
300
200
100
0
-100
-200
-300
-400
-500
-600
-700
-800
-3
-2
-1
0
1
2
3
4
5
cm H2O
mV
ID 44
Linear (ID 44)
y = -148.4x - 107.52
R2 = 0.9999

Site 3, AT3

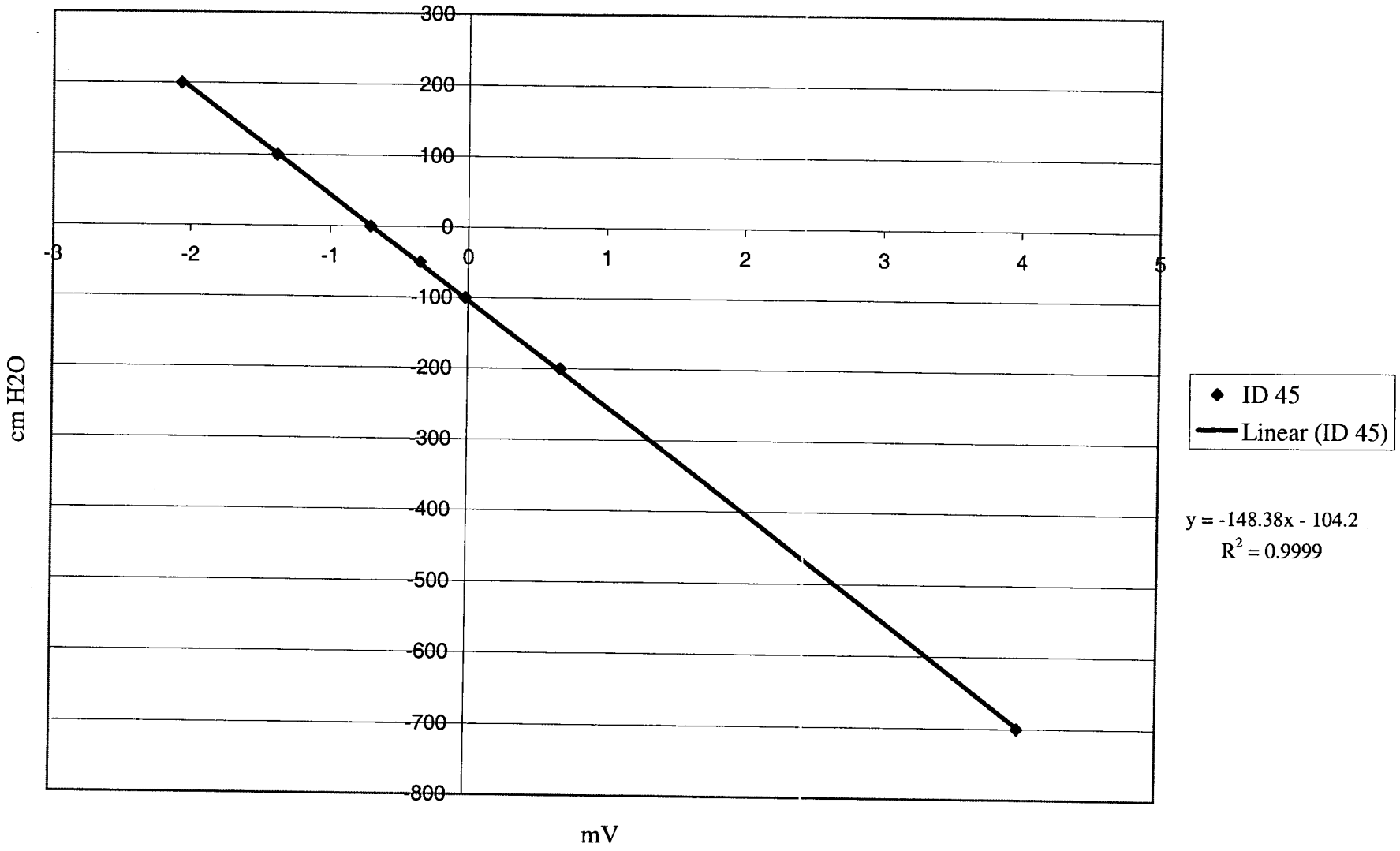
300
200
100
0
-100
-200
-300
-400
-500
-600
-700
-800
-3
-2
-1
0
1
2
3
4
5
cm H2O
mV
ID 45
Linear (ID 45)
y = -148.38x - 104.2
R2 = 0.9999

APPENDIX C

HD sensor calibration data

Site 1	Calibration	Data	
	HDS 5888	HDS 5891	HDS 5893
α (bar^{-1})	0.227	7.232	6.885
n	0.514	3.477	2.489
m	1.487	0.106	0.140
ΔT_{sat}	0.656	0.589	0.594
ΔT_{dry}	2.897	2.586	2.584

Site 2	Calibration	Data
	HDS 5889	HDS 5892
α (bar^{-1})	6.871	7.306
n	2.005	3.141
m	0.153	0.096
ΔT_{sat}	0.597	0.582
ΔT_{dry}	2.526	2.453

Site 3	Calibration	Data
	HDS 5887	HDS 5890
α (bar^{-1})	11.393	6.714
n	6.867	2.323
m	0.053	0.146
ΔTsat	0.809	0.537
ΔT_{dry}	2.123	2.497

ΔT is the temperature rise of the line heat source of the heat dissipation sensor (HDS) due to a 20-sec applied heating; $\Delta T = T_{end} - T_{start}$; T in degrees Celsius

ΔT_{sat} is the vacuum-saturated ΔT for the sensor

ΔT_{dry} is the oven-dried ΔT for the sensor

α, n, m are van-Genuchten-type fitted coefficients

APPENDIX D

Water level pressure transducer calibration curves

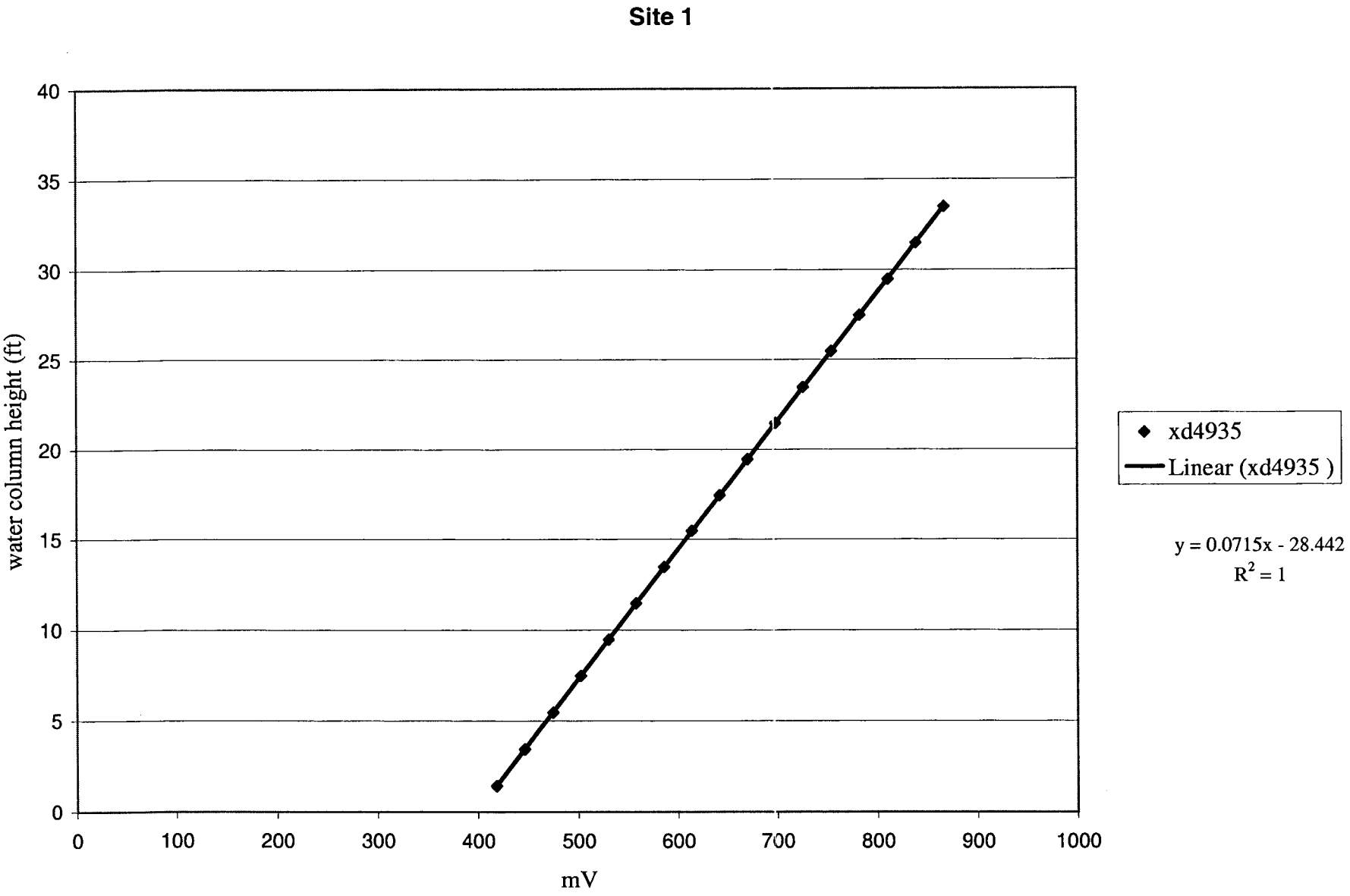
Site 1
water column height (ft)
40
35
30
25
20
15
10
5
0
0
100
200
300
400
500
600
700
800
900
1000
mV
xd4935
Linear (xd4935)
y = 0.0715x - 28.442
R2 = 1

Site 2

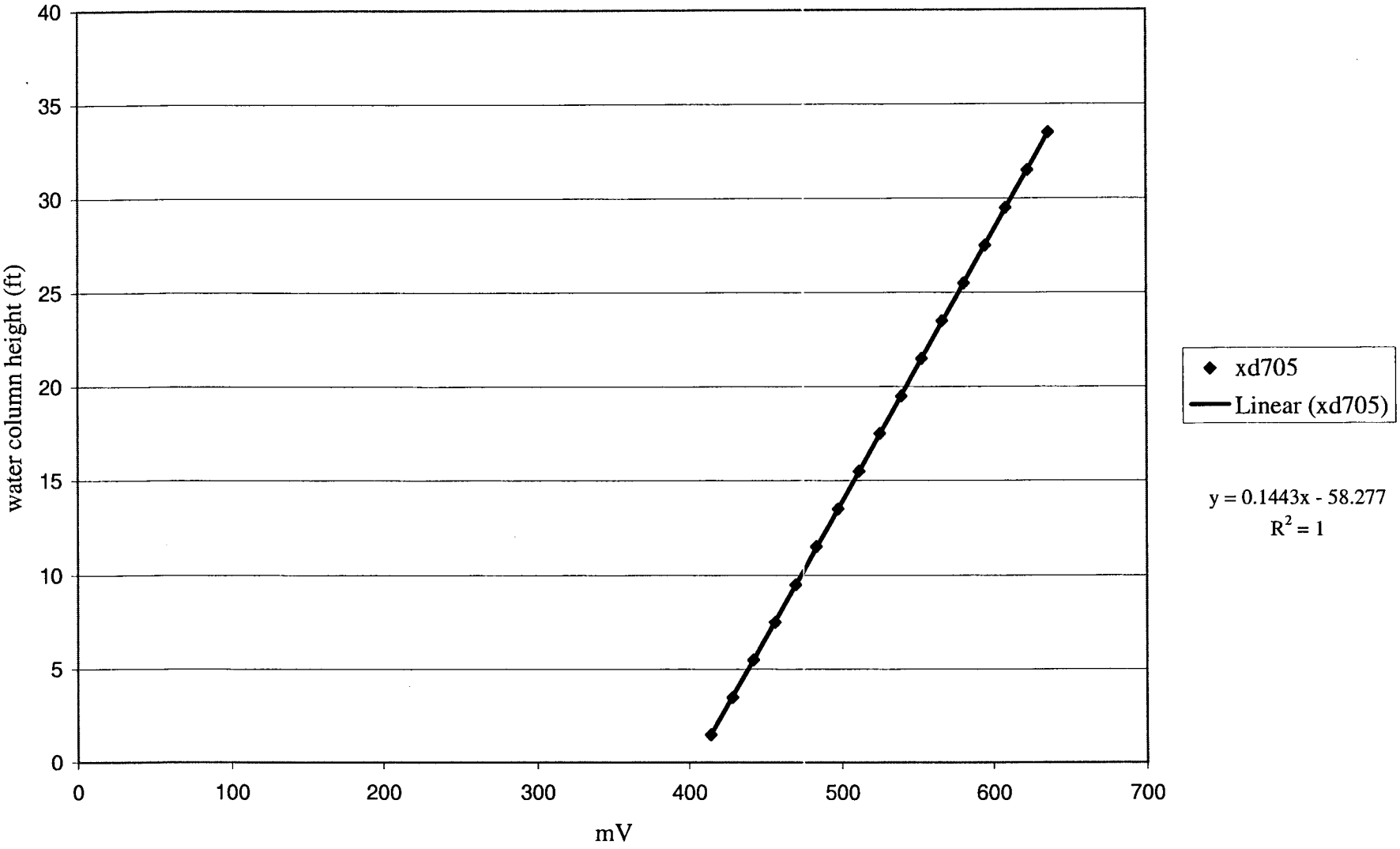
water column height (ft)
40
35
30
25
20
15
10
5
0
0
100
200
300
400
500
600
700
mV
xd705
Linear (xd705)
y = 0.1443x - 58.277
R2 = 1

Site 3

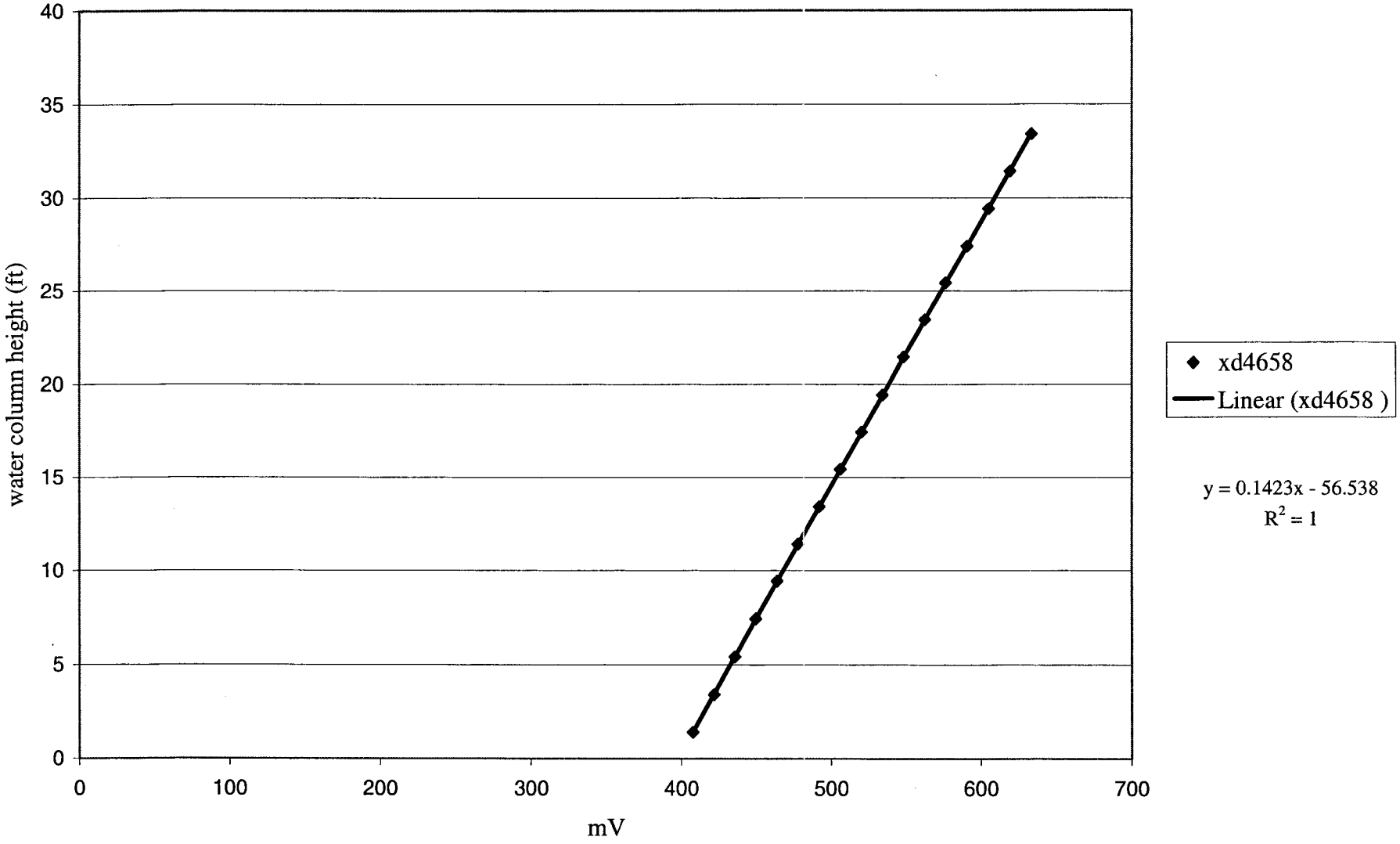
water column height (ft)
0
5
10
15
20
25
30
35
40
0
100
200
300
400
500
600
700
mV
xd4658
Linear (xd4658)
y = 0.1423x - 56.538
R2 = 1

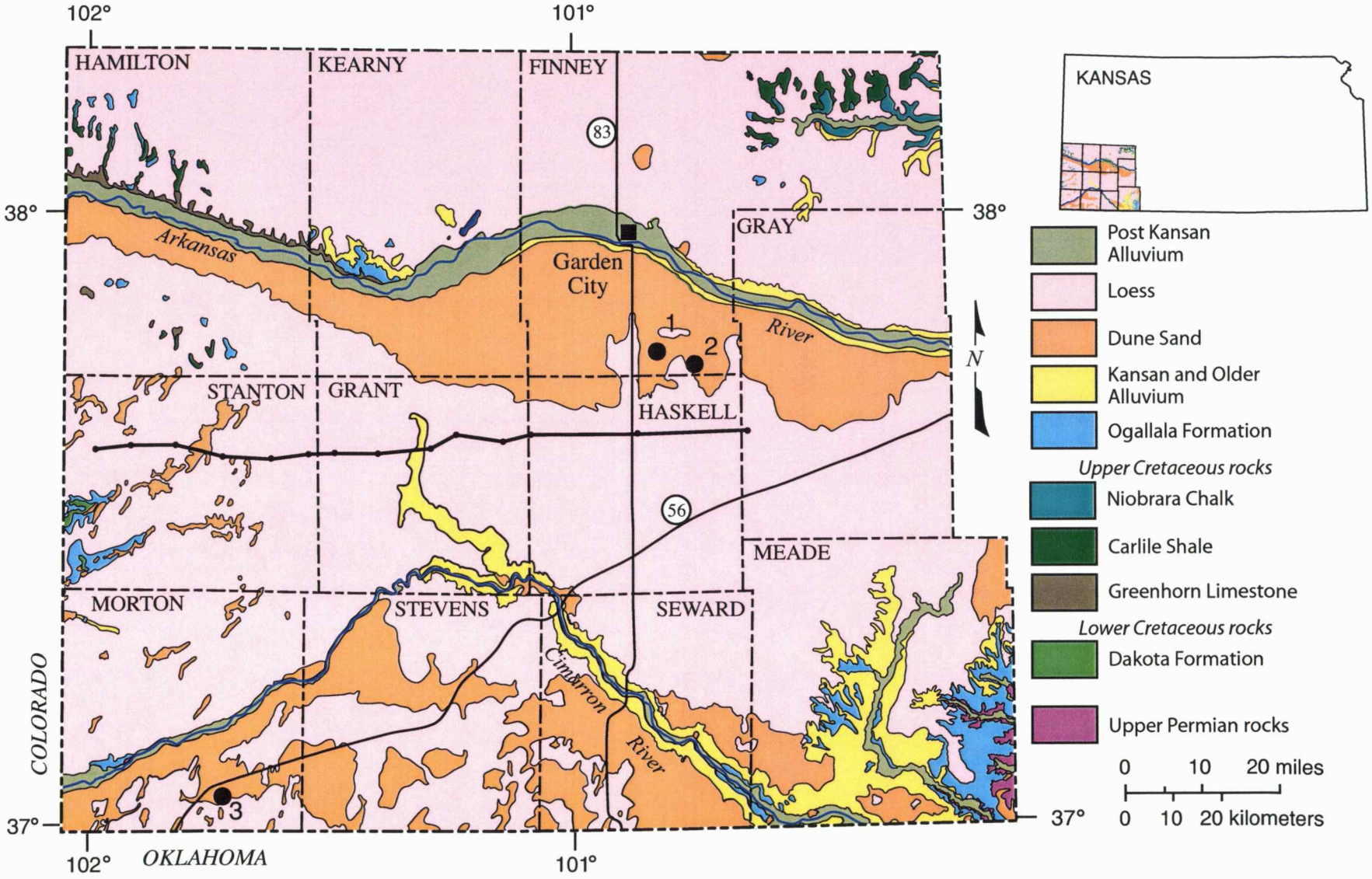
102°
101°
HAMILTON
KEARNY
FINNEY
83
38°
Arkansas
Garden City
GRAY
River
1
2
N
STANTON
GRANT
HASKELL
56
MEADE
MORTON
STEVENS
SEWARD
Cimarron
River
COLORADO
3
37°
OKLAHOMA
KANSAS
Post Kansan Alluvium
Loess
Dune Sand
Kansan and Older Alluvium
Ogallala Formation
Upper Cretaceous rocks
Niobrara Chalk
Carlile Shale
Greenhorn Limestone
Lower Cretaceous rocks
Dakota Formation
Upper Permian rocks
0 10 20 miles
0 10 20 kilometers

Figure 1

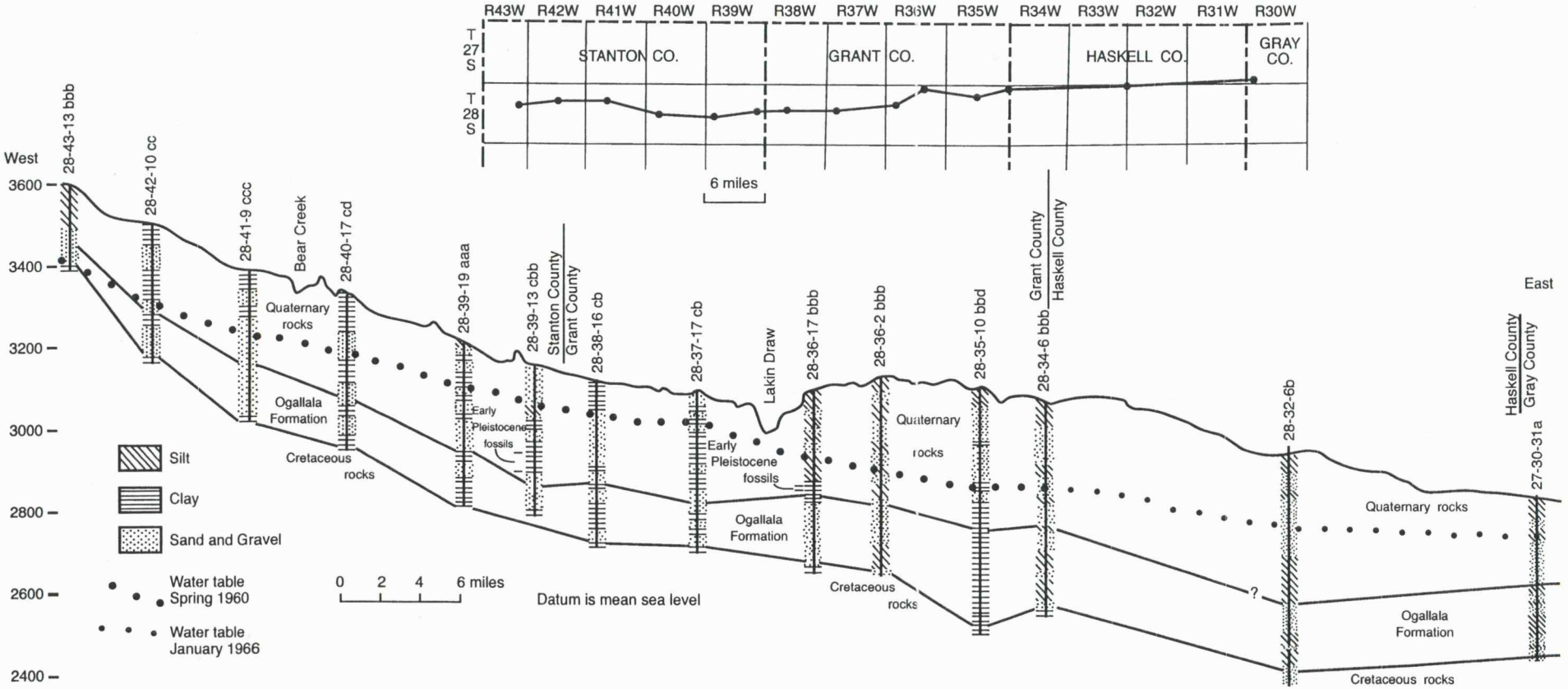
R43W R42W R41W R40W R39W R38W R37W R36W R35W R34W R33W R32W R31W R30W
T 27 S
T 28 S
STANTON CO.
GRANT CO.
HASKELL CO.
GRAY CO.
6 miles
West
East
3600
3400
3200
3000
2800
2600
2400
28-43-13 bbb
28-42-10 cc
28-41-9 ccc
Bear Creek
28-40-17 cd
28-39-19 aaa
28-39-13 cbb
Stanton County
Grant County
28-38-16 cb
28-37-17 cb
Lakin Draw
28-36-17 bbb
28-36-2 bbb
28-35-10 bbd
28-34-6 bbb
Grant County
Haskell County
28-32-6b
Haskell County
Gray County
27-30-31a
Quaternary rocks
Ogallala Formation
Cretaceous rocks
Early Pleistocene fossils
Silt
Clay
Sand and Gravel
Water table Spring 1960
Water table January 1966
0 2 4 6 miles
Datum is mean sea level
?

Figure 2

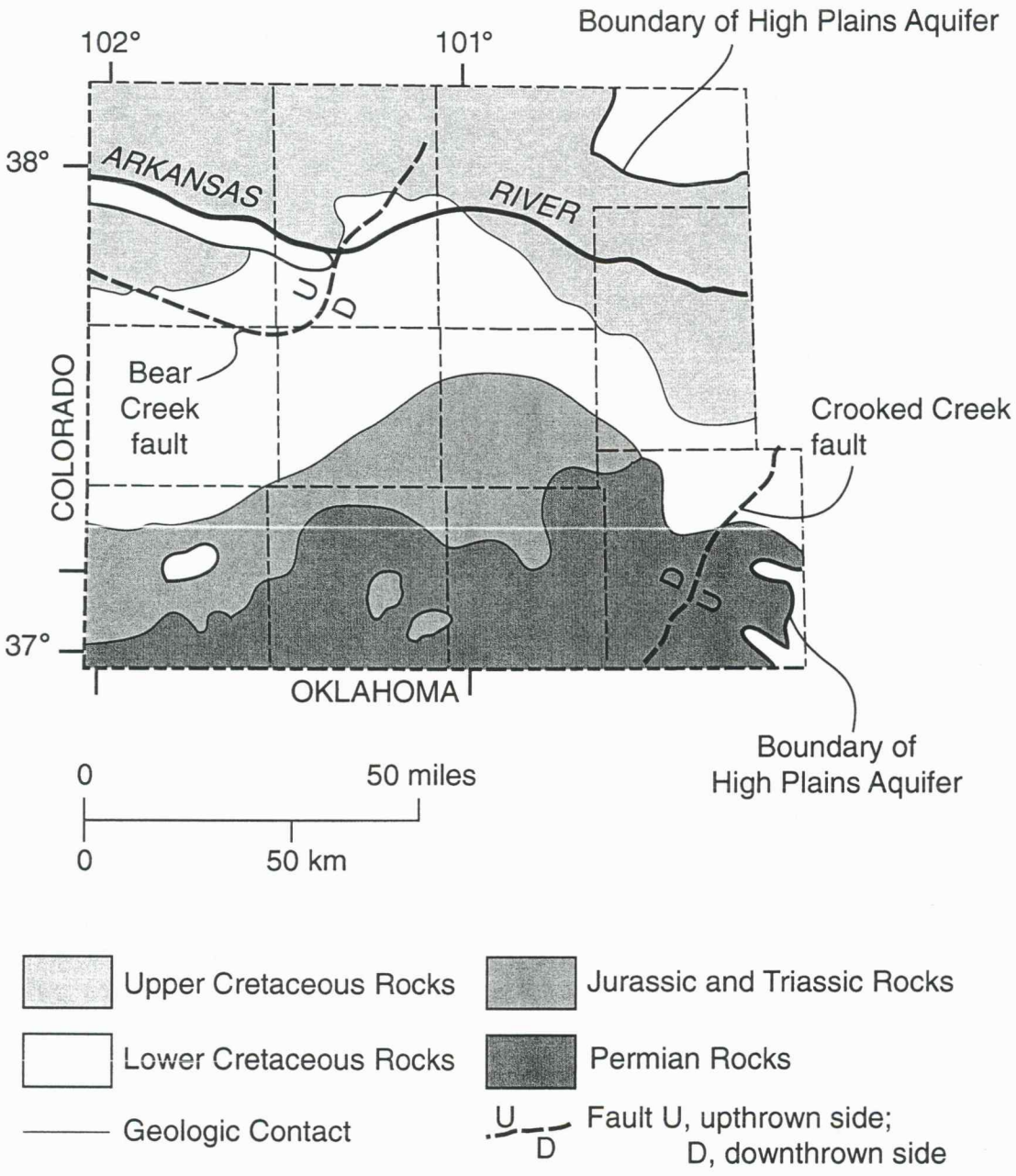
Boundary of High Plains Aquifer
102°
101°
38°
ARKANSAS
RIVER
U
D
Bear
Creek
fault
COLORADO
Crooked Creek
fault
37°
OKLAHOMA
Boundary of
High Plains Aquifer
0
50 miles
0
50 km
Upper Cretaceous Rocks
Jurassic and Triassic Rocks
Lower Cretaceous Rocks
Permian Rocks
Geologic Contact
U
D
Fault U, upthrown side;
D, downthrown side

Figure 3

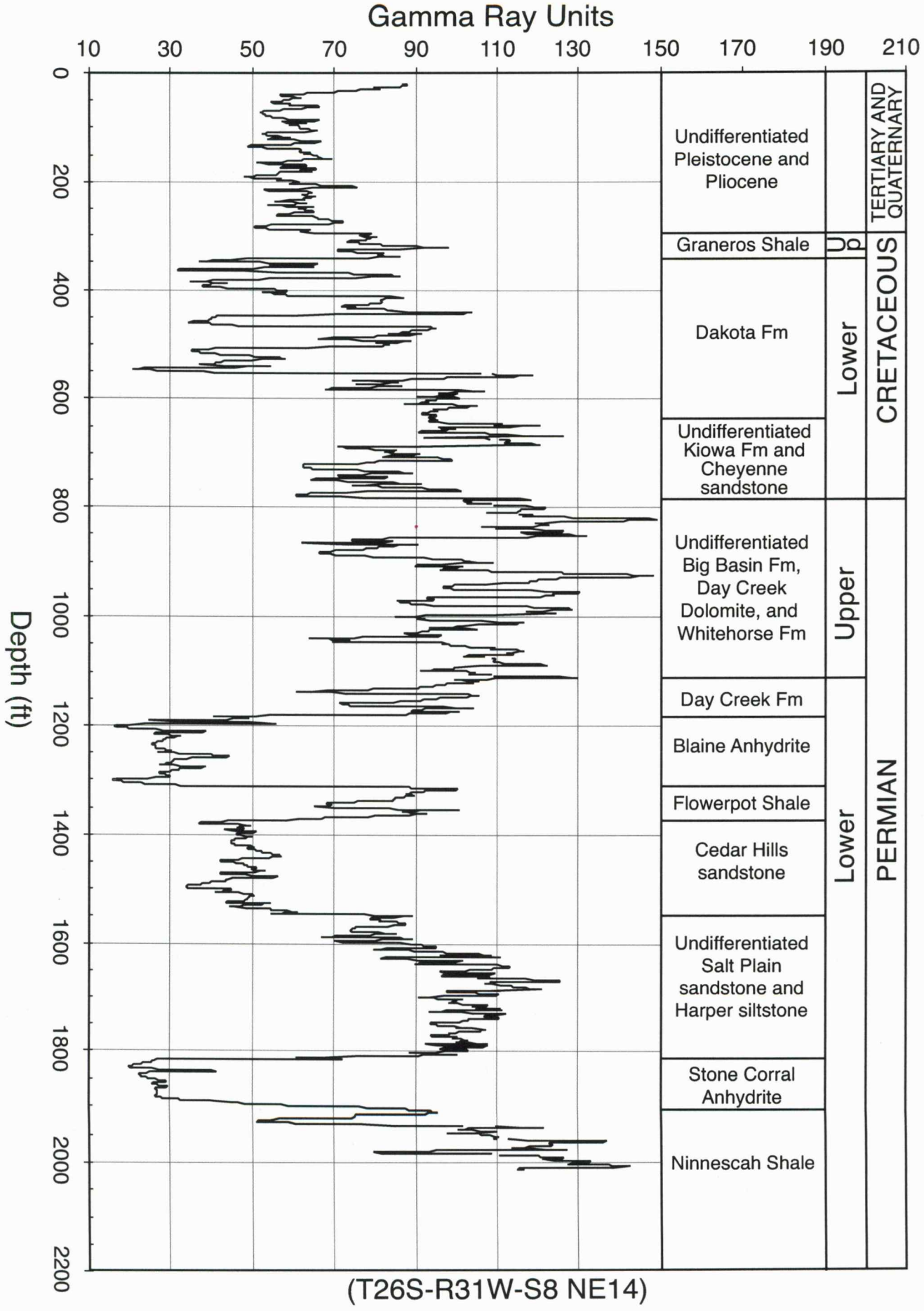
Gamma Ray Units
10
30
50
70
90
110
130
150
170
190
210
Depth (ft)
0
200
400
600
800
1000
1200
1400
1600
1800
2000
2200
Undifferentiated Pleistocene and Pliocene
Graneros Shale
Dakota Fm
Undifferentiated Kiowa Fm and Cheyenne sandstone
Undifferentiated Big Basin Fm, Day Creek Dolomite, and Whitehorse Fm
Day Creek Fm
Blaine Anhydrite
Flowerpot Shale
Cedar Hills sandstone
Undifferentiated Salt Plain sandstone and Harper siltstone
Stone Corral Anhydrite
Ninnescah Shale
Upper
Lower
Lower
TERTIARY AND QUATERNARY
CRETACEOUS
PERMIAN
(T26S-R31W-S8 NE14)

Figure 4

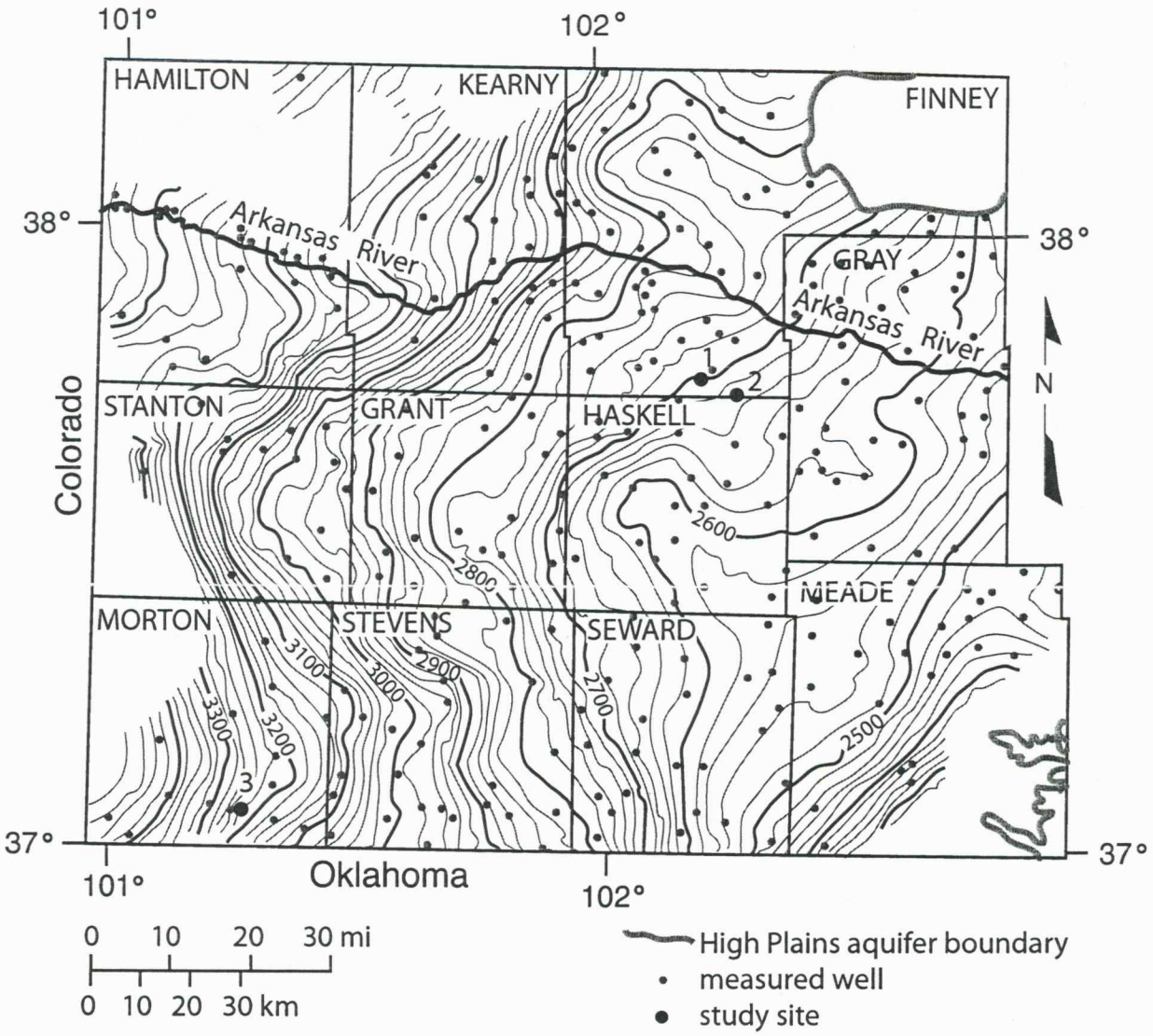
101°
102°
HAMILTON
KEARNY
FINNEY
38°
Arkansas River
GRAY
Arkansas River
N
Colorado
STANTON
GRANT
HASKELL
2600
2800
MEADE
MORTON
STEVENS
SEWARD
3100
2900
3000
2700
3300
3200
2500
1
2
3
37°
101°
Oklahoma
102°
0 10 20 30 mi
0 10 20 30 km
High Plains aquifer boundary
measured well
study site

Figure 5

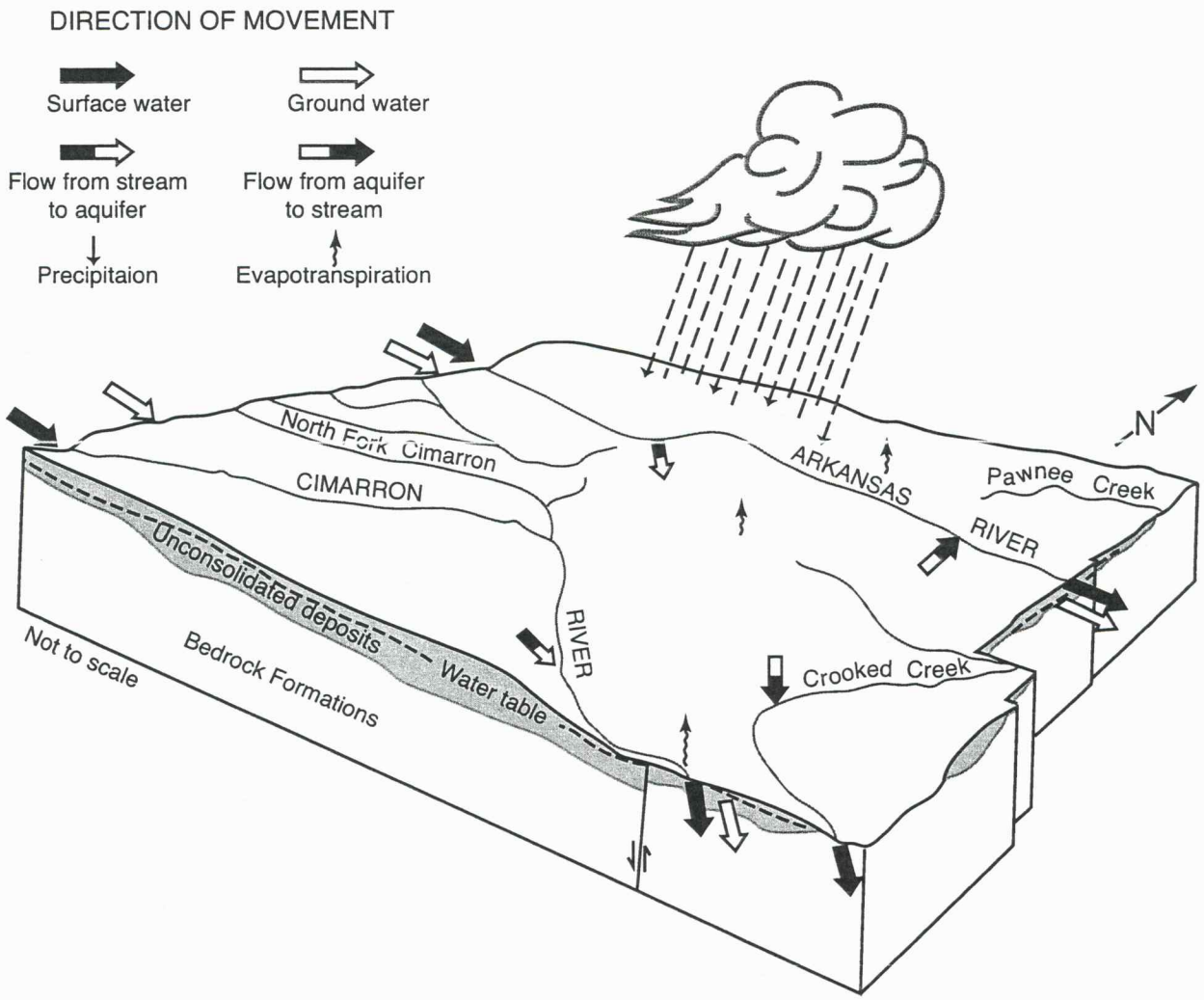
DIRECTION OF MOVEMENT
Surface water
Ground water
Flow from stream to aquifer
Flow from aquifer to stream
Precipitaion
Evapotranspiration
North Fork Cimarron
CIMARRON
RIVER
ARKANSAS
RIVER
Pawnee Creek
Crooked Creek
N
Unconsolidated deposits
Water table
Bedrock Formations
Not to scale

Figure 6

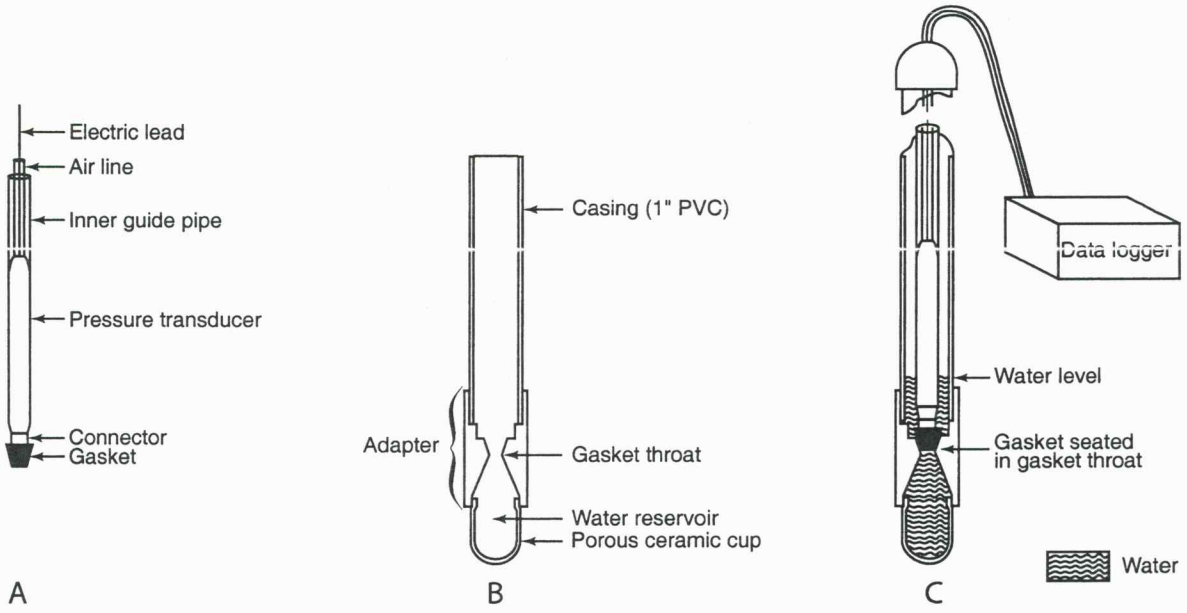
Electric lead
Air line
Inner guide pipe
Pressure transducer
Connector
Gasket
A
Casing (1" PVC)
Adapter
Gasket throat
Water reservoir
Porous ceramic cup
B
Data logger
Water level
Gasket seated
in gasket throat
Water
C

Figure 7

Figure 8

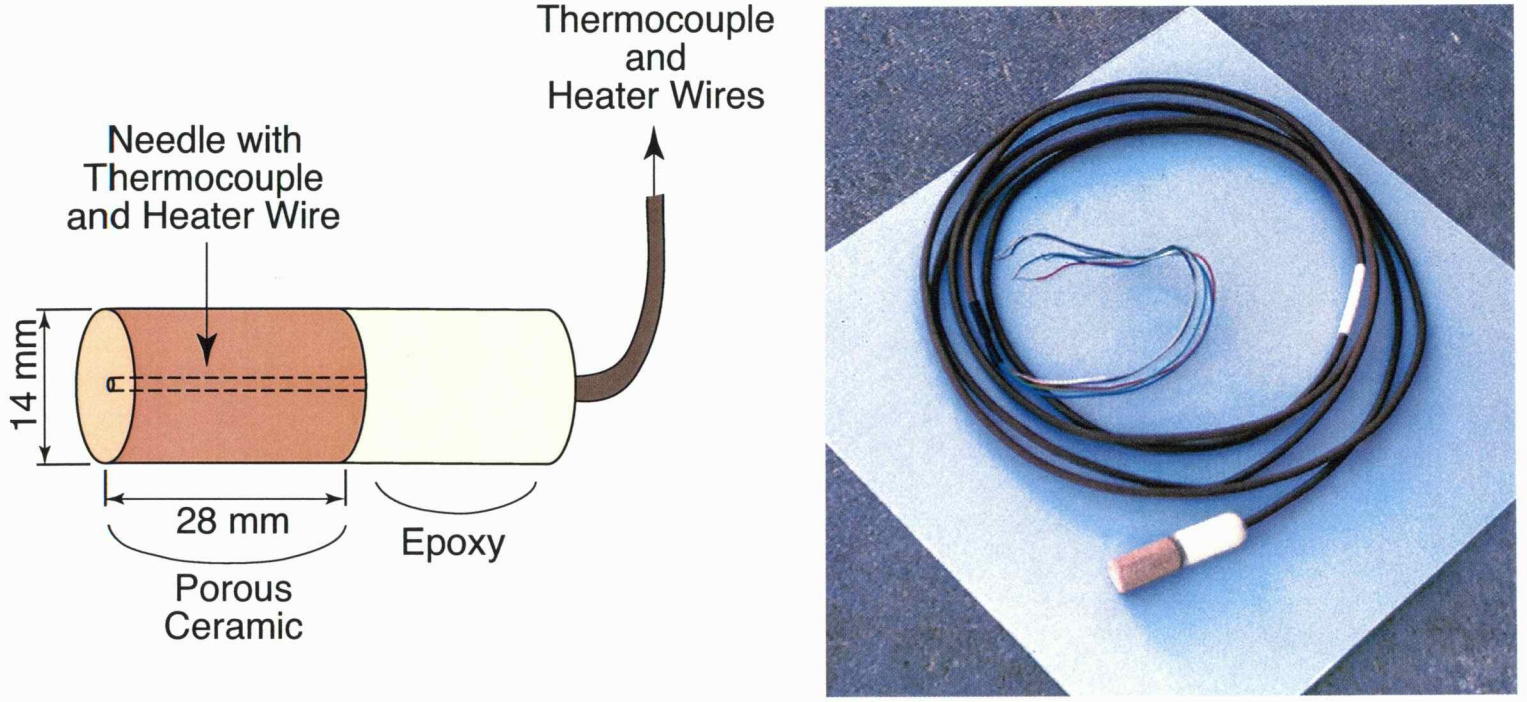
Thermocouple
and
Heater Wires
Needle with
Thermocouple
and Heater Wire
14 mm
28 mm
Epoxy
Porous
Ceramic

Figure 9

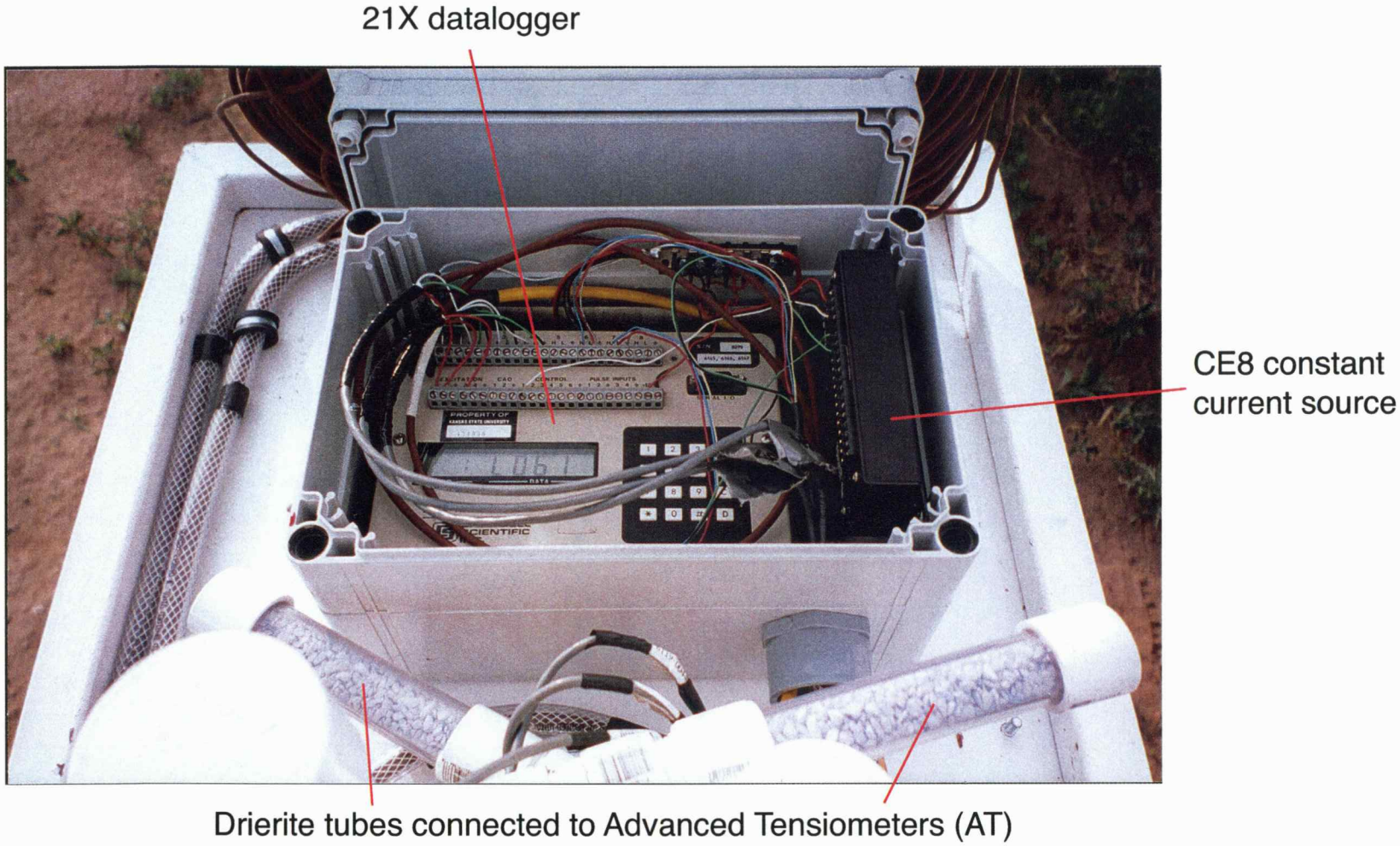
21X datalogger
CE8 constant current source
Drierite tubes connected to Advanced Tensiometers (AT)

Figure 10

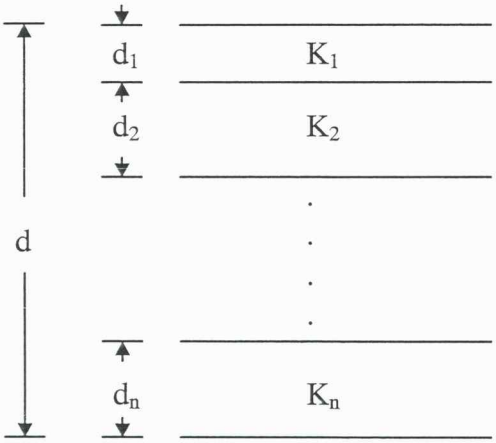

Figure 11

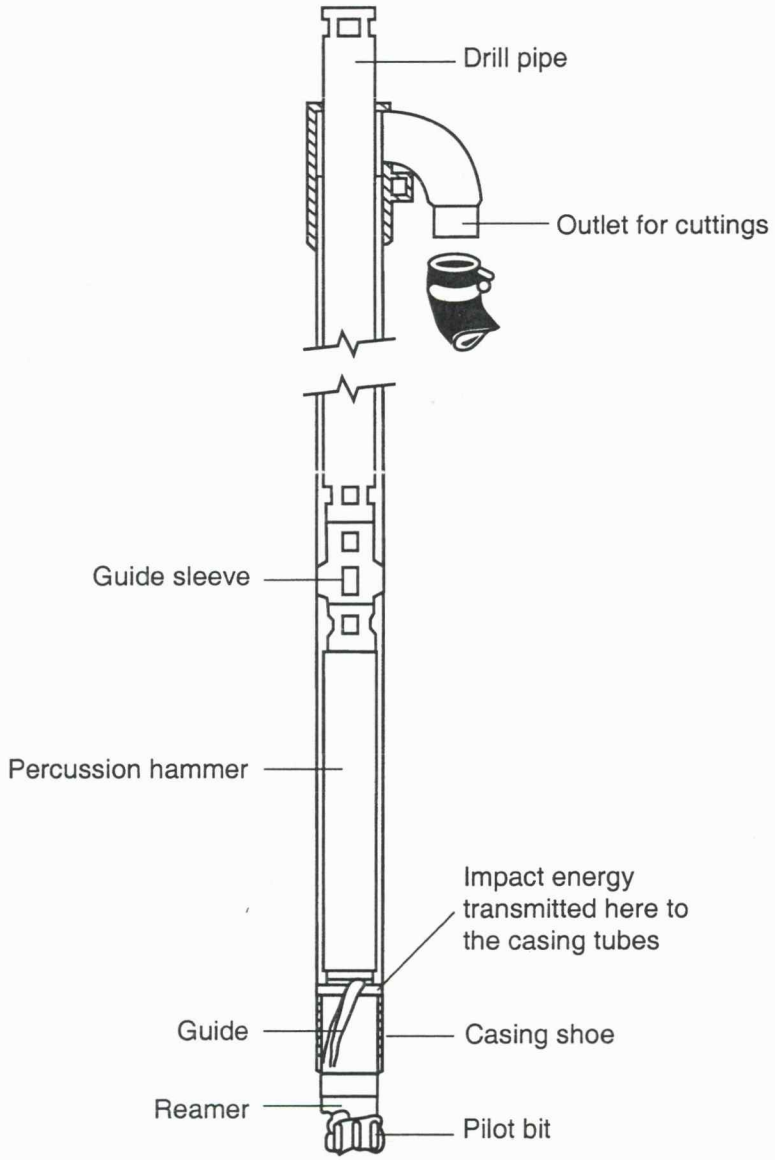
Drill pipe
Outlet for cuttings
Guide sleeve
Percussion hammer
Impact energy
transmitted here to
the casing tubes
Guide
Casing shoe
Reamer
Pilot bit

Figure 12

Figure 13

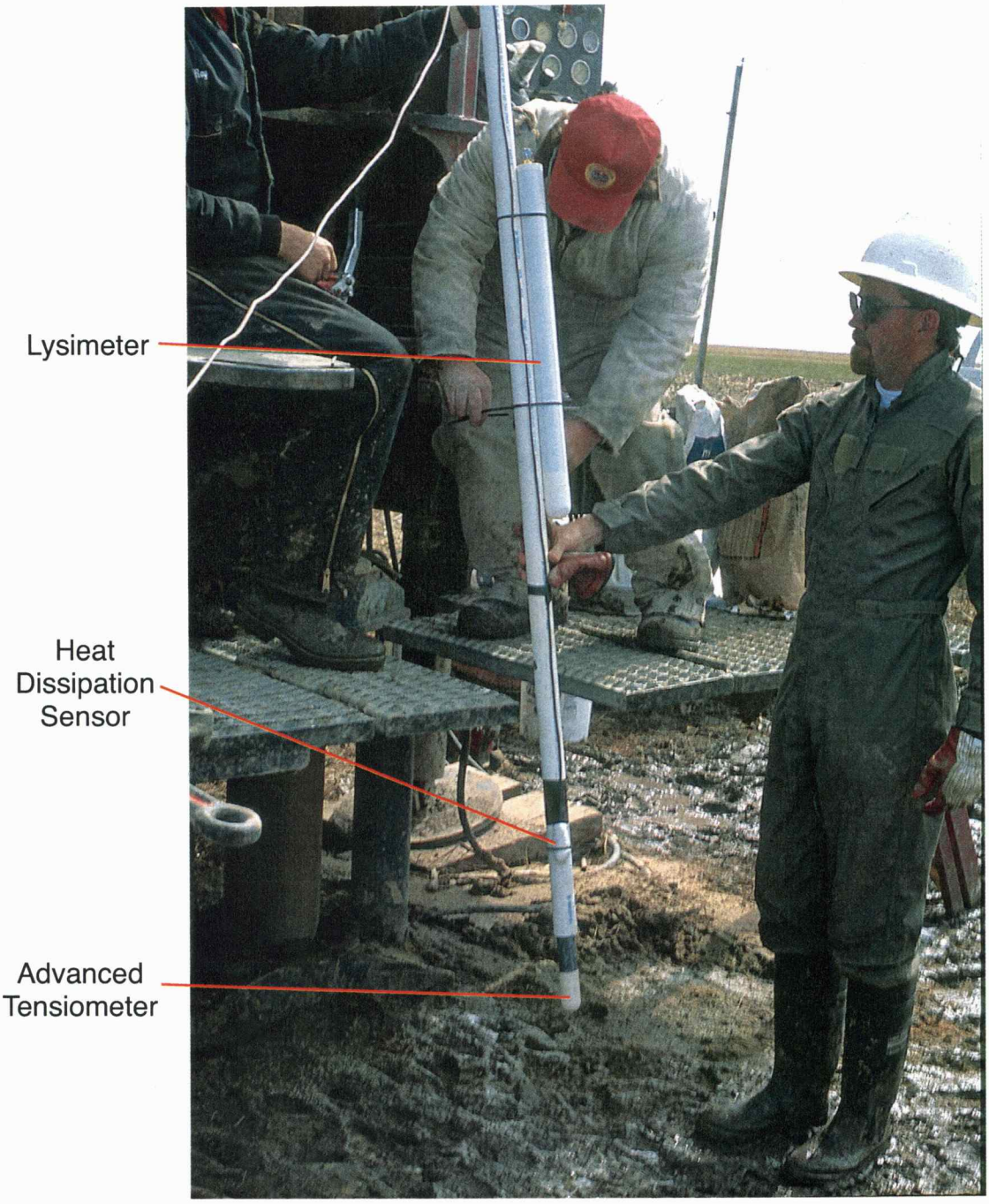

Figure 14

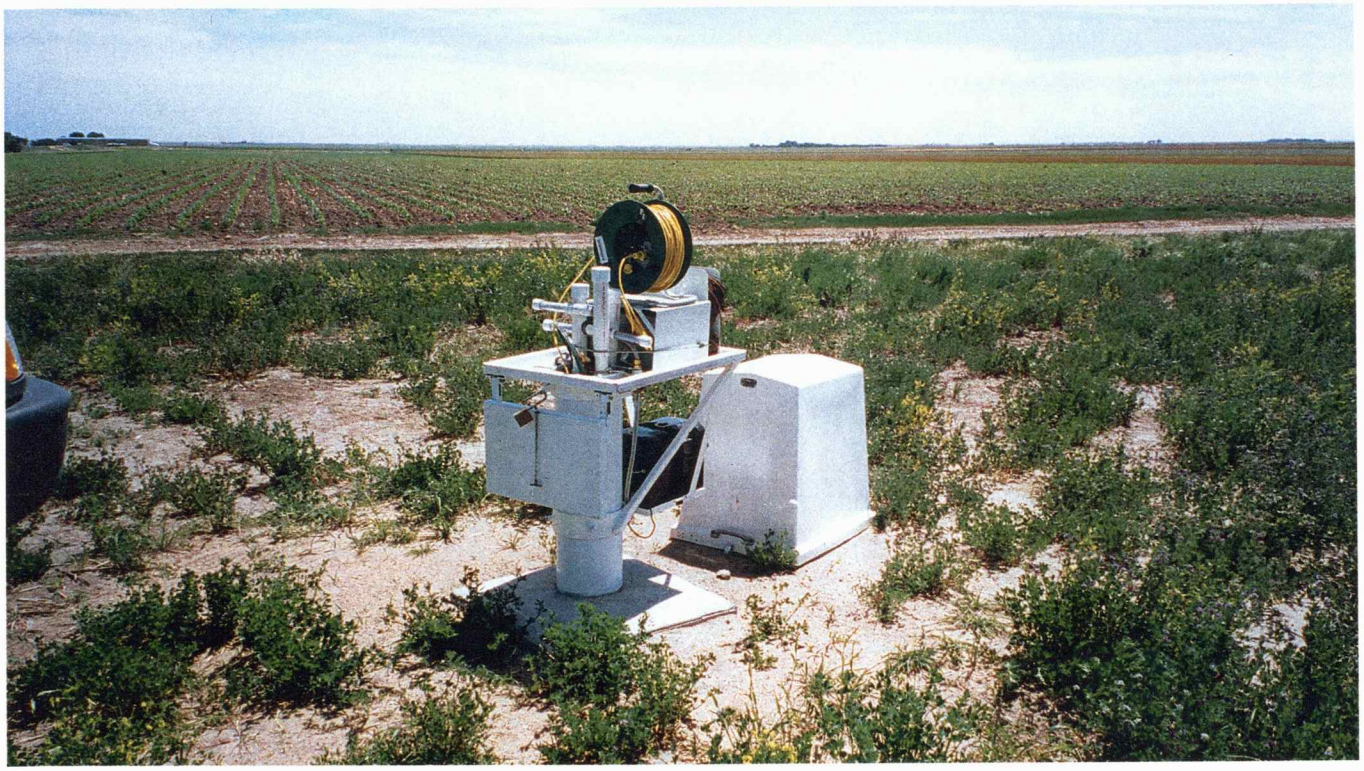

Figure 15

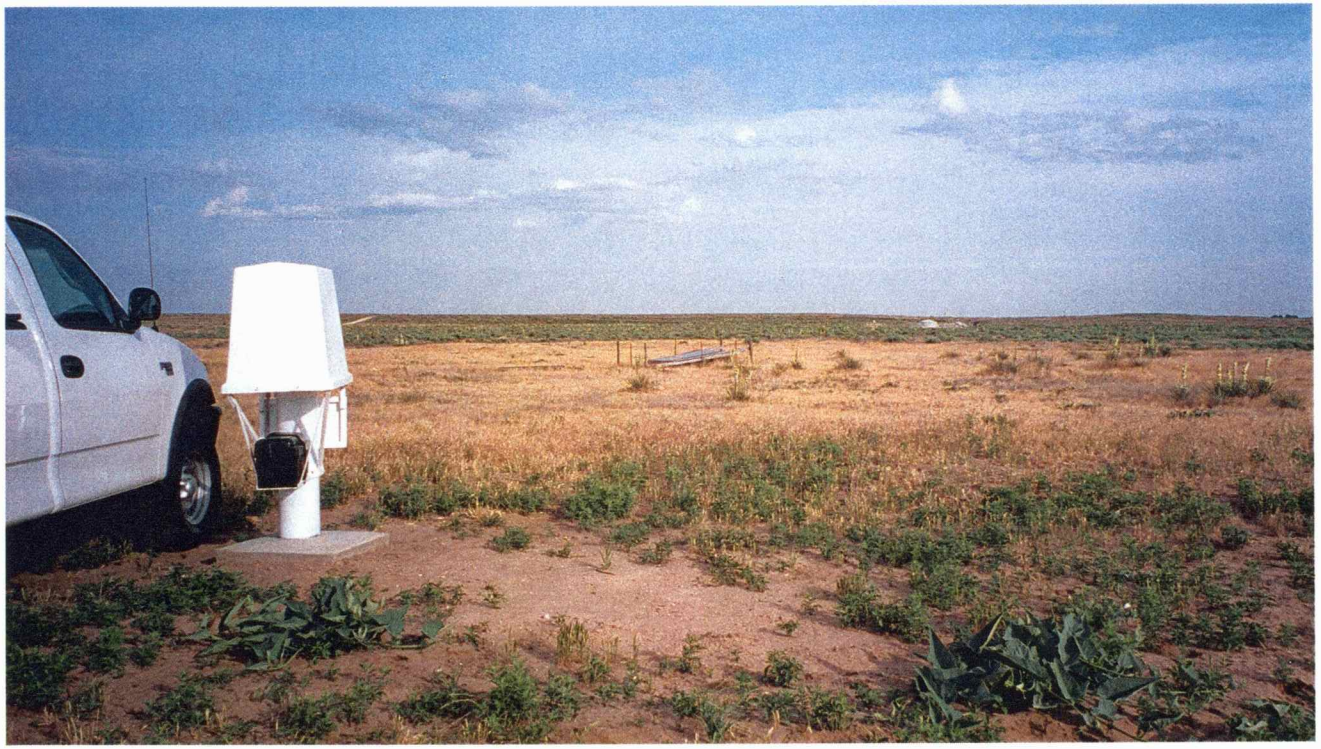

Figure 16

Site 1 (Finney County, KS; T. 26 S.-R. 32 W.-21ADC)

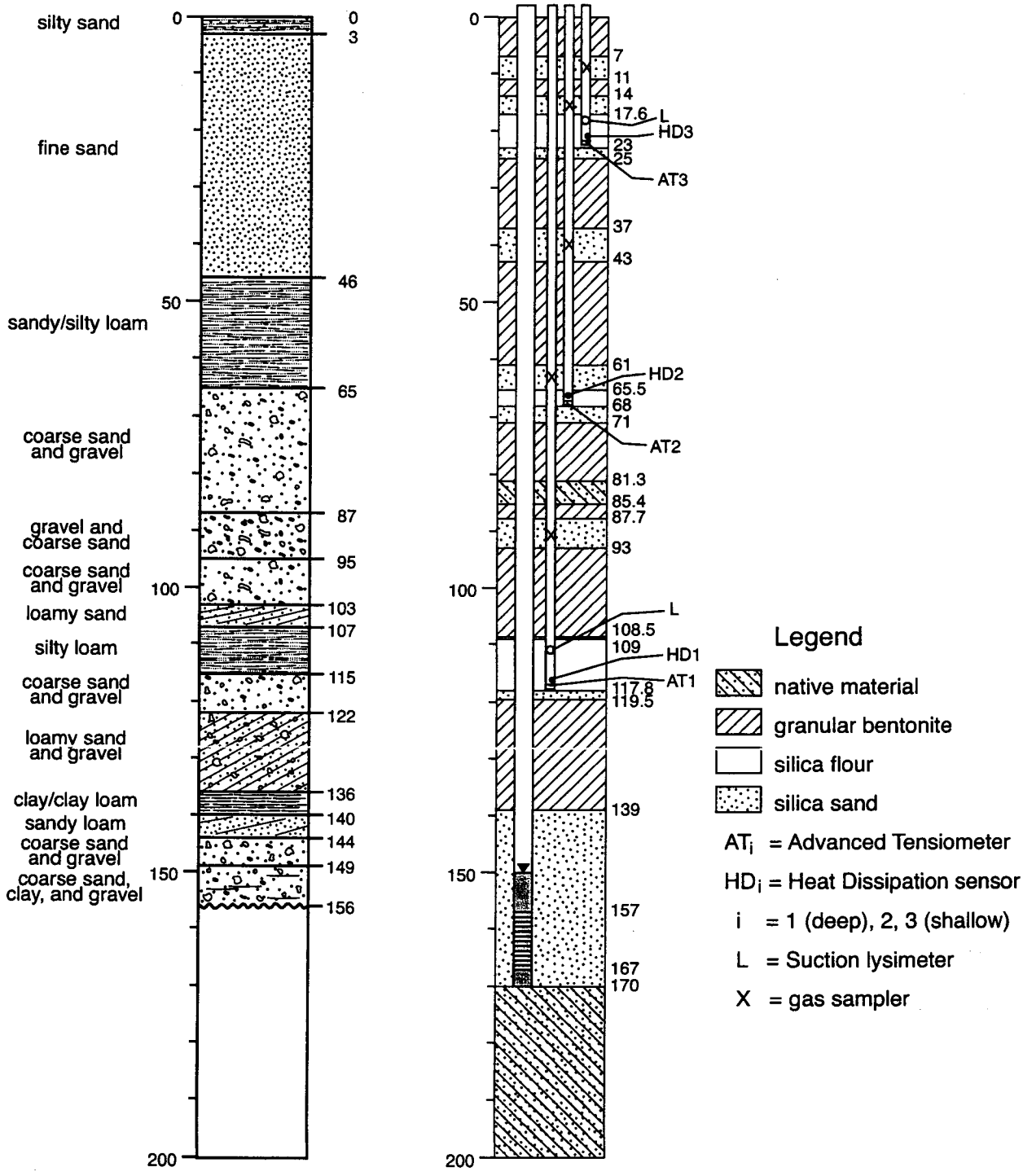

Figure 17

Site 2 (Finney County, KS; T. 26 S.-R. 31 W.-31 CCD)

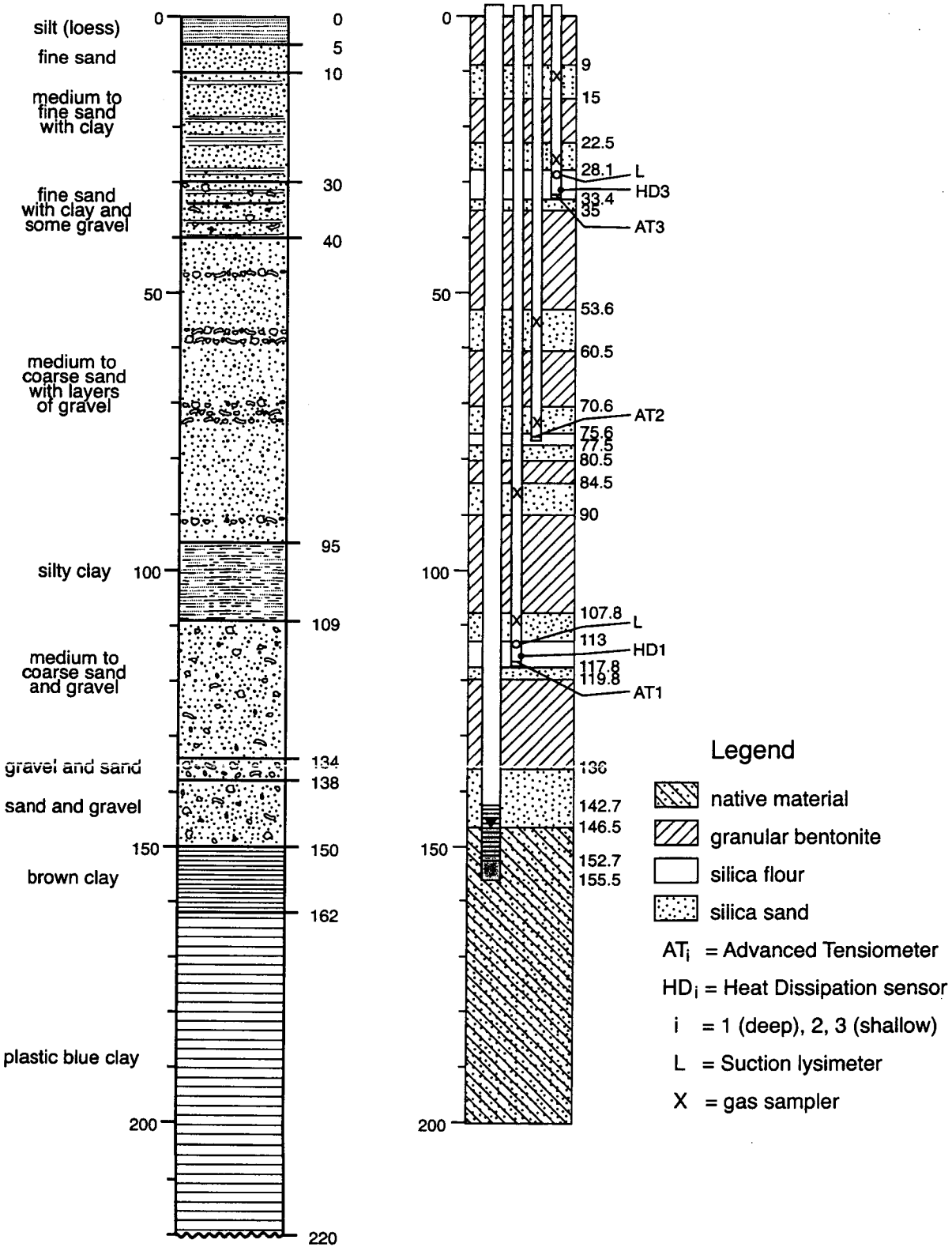

Figure 18

Site 3 (Morton County, KS; T. 34 S.-R. 41 W.-25ADA)

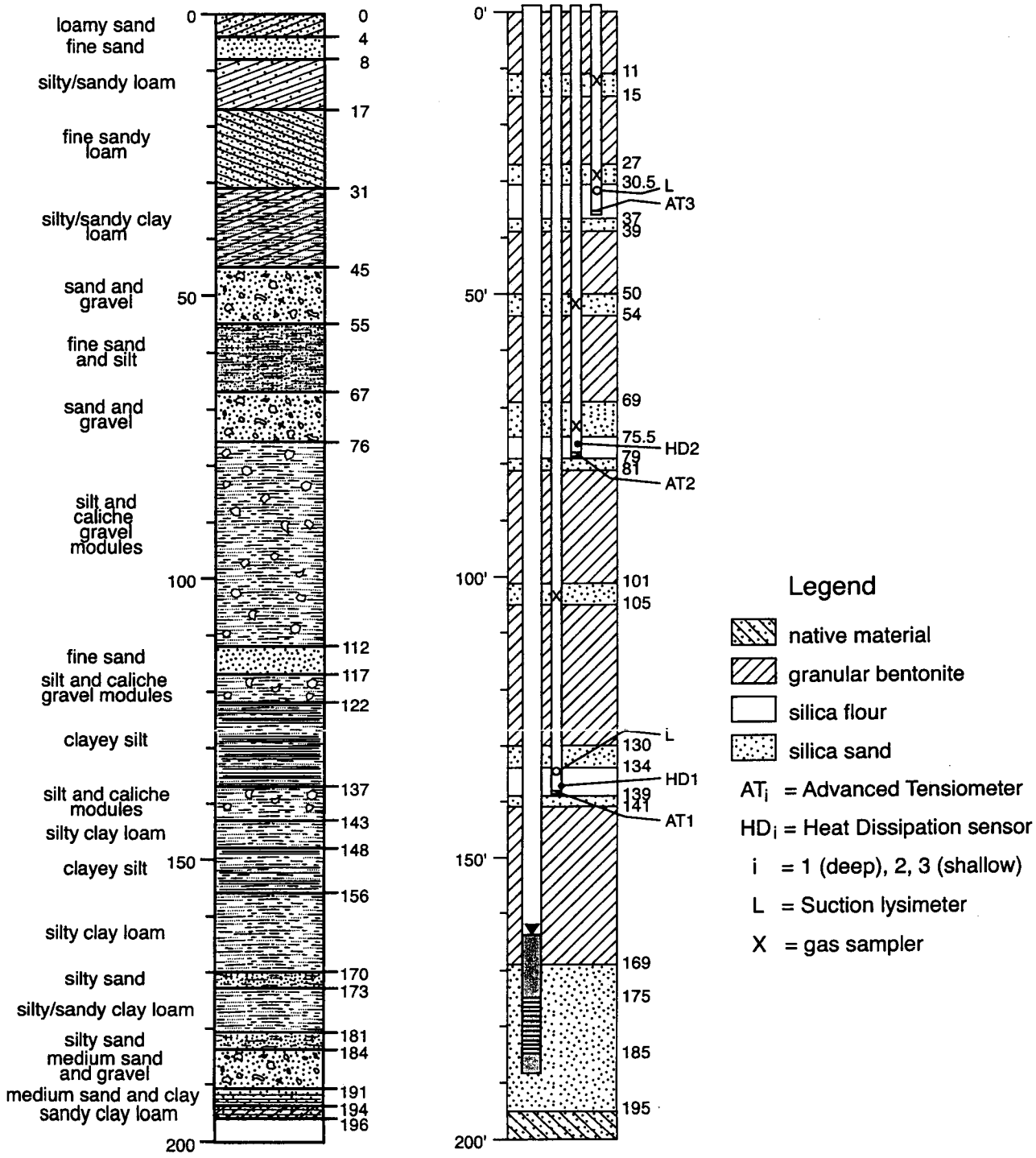

Figure 19

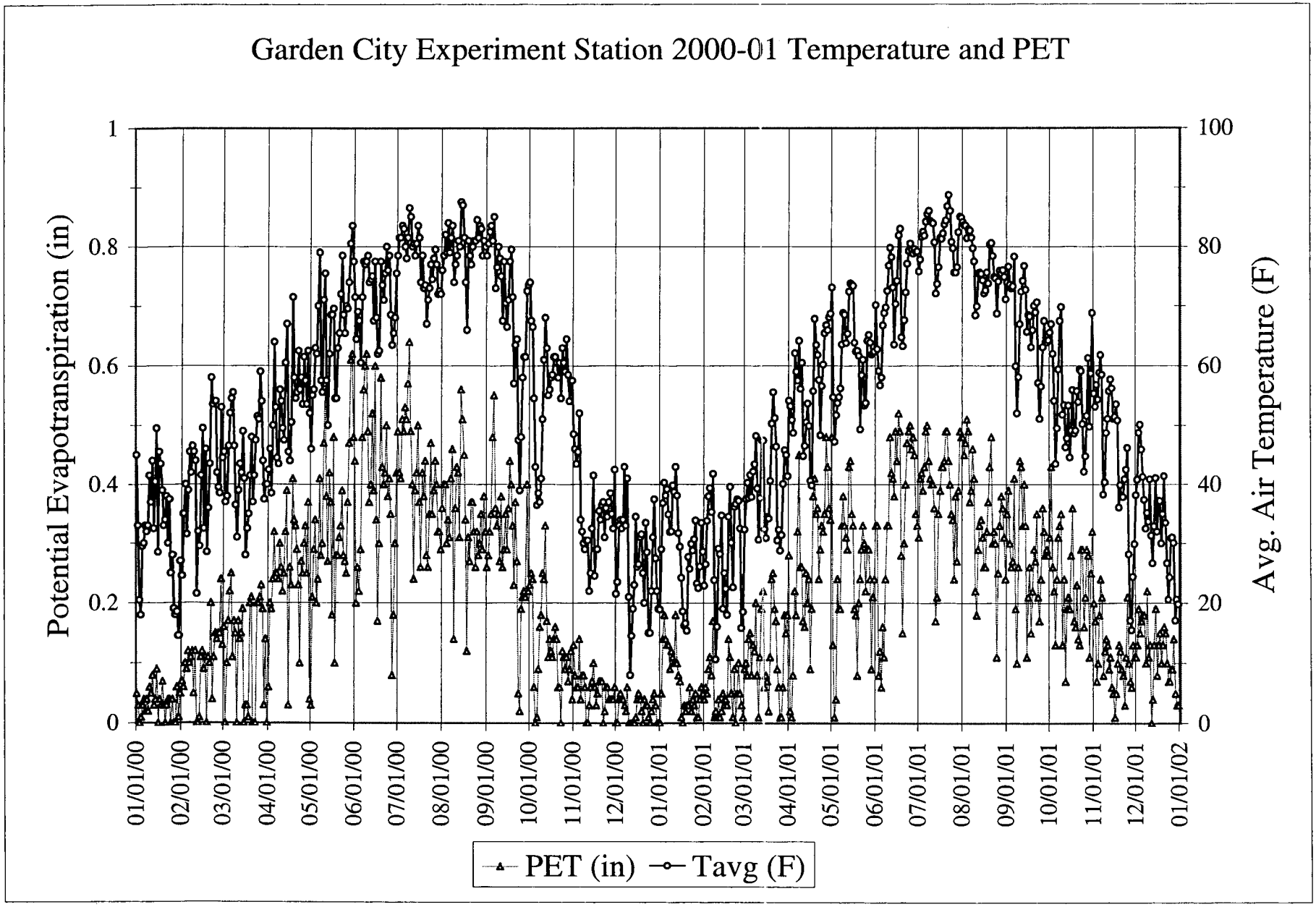
Garden City Experiment Station 2000-01 Temperature and PET
Potential Evapotranspiration (in)
Avg. Air Temperature (F)
1
0.8
0.6
0.4
0.2
0
100
80
60
40
20
0
01/01/00
02/01/00
03/01/00
04/01/00
05/01/00
06/01/00
07/01/00
08/01/00
09/01/00
10/01/00
11/01/00
12/01/00
01/01/01
02/01/01
03/01/01
04/01/01
05/01/01
06/01/01
07/01/01
08/01/01
09/01/01
10/01/01
11/01/01
12/01/01
01/01/02
PET (in)
Tavg (F)

Figure 20

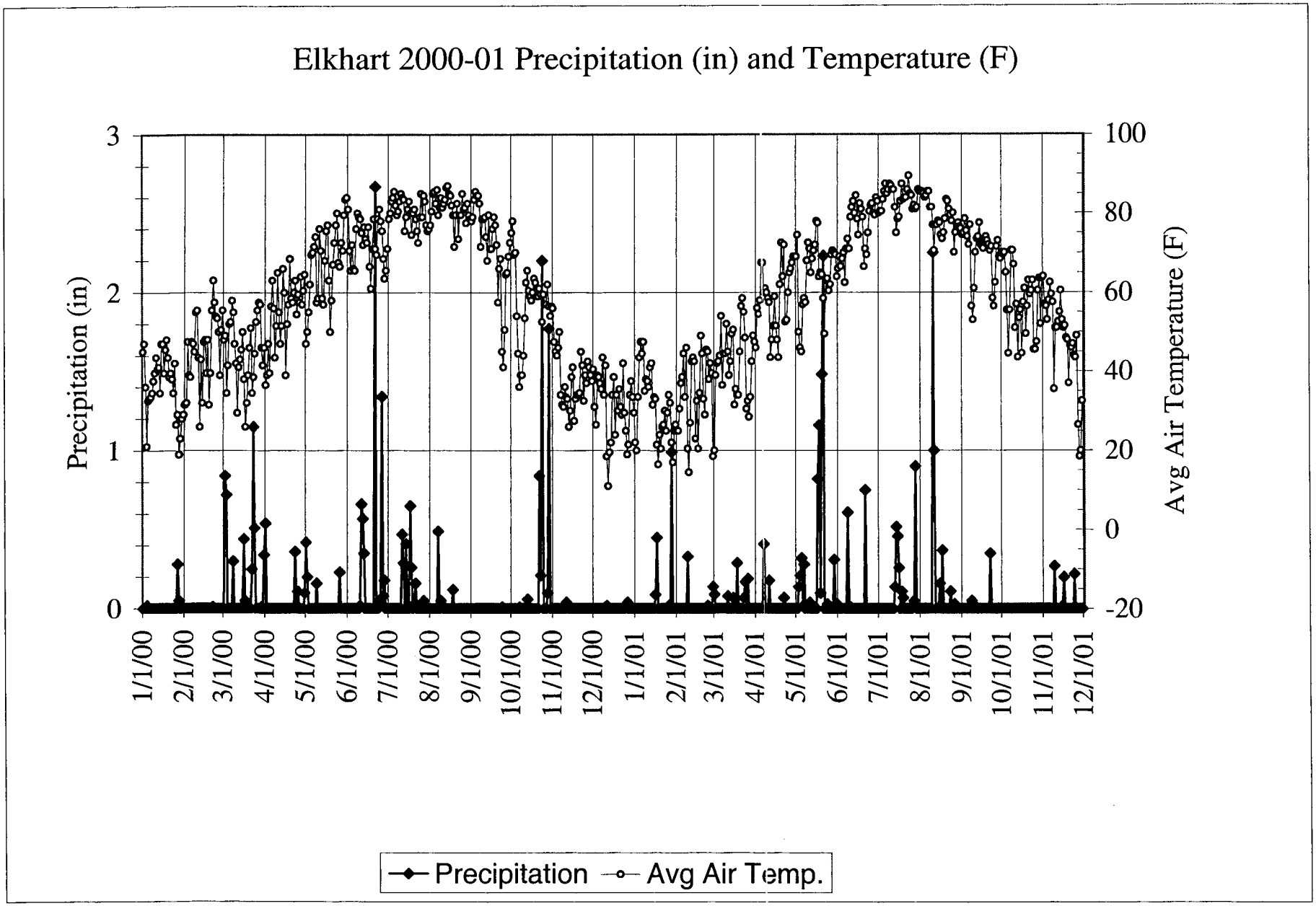
Elkhart 2000-01 Precipitation (in) and Temperature (F)
Precipitation (in)
Avg Air Temperature (F)
3
2
1
0
100
80
60
40
20
0
-20
1/1/00
2/1/00
3/1/00
4/1/00
5/1/00
6/1/00
7/1/00
8/1/00
9/1/00
10/1/00
11/1/00
12/1/00
1/1/01
2/1/01
3/1/01
4/1/01
5/1/01
6/1/01
7/1/01
8/1/01
9/1/01
10/1/01
11/1/01
12/1/01
Precipitation
Avg Air Temp.

Figure 21

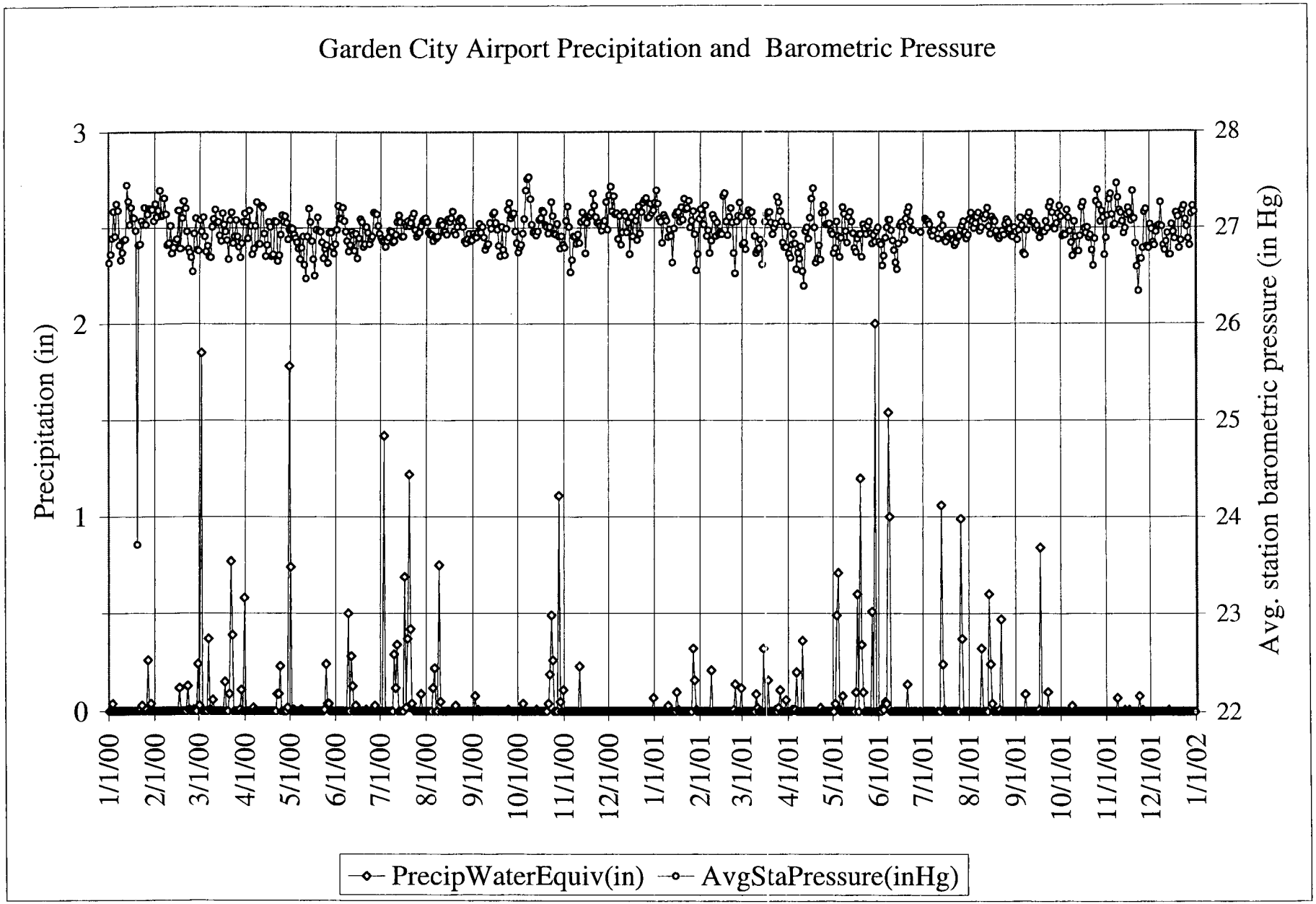
Garden City Airport Precipitation and Barometric Pressure
Precipitation (in)
Avg. station barometric pressure (in Hg)
3
2
1
0
28
27
26
25
24
23
22
1/1/00
2/1/00
3/1/00
4/1/00
5/1/00
6/1/00
7/1/00
8/1/00
9/1/00
10/1/00
11/1/00
12/1/00
1/1/01
2/1/01
3/1/01
4/1/01
5/1/01
6/1/01
7/1/01
8/1/01
9/1/01
10/1/01
11/1/01
12/1/01
1/1/02
PrecipWaterEquiv(in)
AvgStaPressure(inHg)

Figure 22

A

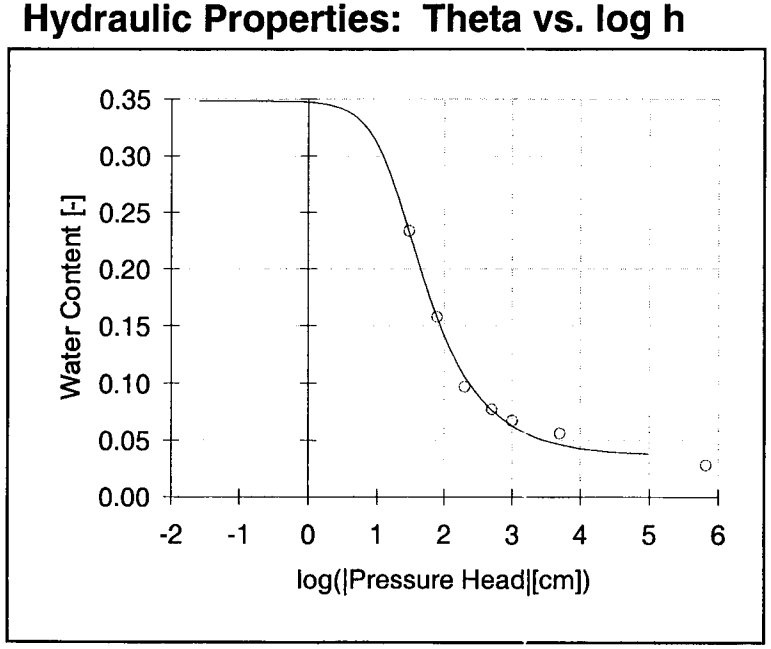
Hydraulic Properties: Theta vs. log h
Water Content [-]
0.35
0.30
0.25
0.20
0.15
0.10
0.05
0.00
-2
-1
0
1
2
3
4
5
6
log(|Pressure Head|[cm])

Figure 23a

B

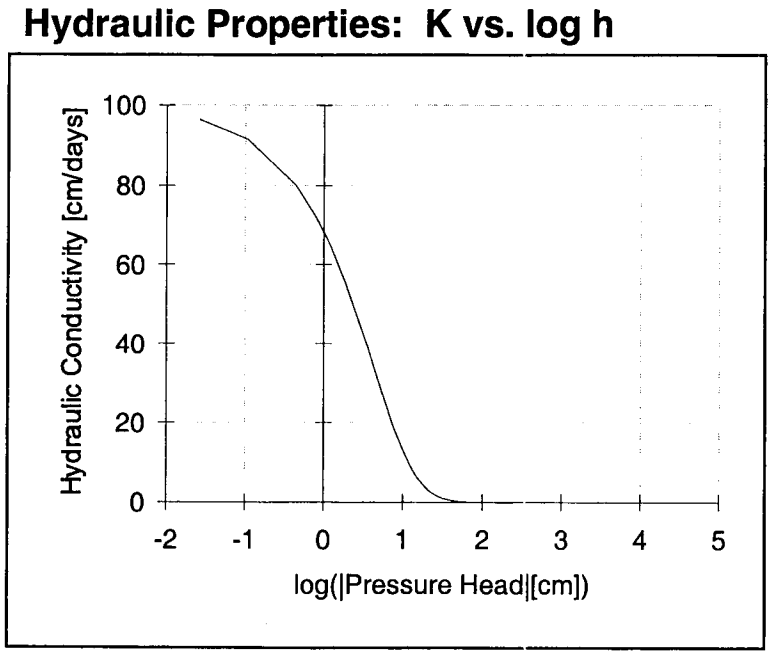
Hydraulic Properties: K vs. log h
Hydraulic Conductivity [cm/days]
100
80
60
40
20
0
-2
-1
0
1
2
3
4
5
log(|Pressure Head|[cm])

Figure 23b

C

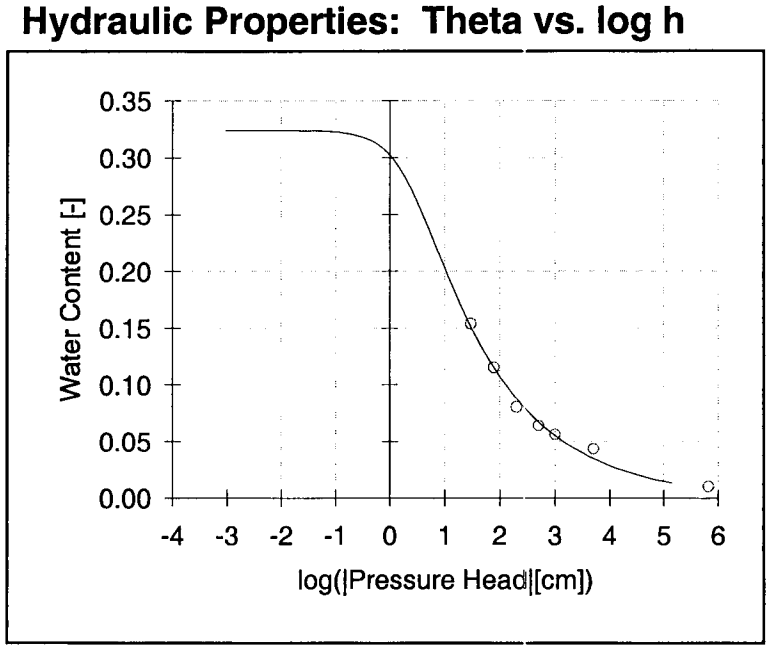
Hydraulic Properties: Theta vs. log h
Water Content [-]
0.35
0.30
0.25
0.20
0.15
0.10
0.05
0.00
-4
-3
-2
-1
0
1
2
3
4
5
6
log(|Pressure Head|[cm])

Figure 23c

D

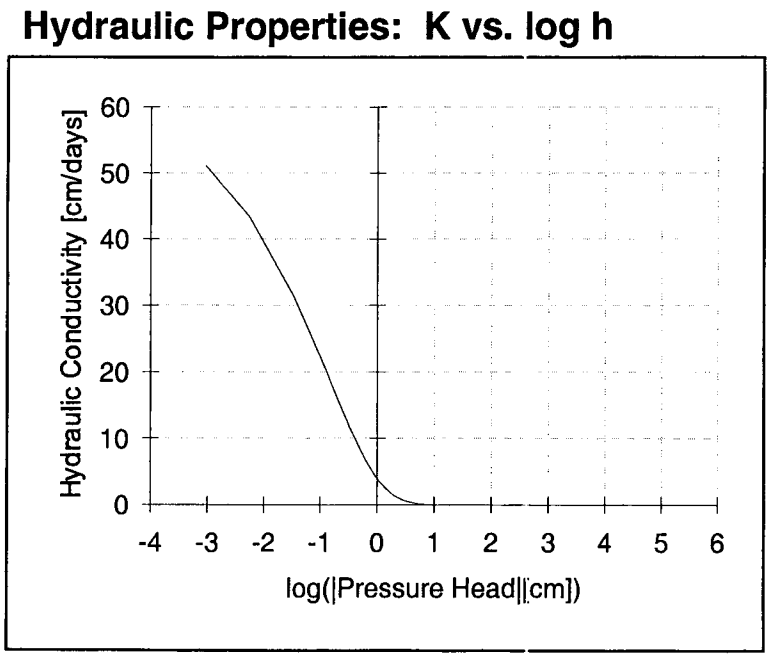
Hydraulic Properties: K vs. log h
Hydraulic Conductivity [cm/days]
60
50
40
30
20
10
0
-4
-3
-2
-1
0
1
2
3
4
5
6
log(|Pressure Head|[cm])

Figure 23d

A

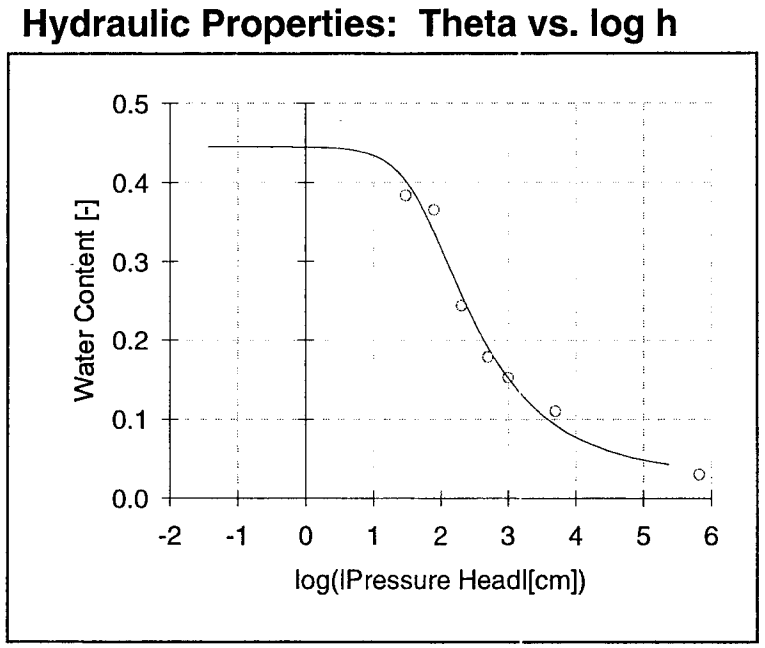
Hydraulic Properties: Theta vs. log h
Water Content [-]
0.5
0.4
0.3
0.2
0.1
0.0
-2
-1
0
1
2
3
4
5
6
log(|Pressure Head|[cm])

Figure 24a

B

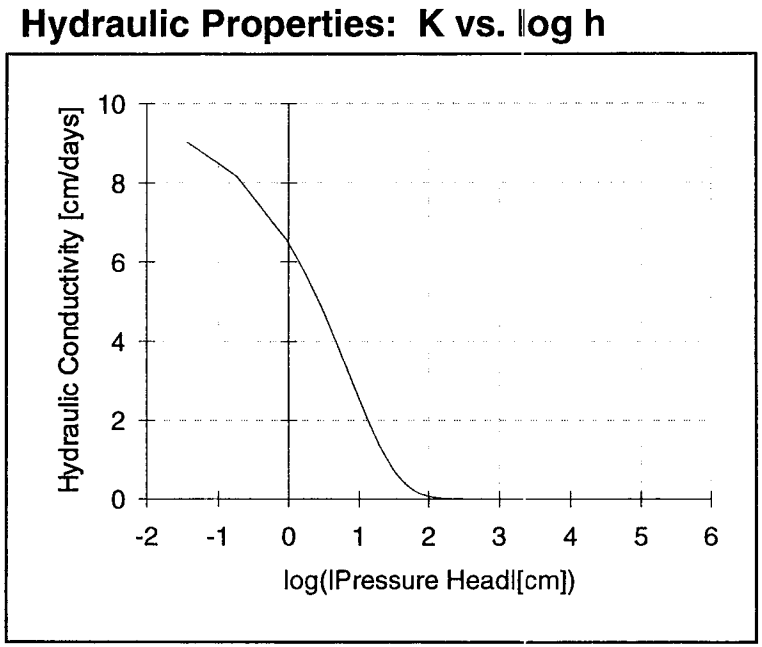
Hydraulic Properties: K vs. log h
Hydraulic Conductivity [cm/days]
10
8
6
4
2
0
-2
-1
0
1
2
3
4
5
6
log(|Pressure Head|[cm])

Figure 24b

C

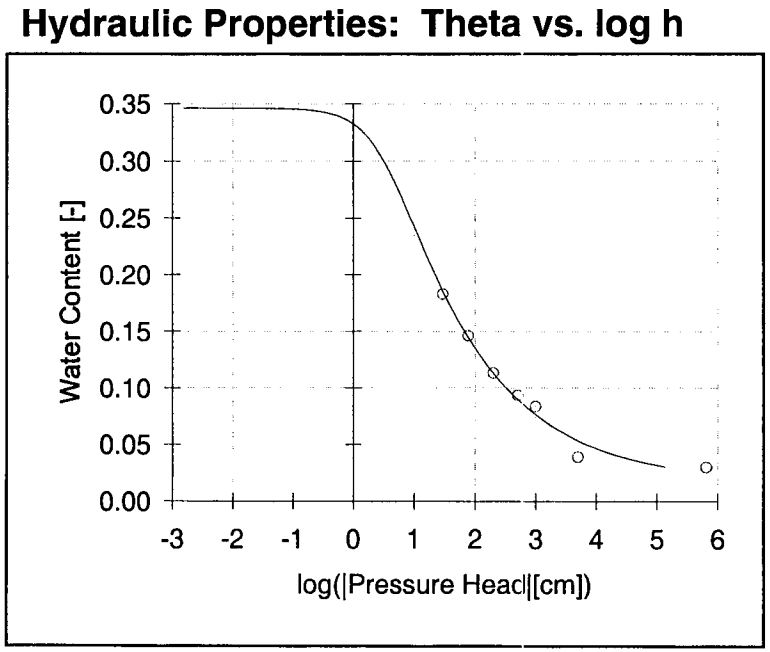
Hydraulic Properties: Theta vs. log h
Water Content [-]
0.35
0.30
0.25
0.20
0.15
0.10
0.05
0.00
-3
-2
-1
0
1
2
3
4
5
6
log(|Pressure Head|[cm])

Figure 24c

D

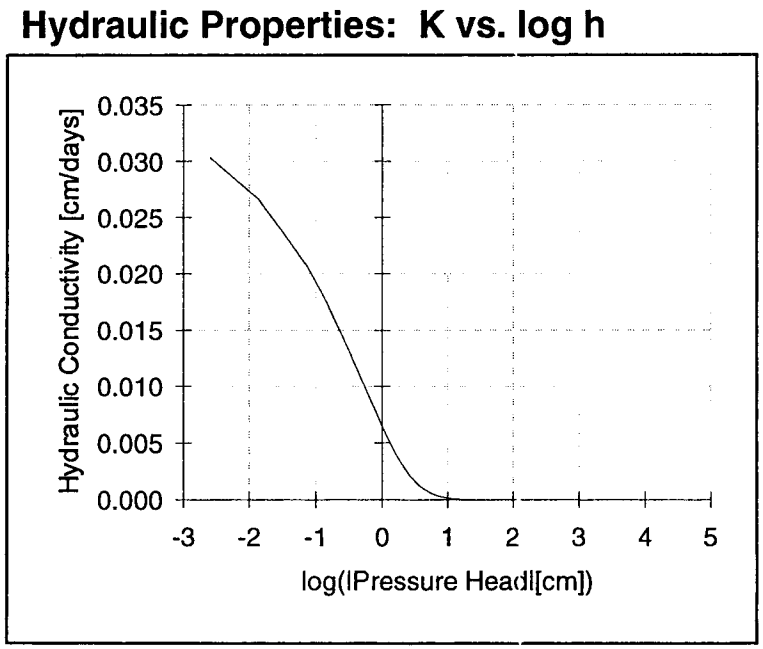
Hydraulic Properties: K vs. log h
Hydraulic Conductivity [cm/days]
0.035
0.030
0.025
0.020
0.015
0.010
0.005
0.000
-3
-2
-1
0
1
2
3
4
5
log(|Pressure Head|[cm])

Figure 24d

A

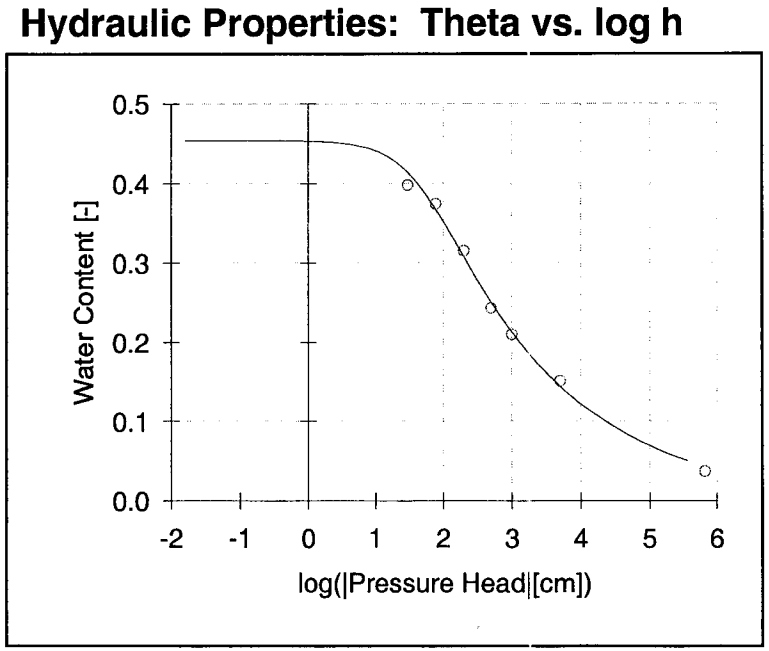
Hydraulic Properties: Theta vs. log h
Water Content [-]
0.5
0.4
0.3
0.2
0.1
0.0
-2
-1
0
1
2
3
4
5
6
log(|Pressure Head|[cm])

Figure 25a

B

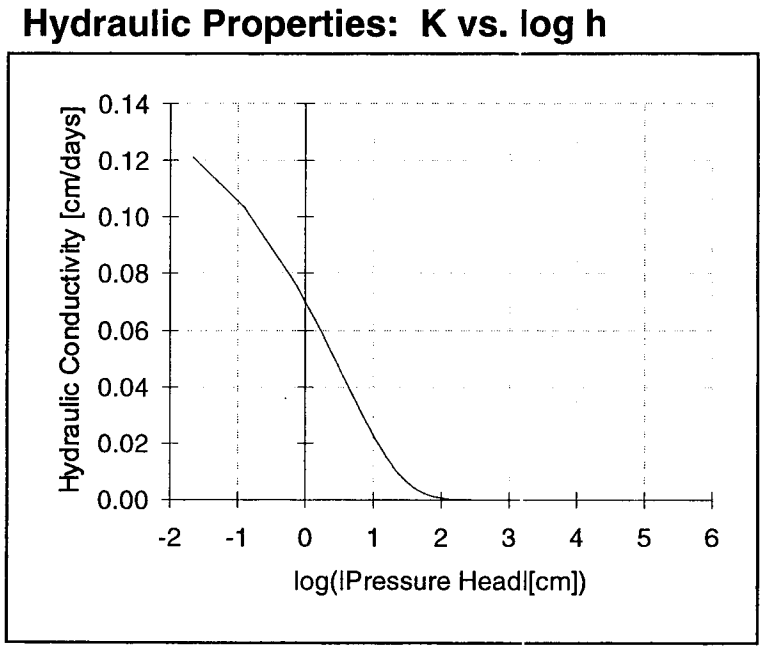
Hydraulic Properties: K vs. log h
Hydraulic Conductivity [cm/days]
0.14
0.12
0.10
0.08
0.06
0.04
0.02
0.00
-2
-1
0
1
2
3
4
5
6
log(|Pressure Head|[cm])

Figure 25b

C

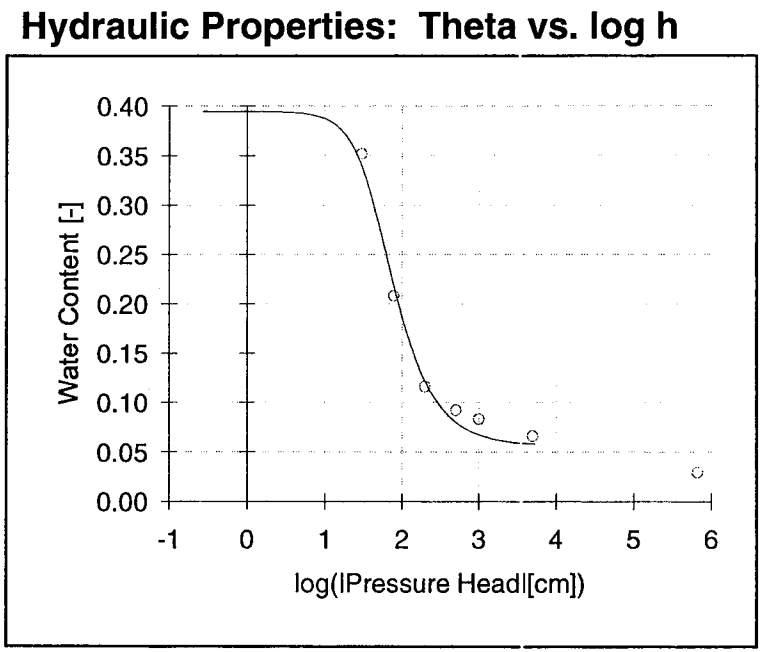
Hydraulic Properties: Theta vs. log h
Water Content [-]
0.40
0.35
0.30
0.25
0.20
0.15
0.10
0.05
0.00
-1
0
1
2
3
4
5
6
log(|Pressure Head|[cm])

Figure 25c

D

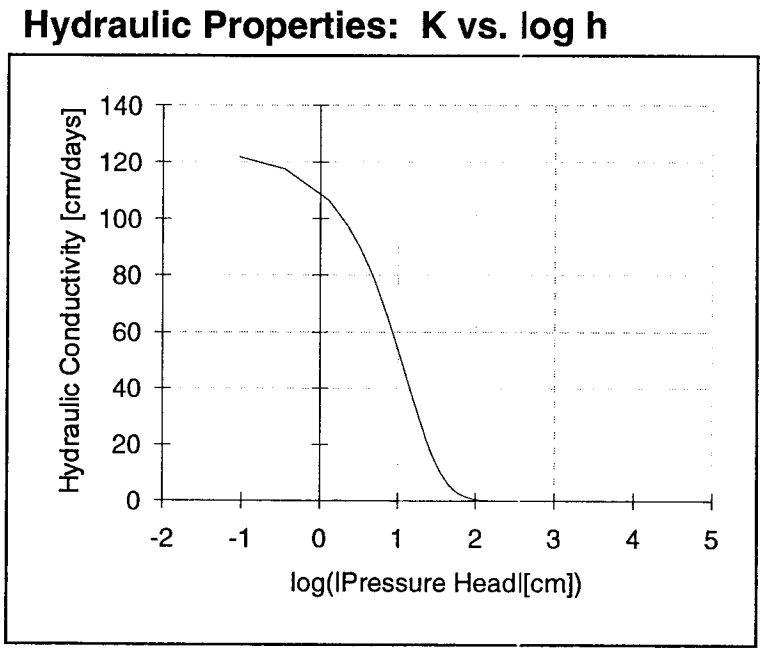
Hydraulic Properties: K vs. log h
Hydraulic Conductivity [cm/days]
140
120
100
80
60
40
20
0
-2
-1
0
1
2
3
4
5
log(|Pressure Head|[cm])

Figure 25d

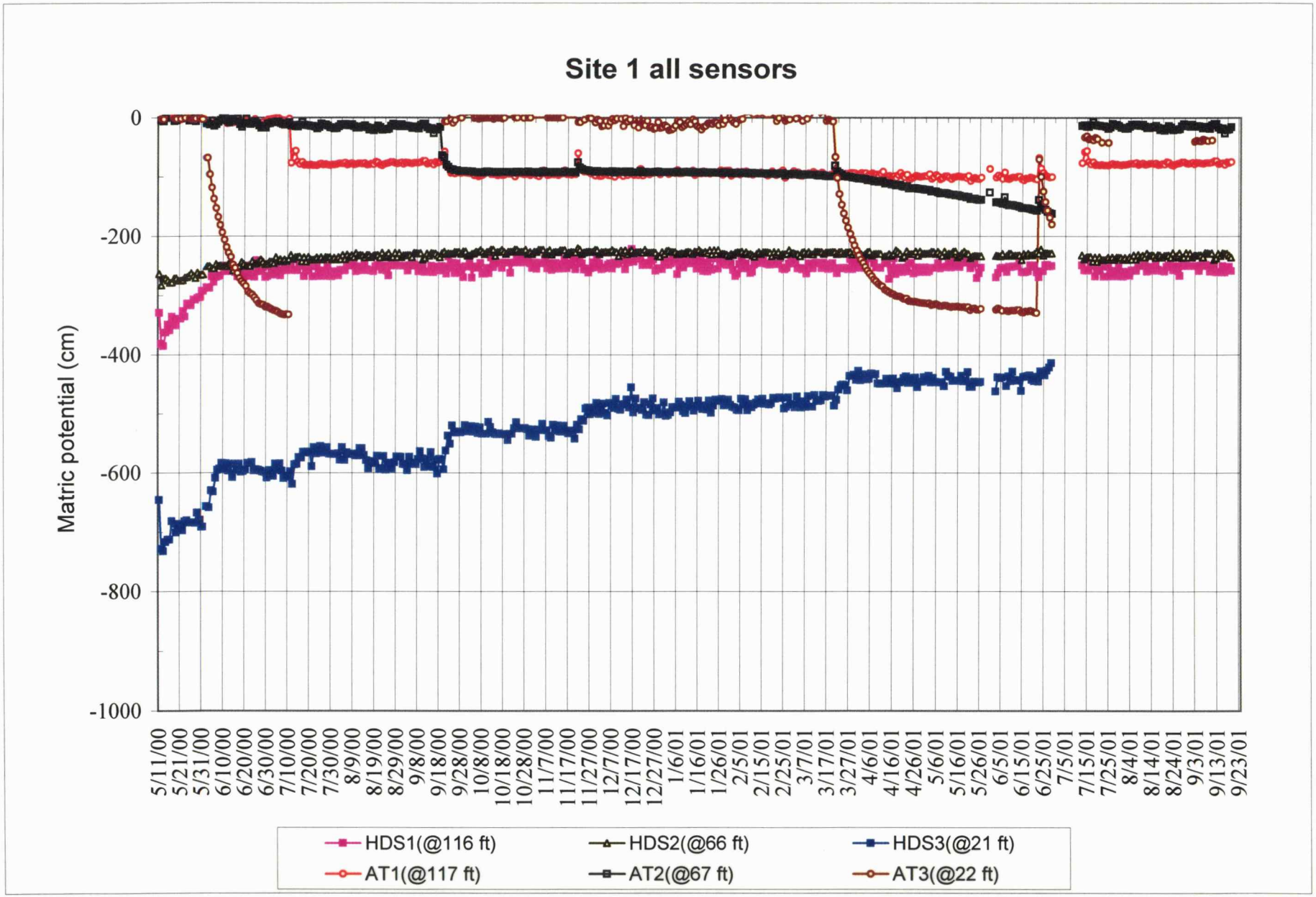
Site 1 all sensors
Matric potential (cm)
0
-200
-400
-600
-800
-1000
5/11/00
5/21/00
5/31/00
6/10/00
6/20/00
6/30/00
7/10/00
7/20/00
7/30/00
8/9/00
8/19/00
8/29/00
9/8/00
9/18/00
9/28/00
10/8/00
10/18/00
10/28/00
11/7/00
11/17/00
11/27/00
12/7/00
12/17/00
12/27/00
1/6/01
1/16/01
1/26/01
2/5/01
2/15/01
2/25/01
3/7/01
3/17/01
3/27/01
4/6/01
4/16/01
4/26/01
5/6/01
5/16/01
5/26/01
6/5/01
6/15/01
6/25/01
7/5/01
7/15/01
7/25/01
8/4/01
8/14/01
8/24/01
9/3/01
9/13/01
9/23/01
HDS1(@116 ft)
HDS2(@66 ft)
HDS3(@21 ft)
AT1(@117 ft)
AT2(@67 ft)
AT3(@22 ft)

Figure 26a

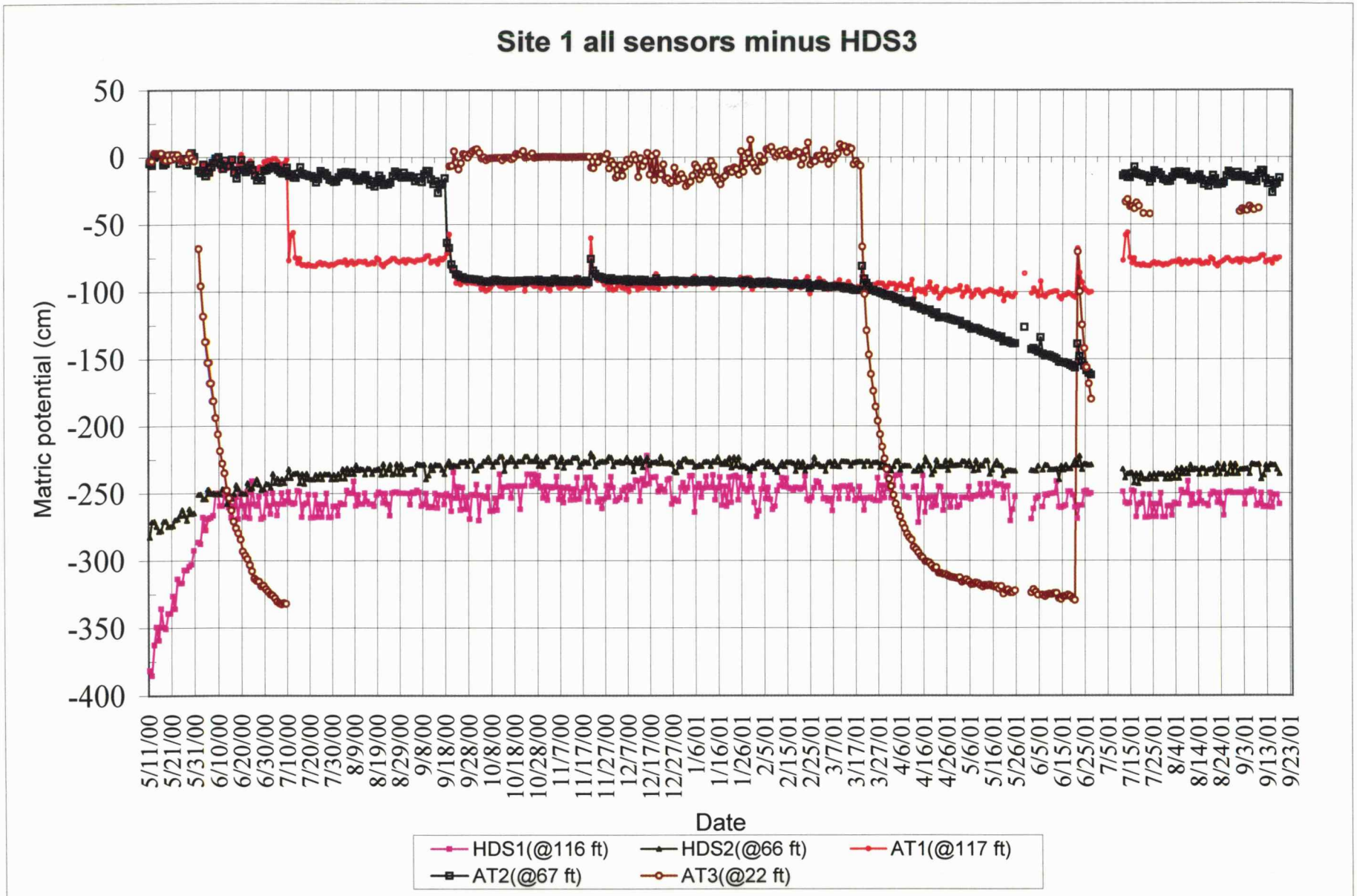
Site 1 all sensors minus HDS3
Matric potential (cm)
50
0
-50
-100
-150
-200
-250
-300
-350
-400
5/11/00
5/21/00
5/31/00
6/10/00
6/20/00
6/30/00
7/10/00
7/20/00
7/30/00
8/9/00
8/19/00
8/29/00
9/8/00
9/18/00
9/28/00
10/8/00
10/18/00
10/28/00
11/7/00
11/17/00
11/27/00
12/7/00
12/17/00
12/27/00
1/6/01
1/16/01
1/26/01
2/5/01
2/15/01
2/25/01
3/7/01
3/17/01
3/27/01
4/6/01
4/16/01
4/26/01
5/6/01
5/16/01
5/26/01
6/5/01
6/15/01
6/25/01
7/5/01
7/15/01
7/25/01
8/4/01
8/14/01
8/24/01
9/3/01
9/13/01
9/23/01
Date
HDS1(@116 ft)
HDS2(@66 ft)
AT1(@117 ft)
AT2(@67 ft)
AT3(@22 ft)

Figure 26b

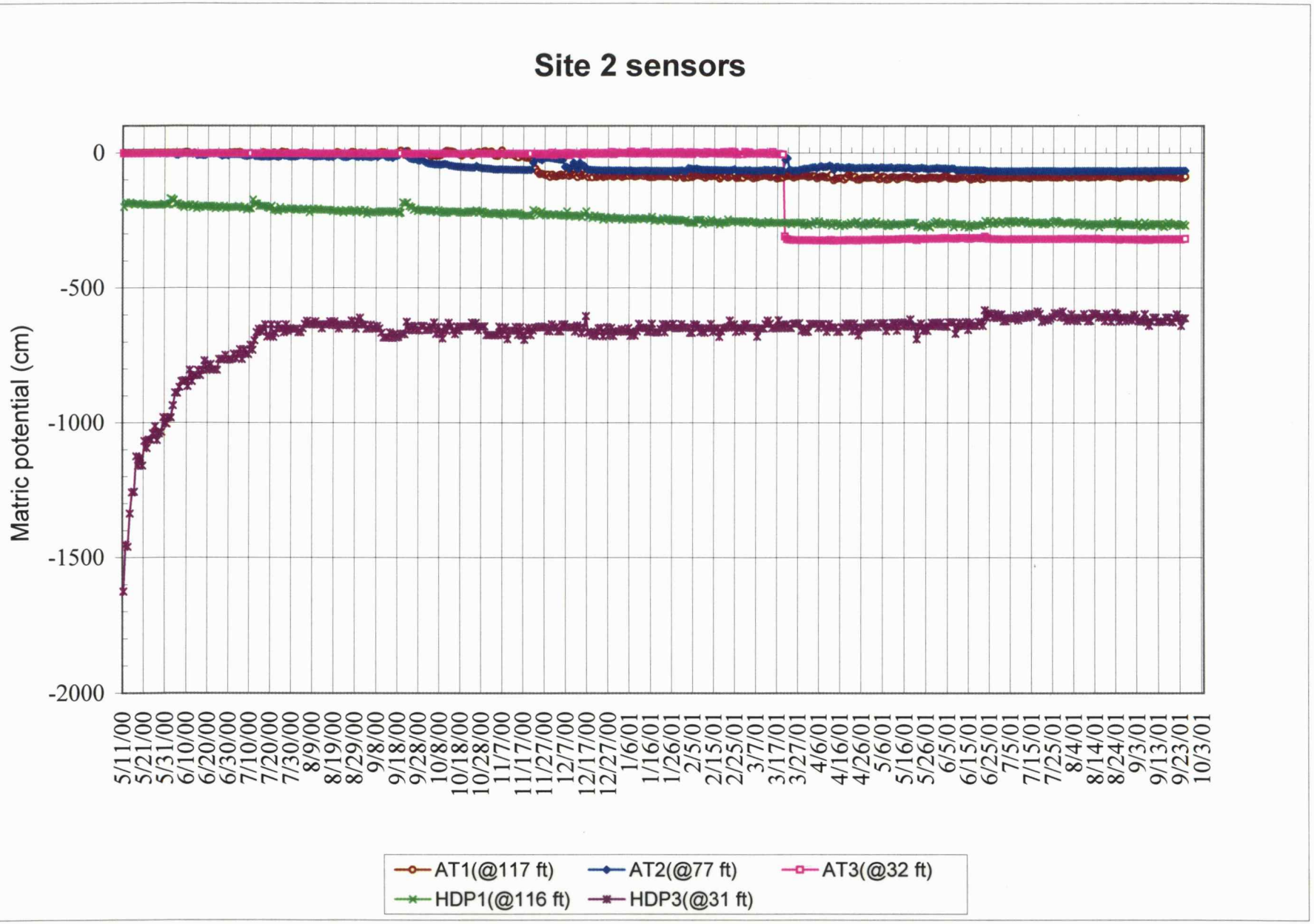
Site 2 sensors
Matric potential (cm)
0
-500
-1000
-1500
-2000
5/11/00
5/21/00
5/31/00
6/10/00
6/20/00
6/30/00
7/10/00
7/20/00
7/30/00
8/9/00
8/19/00
8/29/00
9/8/00
9/18/00
9/28/00
10/8/00
10/18/00
10/28/00
11/7/00
11/17/00
11/27/00
12/7/00
12/17/00
12/27/00
1/6/01
1/16/01
1/26/01
2/5/01
2/15/01
2/25/01
3/7/01
3/17/01
3/27/01
4/6/01
4/16/01
4/26/01
5/6/01
5/16/01
5/26/01
6/5/01
6/15/01
6/25/01
7/5/01
7/15/01
7/25/01
8/4/01
8/14/01
8/24/01
9/3/01
9/13/01
9/23/01
10/3/01
AT1(@117 ft)
AT2(@77 ft)
AT3(@32 ft)
HDP1(@116 ft)
HDP3(@31 ft)

Figure 27a

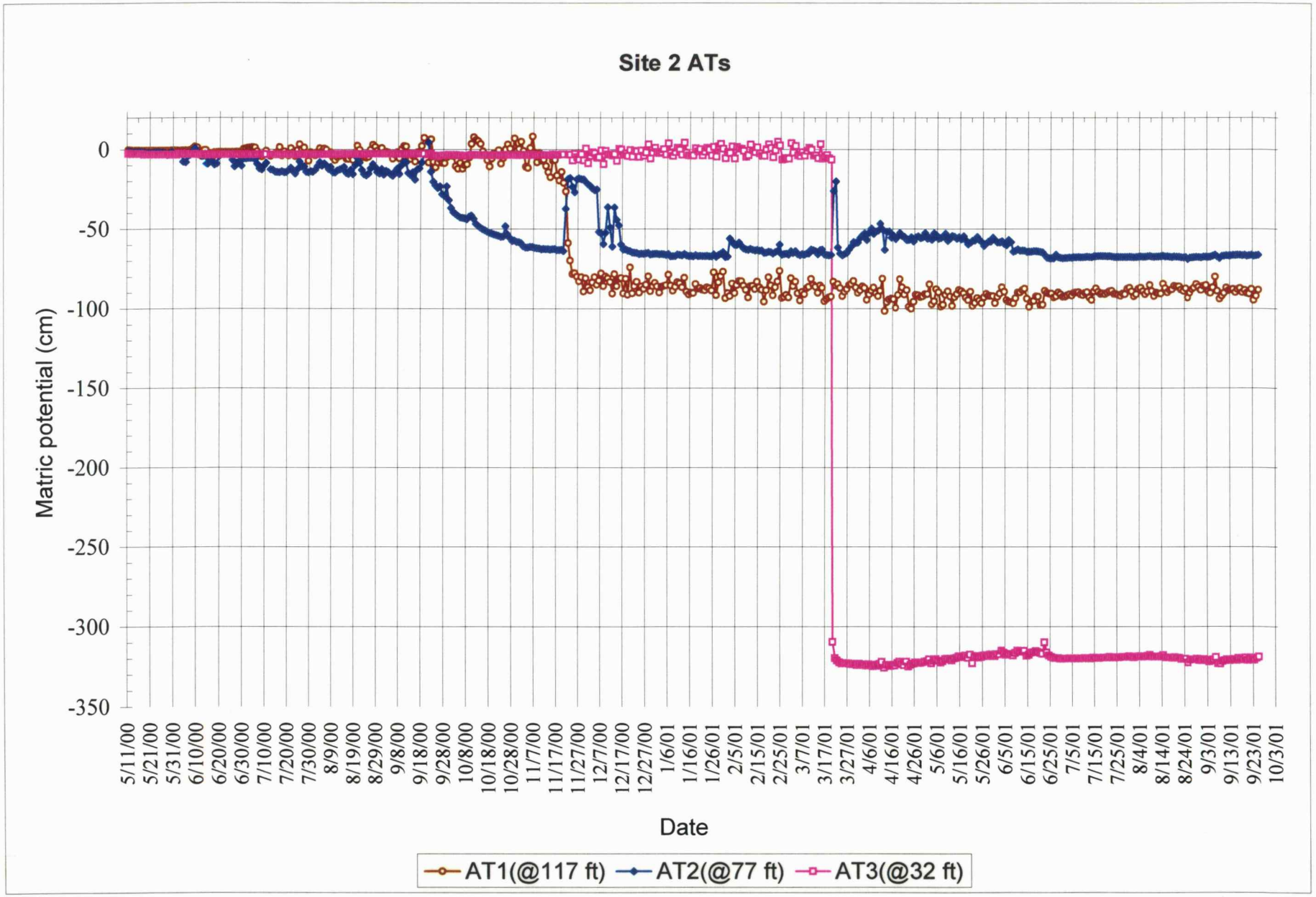
Site 2 ATs
Matric potential (cm)
0
-50
-100
-150
-200
-250
-300
-350
5/11/00
5/21/00
5/31/00
6/10/00
6/20/00
6/30/00
7/10/00
7/20/00
7/30/00
8/9/00
8/19/00
8/29/00
9/8/00
9/18/00
9/28/00
10/8/00
10/18/00
10/28/00
11/7/00
11/17/00
11/27/00
12/7/00
12/17/00
12/27/00
1/6/01
1/16/01
1/26/01
2/5/01
2/15/01
2/25/01
3/7/01
3/17/01
3/27/01
4/6/01
4/16/01
4/26/01
5/6/01
5/16/01
5/26/01
6/5/01
6/15/01
6/25/01
7/5/01
7/15/01
7/25/01
8/4/01
8/14/01
8/24/01
9/3/01
9/13/01
9/23/01
10/3/01
Date
AT1(@117 ft)
AT2(@77 ft)
AT3(@32 ft)

Figure 27b

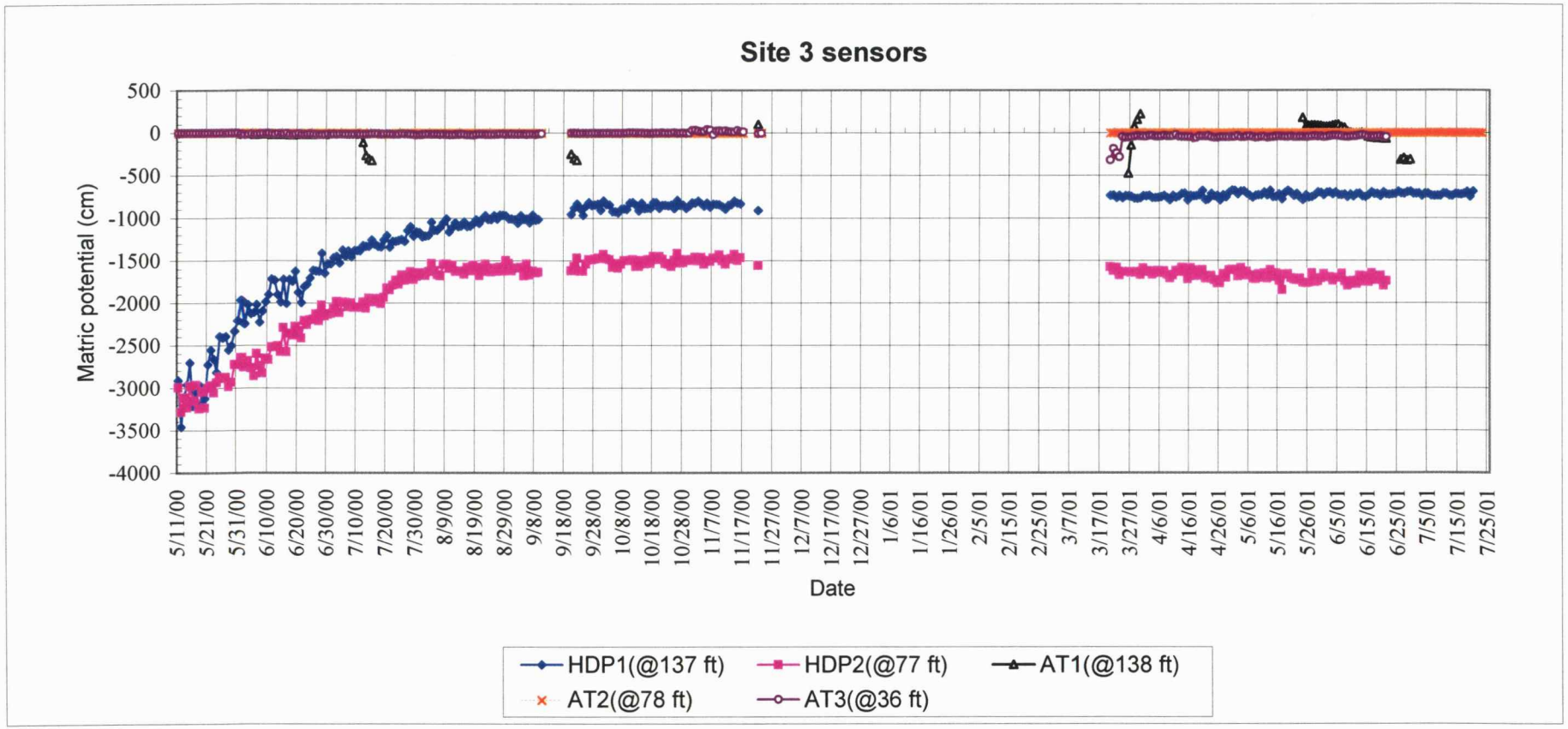
Site 3 sensors
Matric potential (cm)
500
0
-500
-1000
-1500
-2000
-2500
-3000
-3500
-4000
5/11/00
5/21/00
5/31/00
6/10/00
6/20/00
6/30/00
7/10/00
7/20/00
7/30/00
8/9/00
8/19/00
8/29/00
9/8/00
9/18/00
9/28/00
10/8/00
10/18/00
10/28/00
11/7/00
11/17/00
11/27/00
12/7/00
12/17/00
12/27/00
1/6/01
1/16/01
1/26/01
2/5/01
2/15/01
2/25/01
3/7/01
3/17/01
3/27/01
4/6/01
4/16/01
4/26/01
5/6/01
5/16/01
5/26/01
6/5/01
6/15/01
6/25/01
7/5/01
7/15/01
7/25/01
Date
HDP1(@137 ft)
HDP2(@77 ft)
AT1(@138 ft)
AT2(@78 ft)
AT3(@36 ft)

Figure 28

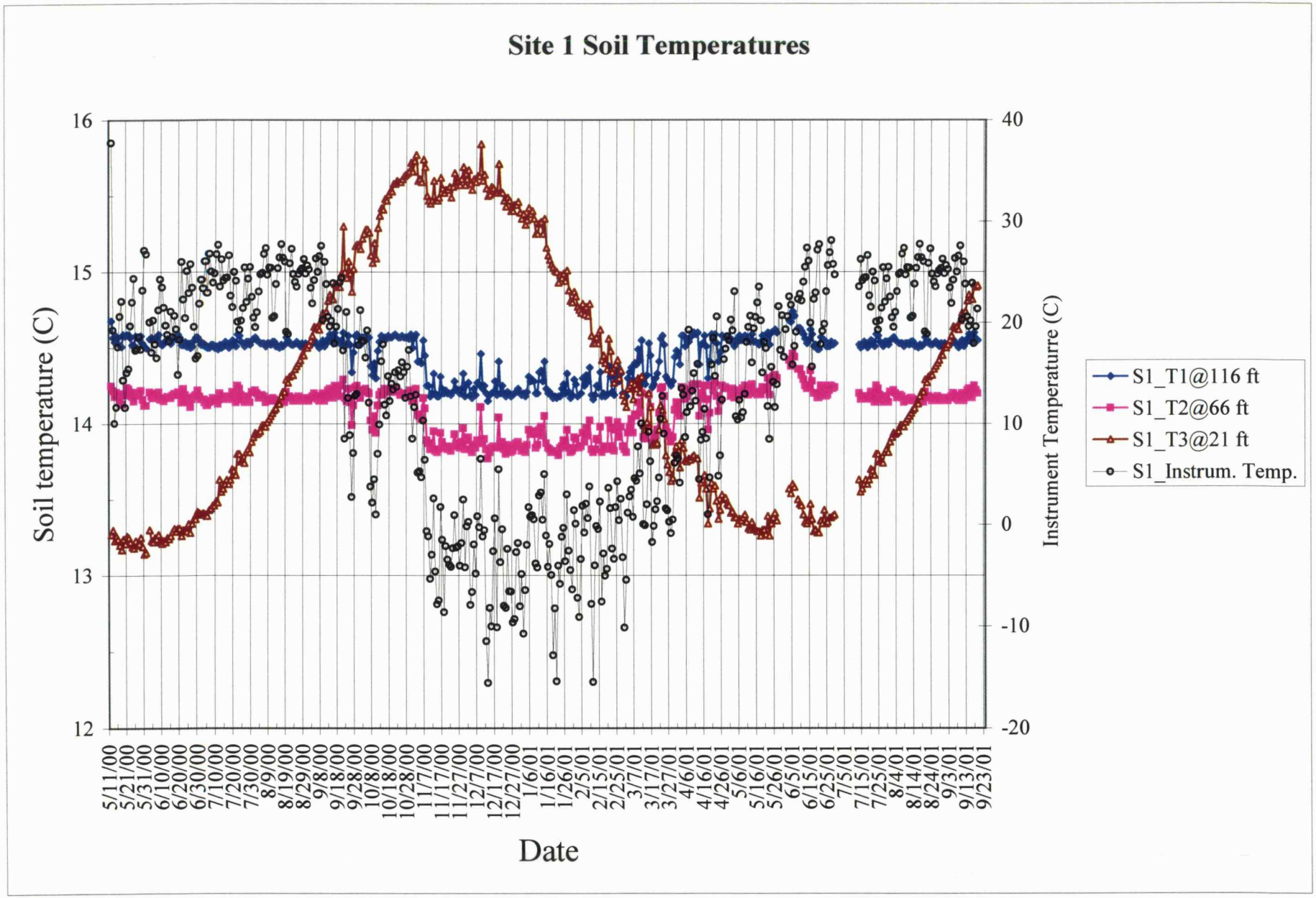
Site 1 Soil Temperatures
Soil temperature (C)
Instrument Temperaturre (C)
Date
16
15
14
13
12
40
30
20
10
0
-10
-20
S1_T1@116 ft
S1_T2@66 ft
S1_T3@21 ft
S1_Instrum. Temp.
5/11/00
5/21/00
5/31/00
6/10/00
6/20/00
6/30/00
7/10/00
7/20/00
7/30/00
8/9/00
8/19/00
8/29/00
9/8/00
9/18/00
9/28/00
10/8/00
10/18/00
10/28/00
11/7/00
11/17/00
11/27/00
12/7/00
12/17/00
12/27/00
1/6/01
1/16/01
1/26/01
2/5/01
2/15/01
2/25/01
3/7/01
3/17/01
3/27/01
4/6/01
4/16/01
4/26/01
5/6/01
5/16/01
5/26/01
6/5/01
6/15/01
6/25/01
7/5/01
7/15/01
7/25/01
8/4/01
8/14/01
8/24/01
9/3/01
9/13/01
9/23/01

Figure 29

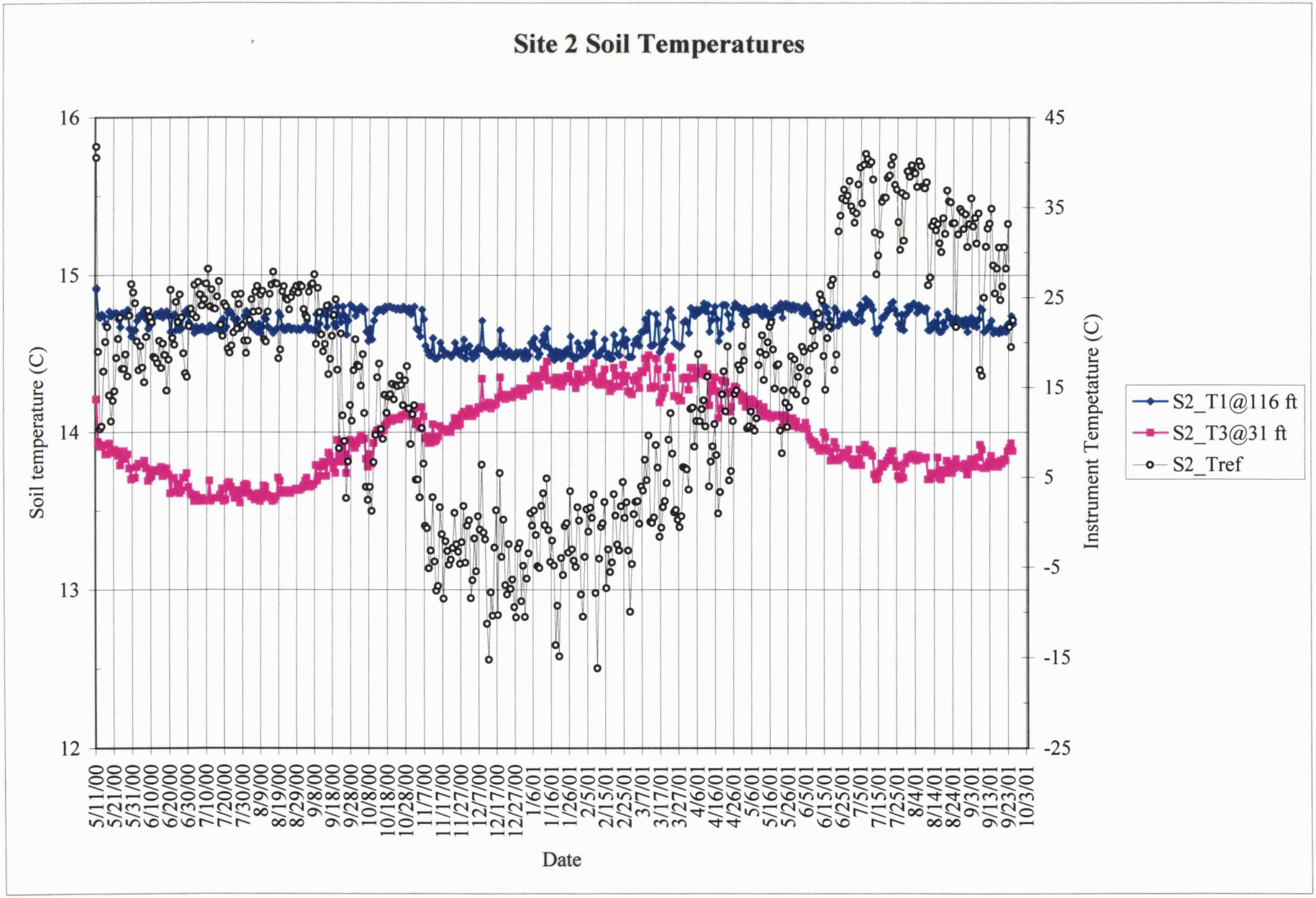
Site 2 Soil Temperatures
Soil temperature (C)
Instrument Tempetature (C)
Date
S2_T1@116 ft
S2_T3@31 ft
S2_Tref
16
15
14
13
12
45
35
25
15
5
-5
-15
-25
5/11/00
5/21/00
5/31/00
6/10/00
6/20/00
6/30/00
7/10/00
7/20/00
7/30/00
8/9/00
8/19/00
8/29/00
9/8/00
9/18/00
9/28/00
10/8/00
10/18/00
10/28/00
11/7/00
11/17/00
11/27/00
12/7/00
12/17/00
12/27/00
1/6/01
1/16/01
1/26/01
2/5/01
2/15/01
2/25/01
3/7/01
3/17/01
3/27/01
4/6/01
4/16/01
4/26/01
5/6/01
5/16/01
5/26/01
6/5/01
6/15/01
6/25/01
7/5/01
7/15/01
7/25/01
8/4/01
8/14/01
8/24/01
9/3/01
9/13/01
9/23/01
10/3/01

Figure 30

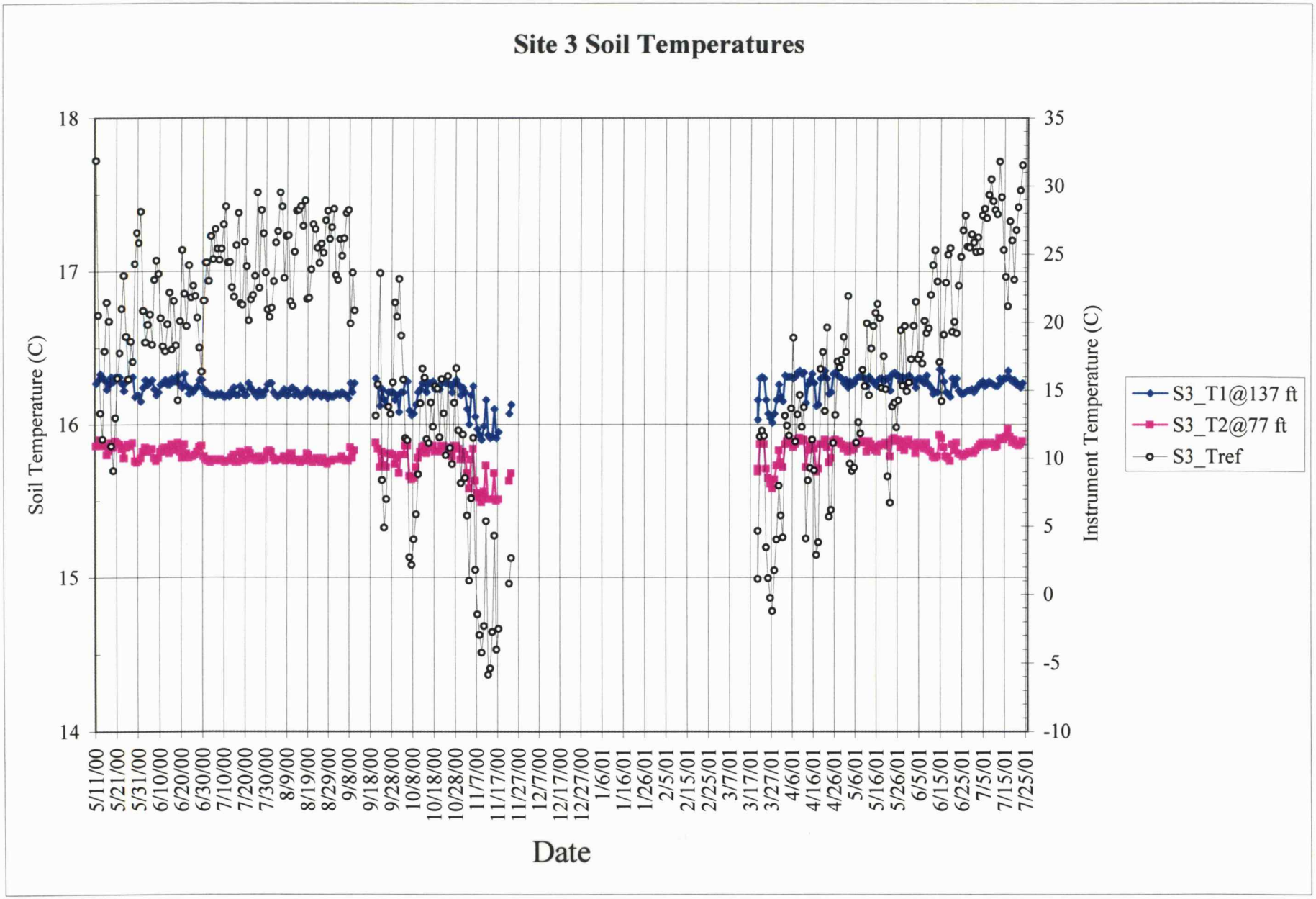
Site 3 Soil Temperatures
Soil Temperature (C)
Instrument Temperature (C)
Date
S3_T1@137 ft
S3_T2@77 ft
S3_Tref
18
17
16
15
14
35
30
25
20
15
10
5
0
-5
-10
5/11/00
5/21/00
5/31/00
6/10/00
6/20/00
6/30/00
7/10/00
7/20/00
7/30/00
8/9/00
8/19/00
8/29/00
9/8/00
9/18/00
9/28/00
10/8/00
10/18/00
10/28/00
11/7/00
11/17/00
11/27/00
12/7/00
12/17/00
12/27/00
1/6/01
1/16/01
1/26/01
2/5/01
2/15/01
2/25/01
3/7/01
3/17/01
3/27/01
4/6/01
4/16/01
4/26/01
5/6/01
5/16/01
5/26/01
6/5/01
6/15/01
6/25/01
7/5/01
7/15/01
7/25/01

Figure 31

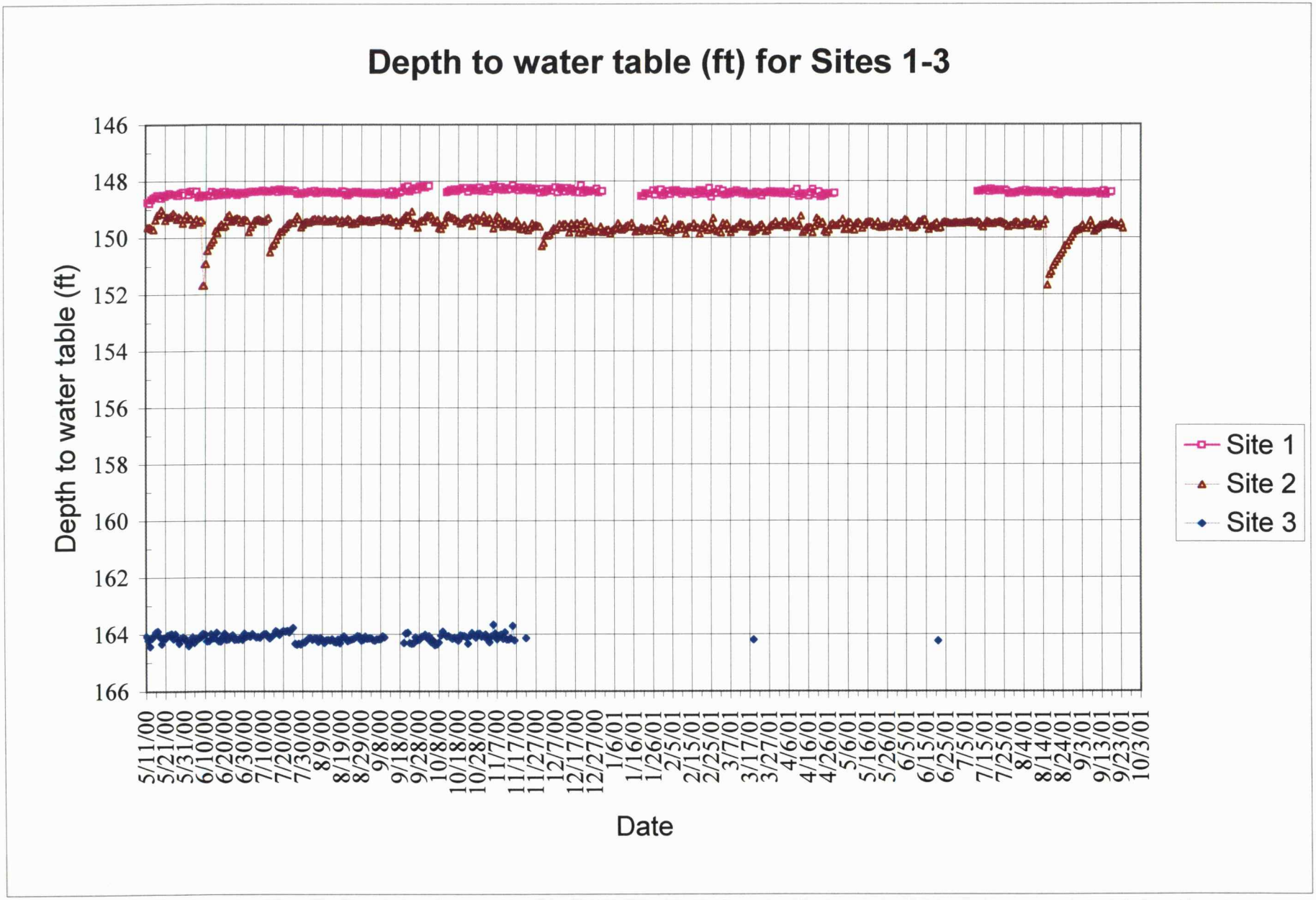
Depth to water table (ft) for Sites 1-3
Depth to water table (ft)
146
148
150
152
154
156
158
160
162
164
166
5/11/00
5/21/00
5/31/00
6/10/00
6/20/00
6/30/00
7/10/00
7/20/00
7/30/00
8/9/00
8/19/00
8/29/00
9/8/00
9/18/00
9/28/00
10/8/00
10/18/00
10/28/00
11/7/00
11/17/00
11/27/00
12/7/00
12/17/00
12/27/00
1/6/01
1/16/01
1/26/01
2/5/01
2/15/01
2/25/01
3/7/01
3/17/01
3/27/01
4/6/01
4/16/01
4/26/01
5/6/01
5/16/01
5/26/01
6/5/01
6/15/01
6/25/01
7/5/01
7/15/01
7/25/01
8/4/01
8/14/01
8/24/01
9/3/01
9/13/01
9/23/01
10/3/01
Date
Site 1
Site 2
Site 3

Figure 32

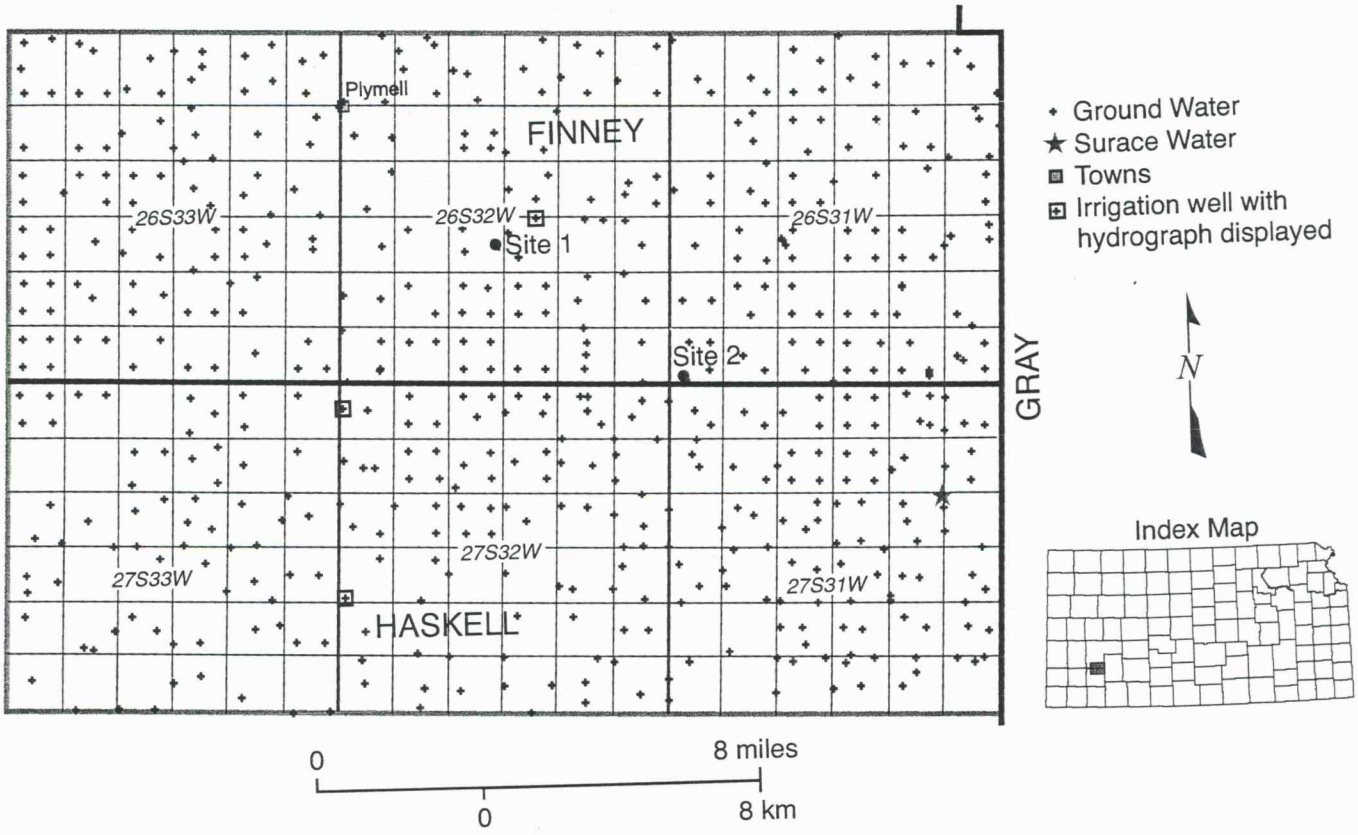
Plymell
FINNEY
26S33W
26S32W
26S31W
Site 1
Site 2
GRAY
27S33W
27S32W
27S31W
HASKELL
Ground Water
Surace Water
Towns
Irrigation well with hydrograph displayed
N
Index Map
0
8 miles
0
8 km

Figure 33

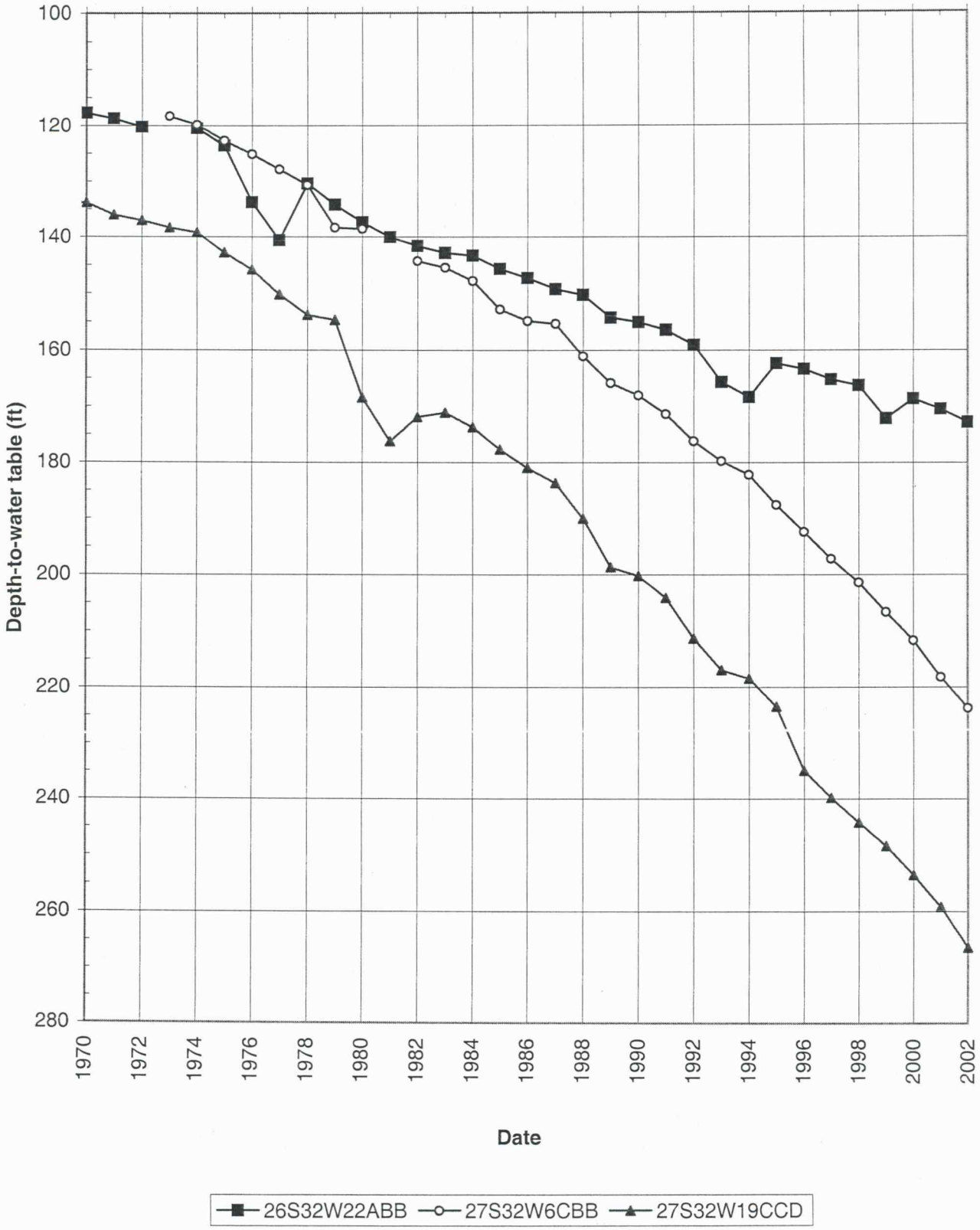
100
120
140
160
180
200
220
240
260
280
Depth-to-water table (ft)
1970
1972
1974
1976
1978
1980
1982
1984
1986
1988
1990
1992
1994
1996
1998
2000
2002
Date
26S32W22ABB
27S32W6CBB
27S32W19CCD

Figure 34